Journal Pre-proof

The Holy Grail: A road map for unlocking the climate record stored within Mars' polar layered deposits

Isaac B. Smith, Paul O. Hayne, Shane Byrne, Patricio Becerra, Melinda Kahre, Wendy Calvin, Christine Hvidberg, Sarah Milkovich, Peter Buhler, Margaret Landis, Briony Horgan, Armin Kleinböhl, Matthew R. Perry, Rachel Obbard, Jennifer Stern, Sylvain Piqueux, Nicolas Thomas, Kris Zacny, Lynn Carter, Lauren Edgar, Jeremy Emmett, Thomas Navarro, Jennifer Hanley, Michelle Koutnik, Nathaniel Putzig, Bryana L. Henderson, John W. Holt, Bethany Ehlmann, Sergio Parra, Daniel Lalich, Candice Hansen, Michael Hecht, Don Banfield, Ken Herkenhoff, David A. Paige, Mark Skidmore, Robert L. Staehle, Matthew Siegler

Please cite this article as: Smith, I.B., Hayne, P.O., Byrne, S., Becerra, P., Kahre, M., Calvin, W., Hvidberg, C., Milkovich, S., Buhler, P., Landis, M., Horgan, B., Kleinböhl, A., Perry, M.R., Obbard, R., Stern, J., Piqueux, S., Thomas, N., Zacny, K., Carter, L., Edgar, L., Emmett, J., Navarro, T., Hanley, J., Koutnik, M., Putzig, N., Henderson, B.L., Holt, J.W., Ehlmann, B., Parra, S., Lalich, D., Hansen, C., Hecht, M., Banfield, D., Herkenhoff, K., Paige, D.A., Skidmore, M., Staehle, R.L., Siegler, M., The Holy Grail: A road map for unlocking the climate record stored within Mars' polar layered deposits, *Planetary and Space Science* (2020), doi: https://doi.org/10.1016/j.pss.2020.104841.

during the production process, errors may be discovered which could affect the content, and all legal disclaimers that apply to the journal pertain.

The Holy Grail: A Road Map for Unlocking the Climate Record Stored within Mars' Polar Layered Deposits

Authors and Affiliations

Isaac B. Smith
      York University, Toronto, Ontario, Canada, M3J 1P3
      Planetary Science Institute, Lakewood, CO 80401
Paul O. Hayne
      University of Colorado Boulder, Boulder, Colorado 80309
Shane Byrne
      University of Arizona, Tucson, Arizona 85721
Patricio Becerra
      Universität Bern, Bern, Switzerland
Melinda Kahre
      NASA Ames Research Center, Moffett Field, California 94035
Wendy Calvin
      University of Nevada, Reno, Reno, Nevada 89557
Christine Hvidberg
      University of Copenhagen, Copenhagen, Denmark
Sarah Milkovich
      Jet Propulsion Laboratory, California Institute of Technology, Pasadena, California 91109
Peter Buhler
      Jet Propulsion Laboratory, California Institute of Technology, Pasadena, California 91109
Margaret Landis
      University of Colorado Boulder, Boulder, Colorado 80309
Briony Horgan
      Purdue University, West Lafayette, Indiana 47907
Armin Kleinböhl
      Jet Propulsion Laboratory, California Institute of Technology, Pasadena, California 91109
Matthew R. Perry
      Planetary Science Institute, Lakewood, CO 80401
Rachel Obbard
      SETI Institute, Mountain View, California 94043
Jennifer Stern
      NASA Goddard Space Flight Center, Greenbelt, Maryland 20771
Sylvain Piqueux
      Jet Propulsion Laboratory, California Institute of Technology, Pasadena, California 91109
Nicolas Thomas
      Universität Bern, Bern, Switzerland
Kris Zacny
      Honeybee Robotics, Pasadena, California 91103
Lynn Carter

43   University of Arizona, Tucson, Arizona 85721
44 Lauren Edgar
45   U.S. Geological Survey, Flagstaff, Arizona 86001
46 Jeremy Emmett
47   New Mexico State University, Las Cruces, New Mexico 88003
48 Thomas Navarro
49   McGill Space Institute, McGill University, Montréal, Québec, Canada
50   University of California, Los Angeles, Los Angeles, California 90095
51 Jennifer Hanley
52   Lowell Observatory, Flagstaff, Arizona 86001
53 Michelle Koutnik
54   University of Washington, Seattle, Washington 98195
55 Nathaniel Putzig
56   Planetary Science Institute, Lakewood, CO 80401
57 Bryana L. Henderson
58   Jet Propulsion Laboratory, California Institute of Technology, Pasadena, California 91109
59 John W. Holt
60   University of Arizona, Tucson, Arizona 85721
61 Bethany Ehlmann
62   California Institute of Technology, Pasadena, California 91125
63   Jet Propulsion Laboratory, California Institute of Technology, Pasadena, California 91109
64 Sergio Parra
65   California Institute of Technology, Pasadena, California 91125
66 Daniel Lalich
67   Cornell University, Ithaca, New York 14853
68 Candice Hansen
69   Planetary Science Institute, Tucson, Arizona 85719
70 Michael Hecht
71   Haystack Observatory, Westford, Massachusetts 01886
72 Don Banfield
73   Cornell University, Ithaca, New York 14853
74 Ken Herkenhoff
75   U.S. Geological Survey, Flagstaff, Arizona 86001
76 David A. Paige
77   University of California, Los Angeles, Los Angeles, California 90095
78 Mark Skidmore
79   Montana State University, Bozeman, Montana 59717
80 Robert L. Staehle
81   Jet Propulsion Laboratory, California Institute of Technology, Pasadena, California 91109
82 Matthew Siegler
83   Planetary Science Institute, Tucson, Arizona 85719

0: Abstract

In its polar layered deposits (PLD), Mars possesses a record of its recent climate, analogous to terrestrial ice sheets containing climate records on Earth. Each PLD is greater than 2 km thick and contains thousands of layers, each containing information on the climatic and atmospheric state during its deposition, creating a climate archive. With detailed measurements of layer composition, it may be possible to extract age, accumulation rates, atmospheric conditions, and surface activity at the time of deposition, among other important parameters; gaining the information would allow us to "read" the climate record. Because Mars has fewer complicating factors than Earth (e.g. oceans, biology, and human-modified climate), the planet offers a unique opportunity to study the history of a terrestrial planet's climate, which in turn can teach us about our own planet and the thousands of terrestrial exoplanets waiting to be discovered.

During a two-part workshop, the Keck Institute for Space Studies (KISS) hosted 38 Mars scientists and engineers who focused on determining the measurements needed to extract the climate record contained in the PLD. The group converged on four fundamental questions that must be answered with the goal of interpreting the climate record and finding its history based on the climate drivers

1. *What are present and past fluxes of volatiles, dust, and other materials into and out of the polar regions?*
2. *How do orbital forcing and exchange with other reservoirs affect those fluxes?*

105   *3. What chemical and physical processes form and modify layers?*

106   *4. What is the timespan, completeness, and temporal resolution of the climate history*

107   *recorded in the PLD?*

108

109   The group then proposed numerous measurements in order to answer these questions

110 and detailed a sequence of missions and architecture to complete the measurements. In all,

111 several missions are required, including an orbiter that can characterize the present climate and

112 volatile reservoirs; a static reconnaissance lander capable of characterizing near surface

113 atmospheric processes, annual accumulation, surface properties, and layer formation

114 mechanism in the upper 50 cm of the PLD; a network of SmallSat landers focused on

115 meteorology for ground truth of the low-altitude orbiter data; and finally, a second landed

116 platform to access ~500 m of layers to measure layer variability through time. This mission

117 architecture, with two landers, would meet the science goals and is designed to save costs

118 compared to a single very capable landed mission. The rationale for this plan is presented

119 below.

120   In this paper we discuss numerous aspects, including our motivation, background of

121 polar science, the climate science that drives polar layer formation, modeling of the

122 atmosphere and climate to create hypotheses for what the layers mean, and terrestrial analogs

123 to climatological studies. Finally, we present a list of measurements and missions required to

124 answer the four major questions and read the climate record.

125 ## *1. Background*

1.A Justification and Timeliness

From a scientific point of view, this is the opportune time to set the direction of future exploration of the polar layered deposits (PLD). The Mars polar science community held a conference in 2016 (Smith et al., 2018) and the Mars Amazonian Climate Workshop in 2018 (Diniega and Smith, this issue) that distilled and summarized many years of research performed on the datasets of numerous missions. Further, the Mars Exploration Program Analysis Group (MEPAG) recently completed an ice and climate study identifying the polar regions as high priority destinations for future exploration (ICE-SAG 2019). Those reports outline mature hypotheses and major themes for future work that cannot be addressed with current assets or those in development. Thus, we are at a turning point in the exploration of the PLD where existing data have been well-studied, hypotheses are waiting to be tested, and new data that can address these high priority topics are many years away.

Furthermore, technological developments have occurred in the past decade that make a landed polar mission more technically feasible and affordable than in the past. For example, entry, descent, and landing technology has evolved to include new methods of placing large payloads on the surface with greater location accuracy, and cryogenic drilling has advanced for both Mars and icy satellite investigations (Zacny and Bar-Cohen 2010).

Much progress has been made in constructing theoretical models that relate different climate states to PLD accumulation and ablation (Levrard et al. 2007; Hvidberg et al. 2012; Manning et al., 2019). Several recent studies have compared Mars Reconnaissance Orbiter (MRO) observations of the layers to these models, and they show broad agreement on the recent accumulation rate of the northern PLD (NPLD, Becerra et al., 2016; Landis et al., 2016;

148 Smith et al., 2016) and southern PLD (SPLD, Buhler et al., 2020). Thus, we, as a community, are

149 ready to measure layer properties for the climate record they contain.

150   In that context, we present a mission architecture that takes advantage of all classes of

151 NASA proposed mission programs. We focus on designing missions that could fit within the

152 NASA Discovery, New Frontiers, and Small Innovative Missions for Planetary Exploration

153 (SIMPLEX) programs i.e. programs that could develop significant payloads to reach Mars surface

154 or orbit within the objectives of the Decadal Survey (National Research Council 2011) Visions

155 and Voyages (2013-2022) but not dominate the funding schedule. Therefore, we develop a

156 campaign that begins with pathfinding exploration and orbital science that paves the way

157 towards subsequent missions with a targeted set of questions to answer. The concepts are

158 presented in Sections 2.C.1 through 2.C.4.

159   Ultimately, Mars polar exploration is of interest for many reasons. A primary interest is

160 the climate record, but human exploration and the search for life may also lead us to the poles.

161 Naturally, with the large quantities of surface ice exposed at the surface and 24+ hours of

162 sunlight over long periods, polar ice could become a resource for human exploration. Likewise,

163 the astrobiological potential of the layers may also be high. With abundant water, salts, and

164 subsurface heating, a transient history of habitable environments may be recorded in the

165 history of the polar caps. Therefore, while this paper focuses on the climate questions driving

166 polar exploration, additional considerations should be included when selecting missions to the

167 poles.

168

169 *1.B Mars Polar Science Overview and State of the Art*

1.B.1 Polar ice deposits overview and present state of knowledge

The poles of Mars host approximately one million cubic kilometers of layered ice deposits (Smith et al. 2001; Figure 1). Discovered by Mariner 9 imaging (Murray et al. 1972), these Polar Layered Deposits (PLD) have long been thought to record martian climate in an analogous way to terrestrial polar ice sheets. Both PLD are composed primarily of water ice (Plaut et al., 2007; Grima et al. 2009) but contain dust up to a few percent of their total mass, as well as materials potentially related to specific geologic events, such as volcanic ash and impact ejecta. The South PLD (SPLD) has an additional ~1% of carbon dioxide ice (CO_2) that resides in a stratified section above the H_2O layers (Phillips et al., 2011) and a thin, ~10 m thick, CO_2 residual cap that persists from year to year (Figure 1). The vertical and horizontal distribution of these materials are thought to record atmospheric conditions including temperature, relative humidity, and aerosol dust content, along with atmospheric and isotopic materials that varied through time.

Figure 1: Images of the north and south polar layered deposits (NPLD and SPLD, respectively) from the High Resolution Stereo Camera on Mars Express. Left: NPLD in late spring without seasonal frost cover. Width of image is ~1250 km. Right: SPLD in late summer. White CO_2 is the south polar residual cap (SPRC) and the youngest deposit visible at high latitudes and elevations. Much of the center of this image is water ice layers with a thick dust lag with similar coloration as the surrounding rocky surfaces. The NPLD also has a dust lag, but much of the white north polar residual cap (NPRC) is uncovered. The NPLD provides the majority of the water vapor budget for the planet.

183   This iconic PLD layering is seen through visible and infrared imaging of bed exposures in

184   troughs and scarps (Figure 2) and radar sounding data (Figure 3). Although the surfaces of the

185   PLD are among the flattest and smoothest surfaces on Mars, they are bounded by steep,

186   marginal scarps that typically expose up to a kilometer of vertical layering on slopes that exceed

187   10° and rarely reach 90°. Additionally, in the interior of the PLD, arcuate troughs expose a few

188   hundred meters of bedding (Pathare and Paige, 2005). The marginal scarps appear to be

189   erosional in nature, with active erosion observed at the steepest north polar examples (Russell

190   et al. 2008). However, geologic structures, including unconformities, within the PLD indicate

191   that the internal troughs are constructional features, and that they experience erosion on their

192   steeper equator-facing walls and re-deposition on the pole-facing walls, leading them to have

193   migrated 10s of kilometers poleward as the PLD accumulated (Howard et al., 1982; Howard

194   2000; Smith and Holt 2010; 2015; Smith et al., 2013).

195   Variations in the orbital configuration of Mars lead to climatic variations, which are

196   thought to be recorded in the PLD. The orbital parameters, whose oscillations primarily drive

197   these climatic changes, are the planet's obliquity, orbital eccentricity, and argument of

198   perihelion (Laskar et al., 2002). Obliquity cycles have characteristic timescales of ~120 kyr and

199   ~1 Myr; eccentricity varies on timescales of ~1.2 Myr; and the argument of perihelion has a

200   precession cycle of ~51 kyr (Laskar et al. 2004). Over the last 20 Myrs, the obliquity of Mars has

201   varied between 15 and 45 degrees. High values of obliquity (>30°) mean that the horizontal

202   surfaces on the poles receive more insolation on average than the mid-latitudes, which leads to

203   the ablation of polar ice and transport to lower latitudes. Conversely, low obliquity promotes

204   accumulation of polar ice. The present obliquity is around 25°, which is low enough that the

205   average insolation at the poles is lower than at the mid-latitudes, but high enough that the net

206   mass balance is difficult to distinguish from zero (Bapst et al. 2018). Obliquity variations

207   between ~15 and ~35° straddle this value in the last 5 Ma and may have led to large variations

208   in the rate of polar accumulation. Additionally, the precession of perihelion from southern

209   summer (present state) to northern summer will affect insolation rates by 50% (Laskar et al.,

210   2004). As with obliquity, this affects accumulation rates and therefore layer thickness.

211   Multiple angular unconformities in the stratigraphic record show periods of net ablation

212   have occurred (Tanaka 2005), and extremely dusty layers may be sublimation lag deposits that

213   represent disconformities in the record (Fishbaugh et al. 2010). Orbital solutions also show that

214   the mean obliquity between 5 and 20 Ma was ~35° – substantially higher than the ~25° from 4

Figure 2: HiRISE image PSP_005103_0995 of layers in the south polar layered deposits (SPLD). Exposed layers imply active and recent erosion; however, a dust lag may slow sublimation on annual time

215   Ma to the present. Unique solutions prior to 20 Ma cannot currently be derived, but statistical

216   arguments show that a high mean obliquity is common and that the most probable obliquity

217   over all of martian history is ~42 degrees (Laskar et al., 2002). Thus, the current thick polar

218   layered deposits may be atypical compared to most of martian history.

219   Impact craters on the uppermost surface of the NPLD yield a young age, implying

220   ongoing resurfacing that is fast enough to erase craters 100 m in diameter over timescales of

221   kyr to 10s of kyr (Banks et al. 2010; Landis et al. 2016). The SPLD crater record is consistent with

222   a surface that is between 30 Ma and 100 Ma in age (Herkenhoff and Plaut, 2000; Koutnik et al.

223   2002). Model simulations of polar ice stability provide another age constraint. Several studies,

224   described in sections below, argue that the high obliquities prior to 4-5 Ma make ice

225   accumulation at the north pole impossible prior to that time. This has been interpreted as an

226   upper limit for the age of the NPLD. However, the insulating effects of lag deposits are

227   incompletely accounted for in these studies, and the obviously older SPLD and ice rich north

228   polar basal unit (Tanaka 2005) do not fit into this simple model. In addition, the SPLD (Becerra

229   et al., 2019) and Basal Unit (Nerozzi and Holt 2019) both most certainly contain climate

230   signatures from their time of deposition.

231   In addition to the icy bedding that makes up most of their structure, the PLD are partly

232   covered with bright residual ice caps that interact strongly with the current climate (Figure 1).

233   The north polar residual ice cap (NPRC) is a thin water ice unit that overlies the NPLD. It is

234   exposed at the end of the spring after seasonal CO_2 and water frosts sublimate. Stereo imagery

235   shows that it has less than a meter of relief and a texture of light and dark patches (or ridges in

236   some locations) in repeating patterns with a horizontal scale on the order of decameters. It also

237   exhibits an evolution of ice grain size and albedo throughout the year (Langevin et al. 2005;

238   Brown et al. 2016). Fine-grained seasonal frost that accumulates in the fall and winter

239   sublimates in the spring and summer, and older large-grained ice is exposed for a portion of the

240   summer, suggesting that net ablation is currently occurring (Langevin et al. 2005). However,

241   this large-grained ice is dust-free, and ablation has not been significant enough to produce a lag

242   deposit, and ice is currently accumulating within polar impact craters (Landis et al. 2016).

243   The gross and net annual exchange of H_2O onto either polar cap is unknown, but the net

244   flux is thought to average 0.5 kg m^{-2} over the last few Myr onto the NPLD. Evidence exists for

245   either NPLD growth or loss in present day (Kieffer, 1990; Langevin et al., 2005; Chamberlain and

246   Boynton, 2007; Brown et al., 2016) and for re-frosting during summer (Appéré et al., 2011),

247   complicating the story. This unknown mass balance value is a critical parameter for even

248   understanding the current climate, so knowledge of this value will help tune and validate GCMs

249   of modern climate, which supports their application to understanding past climatic states.

250   The SPLD possess a partly buried reservoir of CO_2 ice (up to 1 km thick) that is

251   comparable in mass to the current CO_2 atmosphere of the planet (Phillips et al. 2011; Bierson et

252   al. 2016; Putzig et al., 2018). This CO_2 ice is capped by a water ice layer on top of which a much

253 smaller (~1% of the current atmosphere) surface CO_2 South Polar Residual Cap (SPRC) ice

254 deposit exists (Figure 1; Bibring et al. 2003; Byrne and Ingersoll, 2003; Titus et al. 2003; Byrne

255 2009). This deposit has extremely high albedo that changes with seasons (Colaprete et al.,

256 2005; Schmidt et al., 2009) and hosts a wide variety of sublimation-driven erosional features

257 that have been observed to grow and change every Mars year. Rapid changes in the

258 morphology and appearance of the SPRC are evidence of its sensitive interaction with the

259 current climate. Not only do these sublimation features grow by several meters per year

260 (Thomas et al. 2009; 2016; Buhler et al., 2017), but summer dust storm activity has been

261 observed to lead to distinctive bright halos on the edges of these features (Becerra et al. 2015),

262 which may be associated with further wintertime condensation of CO_2 ice. This interaction,

263 which we observe year to year, may be direct evidence for new SPRC structures forming

264 currently; however, they are very different from the water ice beds that comprise most of the

265 SPLD volume

1.B.2 Polar Layered Deposits formation and nature of layers

267 During orbital variations, the transfer of ice, aerosols, and dust from low latitudes to the

268 poles causes the formation of alternating beds with variable ice purities. The bulk content of

269 the NPLD is ~95% water ice (Grima et al. 2009). However, individual beds may be up to 50%

270 dust (Lalich et al., 2017). The dust-rich beds may have formed during periods of high dust

271 accumulation or during periods of ice loss and lag formation. Dust-poor beds must have formed

272 during times when ice deposition was high relative to dust accumulation (Hvidberg et al., 2012).

273 It is therefore necessary to study the visible stratigraphy of the PLD in order to interpret the

274 timing of deposition of observed layers and build a climate record that ties bed sequences to

275   particular insolation cycles in time.

276   *Observing the stratigraphic record*

277   Properties of the PLDs suggest that accumulation has not been uniform in space

278   (horizontally) or time (vertically). Both PLDs are thickest near the pole and thinner at the

279   margins; the thickest SPLD and south polar CO_2 deposits are slightly offset from the pole (Smith

280   et al., 2001; Colaprete et al., 2005; Phillips et al., 2011; Putzig et al., 2018). In the NPLD, there

281   are clear patterns of local and regional accumulation that were affected by existing basal

282   topography (Brothers et al., 2015) or other large structures (e.g. a now buried chasma Holt et

283   al. (2010)). Additionally, the PLDs contain numerous local and regional unconformities (Tanaka

284   and Fortezzo 2012) that are attributed to deposition following erosion by sublimation or wind

285   ablation; however, some may have formed simultaneously (Smith et al., 2016).

286   The differences in relative accumulation with geographic location, unconformities, and

287   post-depositional modification processes affect the final state of the sedimentary record in the

288   PLD that we can observe. Therefore, in order to detect the periodic signals corresponding to the

289   astronomically-forced insolation, we need to be able to observe and describe intrinsic

290   properties of the beds that make up the record, i.e., properties that relate most closely to the

291   environmental conditions at the time of accumulation. These properties may include sintering

292   rate, dust/ice ratio, or concentrations of different isotopes in iced, dust, and trapped gases. On

293   Earth, these properties can be extracted from ice or sediment core samples, but Mars

294   conditions and remoteness make these measurements more difficult than on Earth. Once

295   sampled, however, martian conditions may improve the readability of the layers over their

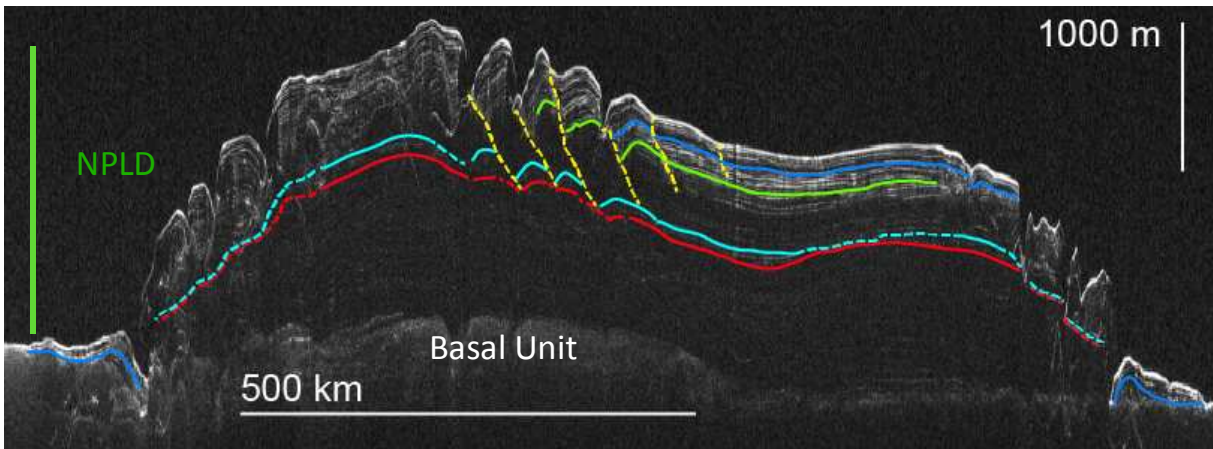296   terrestrial counterpart for several reasons.

Figure 3: Shallow radar (SHARAD) observation 1247002 exhibiting numerous reflections hinting at deposition cycles (Hvidberg et al., 2012). Annotation highlights mapped structures, including unconformities and discontinuities (yellow dashed lines). Modified from Smith and Holt (2015).

297   1. Layers are conformable, particularly at depth, preserving them well compared to highly

298   distorted ice seen in flowing ice on Earth.

299   2. The range of isotopic variation, particularly D/H is an order of magnitude greater than

300   on Earth, making it easier to measure.

301   3. PLD ice's greater hardness due to lower temperature and Mars' lower gravity compared

302   to Earth make drill holes much more stable against collapse (Bar-Cohen & Zacny 2009).

303   4. The PLD likely lack firn (Paige, et al., 1994; Arthern et al., 2000).

304   *Remote sensing observations of exposed bed sequences*

305   Orbital imaging at visible and infrared wavelengths has been used to extract information

306 from the bedding outcrops exposed at the characteristic spiral troughs of the PLD (Cutts, 1973;

307 Schenk and Moore, 2000). Visible imagery datasets provide information on brightness of layers,

308 topography of the outcrop with stereo imaging (Becerra et al., 2016), and color-ratios, while

309 infrared spectrometers provide estimates of the composition of ices, lithics, and alteration

310 phases (e.g. Massé et al., 2012).

311   The High Resolution Imaging Science Experiment (HiRISE) (McEwen et al., 2007) on

312   MRO, provides us with images from which we are able to extract reflectance and topographic

313   information at the scale of ~1–2 meters. There are noticeable variations with depth in

314   topographic expression and brightness for every outcrop that point to an indirect relationship

315   to the composition of the internal bedding (Becerra et al., 2016). Darker exposed layers are

316   hypothesized to contain a higher dust content, and a more protruding layer may also be

317   associated with a high dust content that insulates and protects that particular bed from erosion

318   more than its stratigraphic neighbors (Malin and Edgett, 2001).

319   Surface observations are limited to the top 400 – 800 m of the PLDs, i.e., to the

320   maximum depths of exposures. Additionally, the outcrops are scattered throughout the extent

321   of the PLD, and therefore, correlations must be made between a sequence exposed in one

322   location, and one exposed in a different one, which is not a trivial endeavor (Fishbaugh and

323   Hvidberg, 2006; Milkovich and Plaut, 2008; Becerra et al., 2016).

324   The Compact Reconnaissance Imaging Spectrometer for Mars (CRISM; Murchie et al.,

325   2007), also on MRO, provides visible/near-infrared spectra (VNIR; 0.3-2.6 μm) of the PLD at ~18

326   meter/pixel resolution. This resolution cannot discern individual layers but can resolve broad

327   trends and lag deposits. Lower spatial resolution (~300+ meter/pixel) VNIR spectra from the

328   OMEGA imaging spectrometer onboard Mars Express (Bibring et al., 2005) have also been used

329   to investigate the properties of the surface of the polar plateaus. These datasets have identified

330   seasonal evolution in ice grain size (Langevin et al., 2005; 2007; Calvin et al., 2009; Calvin et al.,

331   2015; Brown et al., 2016) that can be observed for long periods (Piqueux et al., 2015), hydrated

332   salts (possibly including perchlorate and sulfates) within the NPLD (Horgan et al., 2009; Massé

333 et al., 2012), and the presence of primary mafic minerals within the NPLD (Sinha et al., 2019).

334 Hydrated salts may reflect transient aqueous alteration on the polar surface (Horgan et al.,

335 2009) and/or accumulation of atmospheric precipitates (Massé et al., 2012). Mafic minerals

336 within the NPLD include pyroxene, olivine, and glass, both of sand size and finer, which are

337 distinct from the homogeneous global dust that dominates the lag on many exposures. These

338 layers are most likely sourced from a combination of distal and proximal impact ejecta and

339 distal volcanic ash (Horgan et al., 2014; Sinha et al., 2019). The north polar basal unit is also at

340 least partially composed of similar mafic minerals, as the cavi unit is a major source of glass-rich

341 sand feeding the north polar sand sea (Horgan & Bell, 2012).

342

343 *Observations of the subsurface structure with radar*

344   Radar instruments like the Mars Advanced Radar for Subsurface and Ionosphere

345 Sounding (MARSIS; (Picardi et al., 2004)) on board the European Space Agency's (ESA's) Mars

346 Express, and the Shallow Radar (SHARAD; (Seu et al., 2007)) on MRO, are sensitive to the

347 dielectric properties of the target material. Ice is nearly transparent to radar waves, allowing

348 the radio wave to penetrate to the deepest portions of the PLDs, as deep as 3.5 km, and

349 permitting views of the internal structure (Figures 3 and 4). These data show that the deposits

350 are relatively pure, with up to 5 to 10% bulk dust concentrations for the NPLD and SPLD,

351 respectively (Grima et al., 2009; Plaut et al., 2007). Recently, a very high reflection zone was

352 detected at the bottom of the SPLD (Orosei et al., 2018); raising the possibility for a thin layer of

353 water at the polar base.

354   Differences in silicic content (primarily dust, but possibly ash or ejecta) between icy

355   layers will cause changes in dielectric permittivity that change the speed of propagation of the

356   radar wave, causing a reflection (Nunes and Phillips, 2006). The relationship between

357   permittivity, layer structure, and dust content is not completely understood. For example, radar

358   signals from a series of thin, dust-rich beds may have similar properties to a single, thick dust-

359   rich layer (Lalich et al., 2017). However complicated the layering may be, there is consensus

360   that the radar response is related to the dust content of the PLD beds (Grima et al., 2009; Lalich

361   et al., 2017).

362   The vertical resolution of current radar observations is much lower than that of optical

363   imagery, causing a difficulty in matching visible layers and radar reflectors. Where comparisons

364   have been made, radar reflectors mimic the exposed layers in spectral frequency and geometry,

365   most likely because both types of observations observe variable concentrations of dust

366   (Christian et al., 2013; Becerra et al., 2017a). Bed-to-bed correlation between datasets may not

367   become possible until a higher resolution radar sounder flies to Mars in a polar orbit.

368   *Large-scale geologic framework of the PLDs*

369   Establishing broad-scale relationships between layer packets and geologic units in the

370   PLDs provides the geologic framework within which the finer-scale stratigraphy must be

371   analyzed and interpreted. In a major survey, Tanaka et al. (2007, 2008) searched for common

372   characteristics and unconformities to develop a PLD-scale stratigraphic column and geologic

373   map for both PLD. They derived the ages of the units from crater statistics and visual

374   stratigraphic principles. The units most relevant to PLD stratigraphy are the formerly discussed

375   SPRC and NPRC and multiple, thick water ice units (Tanaka et al. 2007; 2008; Tanaka and

376   Fortezzo 2012). The NPLD also reside over a km thick basal unit that contains ~50% sand

377 (Fishbaugh and Head, 2005; Nerozzi and Holt 2019).

378 *Image-based correlation of exposed sequences*

379   Studies of exposed layering rely on properties such as bed protrusion, local slope, and

380 brightness that can be extracted from a Digital Terrain Model (DTM) or a single image of one

381 location on the NPLD and compared to other locations. Images of bed exposures can be used to

382 define and classify discrete layer sequences based on their morphological properties. From

383 there, continuous depth profiles can be extracted and directly compared to synthetic

384 stratigraphic columns built with models of ice and sediment accumulation.
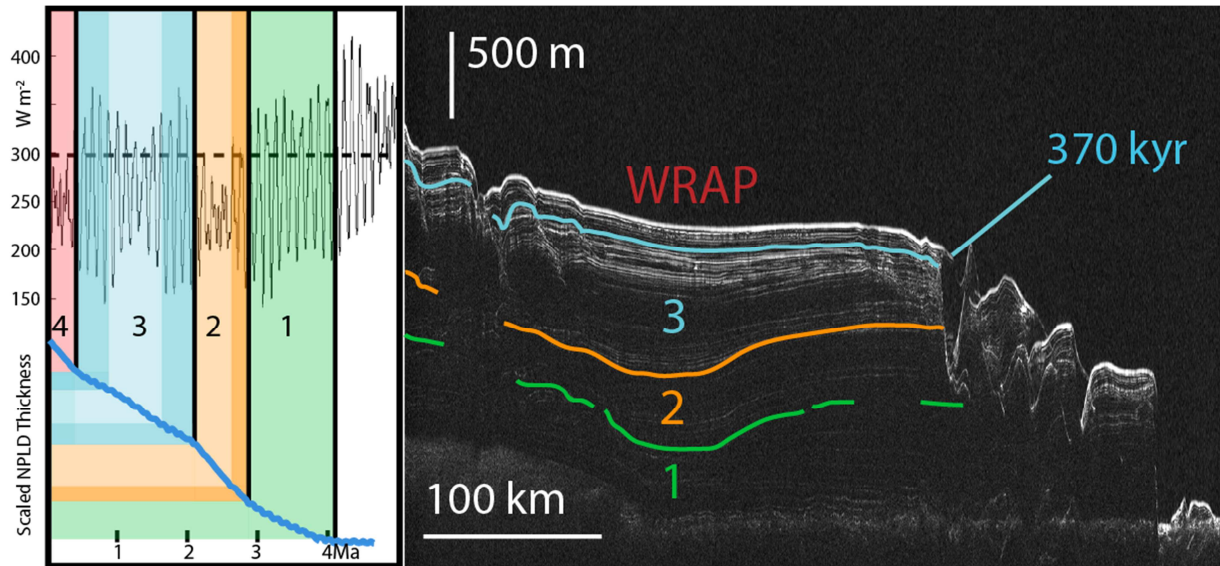
Figure 4: Comparison of model from Levrard et al., (2007) (left) to radar stratigraphic mapping of the NPLD (right). Model calculates solar insolation in Wm^{-2} starting at ~4 Ma and predicts four distinct periods of NPLD accumulation, some at faster rates than others. Blue line in left panel is total accumulation of NPLD ice. Approximately 30 lag deposits are expected to derive from obliquity changes, similar in number to the total number of reflectors that SHARAD detects (right). Bright packets in the radar may correspond to periods when solar insolation cycles had larger amplitudes. WRAP is the Widespread Recent Accumulation Package, possibly associated with the current interglacial period (Smith et al., 2016). Adapted from Smith et al.,

385   Studies of the NPLD (Fishbaugh and Hvidberg 2006) and of the SPLD (Byrne 2004;

386   Milkovich and Plaut 2008; Milkovich et al., 2009) correlated spatially distinct sequences to

387   propose the first relative stratigraphic columns for the two PLD. More recently, near complete

388   imaging coverage of the PLD with the Context Imager (CTX) has allowed for individual beds to

389   be traced hundreds of kilometers along the same trough (Becerra et al., 2016). These profiles

390   can then be directly compared to climate proxies such as insolation or temperature changes

391   with time (Laskar et al., 2002), or analyzed for periodic cycles that match those of the climate

392   signals (Milkovich and Head, 2005; Herkenhoff et al., 2007; Perron and Huybers, 2009; Limaye

393   et al., 2012; Becerra et al., 2017b).

394   *Detailed stratigraphy of the NPLD*

395   Fishbaugh et al. (2010b) were the first to construct a stratigraphic column based on

396   topographic and morphologic considerations from a single HiRISE DTM. They defined two

397   principal types of beds or bedding packets. These they called marker beds (MBs) after Malin

398   and Edgett's (2001) identification of the "original" Marker Bed in various sites on the NPLD.

399   Marker beds are thick, dark, have a characteristic hummocky texture, and thin, resistant layer

400   sets each ~1–2 m in thickness. In the spacing between MBs, the authors reported finding the 30

401   m periodicity previously observed by Laskar et al. (2002) and Milkovich and Head (2005); and in

402   the spacing between bedding packets (thin layers sets), they observed the 1.6 m wavelength

403   from Perron and Huybers, (2009). Later, Limaye et al. (2012) measured bed thicknesses from

404   digital terrain models (DTMs) and found a low variance, with the majority of beds only few

405   meters thick. Analysis by Limaye et al. (2012) confirmed the 1.6 m wavelength, but not the 30

406   m wavelength.

407   Recent work compiled a number of HiRISE DTMs to measure linear protrusion profiles

408   and identified two dominant stratigraphic wavelengths in all profiles that have a common ratio

409   of wavelengths of 1.98±0.15 (Becerra et al., 2017a; 2017b). This was systematically lower than

410   the 2.35 ratio of the orbital signals in the 2 Ma insolation (Laskar et al., 2002) but matches that

411   of synthetic stratigraphy generated by the accumulation model of Hvidberg et al. (2012). These

412   results appear to imply that the uppermost 500 m of the NPLD have accumulated at 0.54

413   mm/yr.

414   *Radar-based stratigraphy*

415   The ability to directly probe the vertical structure of the internal PLD, made possible by

416   subsurface sounding radar, signified a substantial step forward in the study of Mars Polar

417   Science (Figures 3, 4). One of the first major discoveries by SHARAD was that the NPLD beds are

418   laterally continuous throughout almost the entire extent of the dome, over 1000 km (Phillips et

419   al., 2008). When radar data coverage is dense enough, various radar units can be mapped

420   throughout the whole PLD, resulting in thickness measurements of prominent units and, in

421   essence, a radar-based stratigraphy (Putzig et al., 2009; Smith and Holt, 2015; Nerozzi and Holt

422   2017). Additionally, a three-dimensional radar volume has been developed for observing in

423   geometries not permitted with only two-dimensional, orbit parallel profiles (Foss et al., 2017;

424   Putzig et al., 2018).

425   NPLD Reflections are location dependent, but radar images typically reveal ~four

426   packets of finely spaced bright reflectors separated by homogeneous interpacket regions and

427   few reflectors (Figure 4). Phillips et al. (2008) suggested that the packet/interpacket structure

428   related to approximately million-year periodicities in Mars' obliquity and/or orbital eccentricity.

429   Putzig et al. (2009) extended this work to suggest uniform deposition and erosion patterns

430   were common throughout most of NPLD history. Studies with the SHARAD dataset also allowed

431   researchers to explain the formation of Chasma Boreale (Holt et al., 2010) and the onset,

432   migration, and morphological diversity of the iconic spiral troughs (Smith and Holt, 2010; 2015).

433   Further, intermediate scale undulations reflect regional winds and leave behind stratigraphy

434   that the radar detects (Herny et al., 2014). A full discussion of spiral trough formation

435   hypotheses, including undulations, can be found in Smith et al. (2013).

436   Recent analysis of SHARAD data found a cap-wide unconformity that varied between 80

437   and 300 m beneath the current surface (Figure 4, Smith et al., 2016). This was interpreted to

438   represent a climatic shift from a period of net NPLD loss to one of rapid accumulation. Previous

439   modeling had predicted thicknesses of ~300 m (Levrard et al., 2007) and volumes of

440   approximately 1-meter global equivalent layer of ice (Head et al., 2003) would have

441   accumulated on the NPLD in the last 370 kyr. This thickness and volume compared favorably

442   with the measured values, and Smith et al. (2016) interpreted this to mean that the

443   unconformity occurred at this time and derived an average accumulation rate of 0.32 mm/yr

444   since then.

445   *Forcings*

446   The climatic state of Mars is driven by changes in the orbital parameters of the planet

447   and by the presence and longevity of volatile and dust reservoirs. As described above, obliquity

448   variations are the most important orbital parameter driving the movement of water ice,

449   potentially transferring the majority of Mars' water inventory between the mid-latitudes, poles,

450   and equator on ~105 yr timescales (Levrard et al., 2007). Additionally, smaller effects on the

451   pattern of global insolation occur due to precession of the argument of perihelion and

452   variations in the eccentricity of Mars' orbit (Laskar et al., 2004). Combined, these three orbital

453   cycles drive most of Mars' climate variations.

454   External forcings of Mars' climate include solar winds, Jeans Escape, cosmic rays,

455   impactors, etc., that act to strip material away from the upper atmosphere or, on smaller

456   scales, implant new materials. Secular mass loss driven by the solar wind put Mars into its

457   current, low-pressure state billions of years ago (Jakosky and Phillips, 2001). On timescales

458   relevant to the polar ice, atmospheric stripping may have affected fractionation rates for

459   isotopes in parallel with solar cycles (Fisher 2007).

460   There are also internal climate forcings. The major internal climate driver is the poorly

461   understood dust cycle. Several local and regional dust storms occur repeatedly on annual time

462   scales (Montabone et al., 2015). The biggest perturbation of the atmosphere by dust is from

463   planet-encircling dust events that cover all longitudes and are so optically thick that visible

464   imagers cannot detect the surface. In these events, atmospheric temperatures increase

465   globally, affecting water vapor distribution and transport. Observations record dust storms

466   every few martian years.

467   Volcanic outgassing must play a role in the variability of atmospheric composition and

468   maybe pressure (Craddock and Greeley 2009). The most recent volcanic eruptions are dated at

469   only ~10 Myr, so they are relevant to Amazonian climate (Bermann and Hartmann 2002).

470   Evidence of eruptions, through fine grained pyroclastic ash fall or alteration of isotopic ratios

471   into the atmosphere, may exist within the PLDs.

Isotope Variability in Layers

473   Because PLD layers form from meteoric constituents, they likely retain a combination of

474   ices (H_2O, CO_2), dust, and trapped gasses. Water vapor and carbon dioxide will undergo

475   fractionation processes during deposition to a solid, but trapped gases, if retained during

476   sintering, can provide samples of the past atmosphere. Because of the numerous reservoirs

477   that can contribute, the layers may be a collection of mixed sources.

478   The ratio of deuterium to hydrogen (D/H) in PLD water ice is a valuable measurement.

479   The seasonal signal of D/H from atmosphere-ice exchange in the northern hemisphere imparts

480   a distinctive isotopic signature in the atmosphere of >1000 per mil (Villanueva et al., 2015) that

481   may be recorded in the currently forming ice layer. Over time, and through orbital cycles, the

482   D/H ratio of layered ice will vary based on the source reservoirs that supply the materials (Vos

483   et al., 2019). This deposition can tell us about the climate signal of orbital parameters driving

484   variations in obliquity, which in turn provides information on what reservoirs are accessed at

485   different orbital states (e.g., Montmessin et al., 2005; Fisher 2007).

486   Even though multiple sources likely supplied the atmospheric water vapor that

487   contributed to deposition in the PLDs, finding the ratio of D/H within solid ice will provide

488   insight into the long-term (>3 Ga) climate history of Mars (Vos et al., 2019). This in turn will

489   teach us about the loss rate of water to space (Jakosky 1990) and Mars' earlier environment.

490   A key aspect of interpreting the PLD climatic record is establishing an absolute

491   chronology in addition to relative timing. As with Curiosity (Farley et al., 2014), in situ

492   geochronology with mass spectroscopy may be possible for the ice cores, particular for those

493   layers enriched in dust. Methods measuring decay products of radioactive elements (e.g. He,

494   Ne, Be, Ar) and the concentrations of cosmogenic radionuclides need further study to vet their

495   application for the chronology of PLD (Section 2.A.5).

496   *Polar Ice Flow*

497   Terrestrial ice sheets experience rapid, large-scale flow that affects layer properties,

498   including thickness, slope, and stratigraphic continuity. These post-deposition modifications

499   alter the climatological record, complicating our efforts to interpret it. If the PLD of Mars have

500   undergone measurable flow, then we must be prepared to take this into account when

501   choosing sampling locations and interpreting the Martian climate record.

502   The magnitude of flow at the NPLD is debated. Predictions of large-scale flow at the

503   NPLD have been made for decades (e.g. Fisher 1993; 2000; 2010; Winebrenner et al., 2008; Sori

504   et al,. 2016), but observational investigations directly testing these hypotheses with

505 stratigraphic comparisons do not support predictions of widescale flow (Karlsson et al., 2011;

506 Smith and Holt 2015), even though some forms of predicted flow may not result in evidence of

507 stratigraphic thinning or thickening (Fisher 2010). Additionally, the thickness of layers in the

508 lowermost 1 km should vary with distance from the accumulation to ablation zones or vary

509 based on elevation gradients; however, they are essentially constant across the entire cap

510 within the resolution of radar sounding investigations (Phillips et al., 2008, Putzig et al., 2009;

511 Nerozzi and Holt 2017).

512   In this paper we acknowledge the importance of flow in terrestrial ice sheets and their

513 potential importance at Mars. Therefore, each recommended investigation below should be

514 taken in context of the state of knowledge regarding flow.

515 *Layer Formation*

516   Modern processes related to layer formation are not well known, and yet the current

517 surface will one day become incorporated into the PLD, analogous to layers below. Thus,

518 reading the variability in layer composition through time requires an understanding of what

519 goes into making a layer today. Importantly, layer formation doesn't end upon burial. Like on

520 Earth, there is a zone in which communication with the atmosphere still occurs, cosmic

521 radiation interacts with materials, and internal forces can recrystallize the ice and exclude or

522 incorporate impurities. Because of this, determining all of the processes that are recorded in a

523 layer is a critical step towards reading the sequence of layers for a climate record.

524   Formation of a layer within the PLD begins with the accumulation and densification of

525 atmospheric ice as snow into firn or by direct deposition that eventually fills pores by

526 compaction, sintering, and gas diffusion. The ratio of these types of accumulation is unknown,

527   but models of PLD accumulation and thermal inertia measurements suggest that the surface

528   layer is dense, implying that densification may be rapid and the firn only a few cm thick

529   (Arthern et al 2000).

530   Observations by the near-polar Phoenix lander showed accumulation by both water ice

531   crystals and surface frosts (Whiteway et al. 2009), but the accumulation ratios there were not

532   quantified. Some of the water ice may also fall as nucleation centers in CO_2 ice, which comes

533   seasonally and forms a meter-thick layer before subliming in the spring, potentially leaving the

534   water ice and other constituents for incorporation into the uppermost layer (Colaprete et al.,

535   2008; Brown et al., 2014).

536   Surface ice crystals begin small but grow with time. Terrestrial models and observation

537   of this growth process show that it is limited by impurities (e.g. Durand et al., 2006; Barr and

538   Milkovich). Past models of the martian PLDs (Kieffer, 1990) can relate ice grain size to depth in

539   the upper meters to surface accumulation rate. These effects must be integrated through time

540   to the depth at which atmospheric communication is cut off and metamorphosis ceases. Thus,

541   measuring a buried layer without knowing what forms and modifies a layer will provide less

542   information than if we have context on all of the formation mechanisms.

543   Besides meteoric ice, the PLD are expected to contain many other constituents. In

544   decreasing order by volume, we expect the composition to include dust, salts, lithic materials,

545   gas bubbles, and HDO, an isotopologue of H_2O, and daughter products of nuclear fission. Dust is

546   incorporated either by falling out of the sky or scavenging during snow formation. Salts are also

547   likely meteorically deposited or are brought in from winds that cross the pole. Depending on

548   location, some of these materials may be recycled from older PLD layers that erode or sublime

549 and are then transported to another place for incorporation. Lithic material, such as volcanic

550 ash or impact ejecta probably fall irregularly. Bubbles of atmospheric gas likely form as new ice

551 accumulates above. Additionally, cosmic radiation will bombard the uppermost PLD, triggering

552 reactions that leave measurable products that vary with depth.

553 Investigating layer formation is critical to reading the climate record, because layers

554 comprise the record. Many processes occur exactly at the surface, including ice crystallization,

555 dust entrainment, isotope fractionation, heat loss or gain, and grain growth. Furthermore,

556 processes continue even after burial, such a sintering, phase partitioning, and impurity

557 exclusion. A firn layer permits gas exchange with the atmosphere, so the top centimeters may

558 be actively forming. Prior work has found conflicting lines of evidence about the current mass

559 balance of the NPLD (Kieffer, 1990; Langevin et al., 2005; Chamberlain and Boynton, 2007;

560 Brown et al., 2016), so it is unclear even if the NPLD is currently gaining or losing mass.

561 ### *1.B.3. Reservoirs other than the PLDs*

562 It is important to identify the reservoirs of volatiles that can be mobilized. The

563 atmosphere is the most active reservoir, and other reservoirs of dust and water ice are

564 abundant on the planet. Each provides input to the climate state and PLD growth.

565 Carbon dioxide is the primary constituent of the martian atmosphere, with a mass of

566 ~2.5×10^{16} kg (James and North, 1982). This fluctuates by approximately 1/3 each season as the

567 atmosphere freezes to the winter pole (Tillman et al., 1993; Forget and Pollack, 1996). The SPRC

568 contains additional CO_2 mass (<1% the mass of the atmosphere; Thomas et al., 2016). The other

569 major reservoir of CO_2 ice is buried beneath the surface of the SPLD. The volume of this ice is

570 estimated to be as much as 16,500 km^3 (Putzig et al., 2018) and if released to the atmosphere

571   would more than double the surface pressure everywhere. This unit has sequences of

572   deposition (Bierson et al., 2016), suggestive of climate signals (Manning et al., 2019; Buhler et

573   al., in press) going back as far as many 10^5 years. Smaller CO_2 reservoirs exist that may play

574   important roles in climate: regolith, minerals, and potentially clathrates.

575   Water ice is the volatile in greatest quantity on the planet, outweighing CO_2 by many

576   orders of magnitude. Combined, the PLDs contain more than 2/3 of the known water budget of

577   Mars (Levy et al., 2014). Additionally, mid-latitude glaciers and ice sheets make up another

578   large fraction of the water budget (Levy et al., 2014; Karlsson et al 2015). Smaller known

579   reservoirs include water bound in the regolith to minerals or salts, in the atmosphere as clouds,

580   and pore filling ice. Water may also be injected into the atmosphere via volcanoes or comets.

581   Deep water reservoirs are predicted to exist, but they may not interact with the surface of the

582   planet in a measurable way (Grimm et al., 2017).

583   Finally, dust reservoirs are found across much of the planet. The PLD may contain

584   upwards of 5% dust for the north or 10% for the south based on dielectric (Plaut et al., 2007;

585   Grima et al., 2009) and gravity (Zuber et al., 2007) measurements. Other locations on the

586   planet, such as pedestal craters, contain stratified ice and dust as well (Kadish et al., 2008;

587   Nunes et al., 2011). Atmospheric dust is visible from ground-based imagery, and many locations

588   on Mars have a fine layer of surface dust.

589   Forcings, as discussed above, act on the volatile and dust reservoirs. However, there is

590   abundant evidence that some of these reservoirs are much older than their expected response

591   time to orbital variations (Levrard et al., 2007; Bramson et al., 2017 and references within). The

592   presence of the SPLD is the biggest enigma because, unlike the NPLD, the surface age is an

593 order of magnitude older than climate models would suggest (Herkenhoff and Plaut, 2000;

594 Levrard et al., 2007). Also, mid-latitude ice shows crater counts that suggest ages of 10^8 years in

595 some cases. These reservoirs have likely been sequestered from exchange with the atmosphere

596 due to a dust/debris cover and have contributed little to global cycles for long periods (Toon et

597 al., 1980; Bramson et al., 2017).

598

599 ### 1.B.3 Climate models and PLD formation

600 *Introduction and Methodology*

601 Models are critical tools for investigating the past climate of Mars, and global climate

602 models (GCMs) have been used to study aspects of the Amazonian (last ~2.8 Gyr of Martian

603 history) climate and the formation of the PLDs. Since the Amazonian period is characterized by

604 a solar luminosity similar to the current solar luminosity and an atmospheric mass comparable

605 to what it is today, we can study the climate by considering how changes to the orbital

606 parameters would affect the present-day Mars climate. Thus, the general methodology for

607 these studies is to execute a GCM that does a reasonable job of reproducing the current Mars

608 climate with modified orbit parameters (obliquity, eccentricity, argument of perihelion).

609 *Modeling the Current Climate*

610 The cycles of CO_2, dust, and water, including sublimation and deposition, dominate the

611 climate of Mars. The GCM community has invested significant effort over the past few decades

612 towards improving how GCMs handle and predict these cycles. This requires the

613 implementation of a wide range of physical processes that govern how dust, CO_2, and water

614   cycle into, through, and out of the atmosphere considering surface and orbital properties.

615   CO_2 is the most straightforward cycle to simulate. Surface energy balance methods are

616   used to compute CO_2 condensation and sublimation as CO_2 cycle into and out of the seasonal

617   CO_2 polar caps. Atmospheric condensation of CO_2 is usually handled with a simple scheme in

618   lieu of representing the more complex microphysical processes of cloud formation (Forget et

619   al., 1999; Haberle et al., 2008; Guo et al., 2009), and recent work has improved how CO_2 clouds

620   are simulated in GCMs (Listowski et al., 2013; Dequaire et al., 2014).

621   Significant effort has been invested in improving the handling of water cycle physics in

622   GCMs (Figure 5) based on modern observations. Even though there are other contributors, in

623   modeling, the NPRC and NPLD outliers are generally considered to be the primary source of

624   water to the present atmosphere (Navarro et al., 2014), but investigations may include a

625   regolith source (Böttger et al., 2005) that accesses ancient ice deposits. Sophisticated

626   microphysical schemes can explicitly include the physics of nucleation, growth, and size-

627   dependent sedimentation (Montmessin et al., 2002; 2004). The inclusion of cloud radiative

628   effects has proven quite challenging due to the many complex feedbacks involved, but

629   significant progress has been made in realistically representing the seasonal cycles of water

630   vapor and clouds (Navarro et al., 2014; Haberle et al., 2018).

631   The dust cycle remains the most challenging of the three climate cycles to simulate fully.

632   Investigations that include the physics of dust lifting based on resolved surface wind stress and

633   dust devils (and/or unresolved small-scale lifting) can capture general behaviors of the

634   observed dust cycle but are thus far unable to realistically simulate others (Newman et al.,

635   2002; Basu et al., 2004; Kahre et al., 2006). In particular, capturing the observed inter-annual

636   variability of global dust storms remains elusive. In lieu of using fully interactive methods,

637   studies that focus on other aspects of the martian climate generally use prescribed or semi-

638   prescribed dust methods based. In these studies, the horizontal and/or vertical distribution is

639   constrained by observations (Montabone et al., 2015). Caution is warranted when using the

640   dust observations for past climate studies because it is unlikely that the seasonal patterns of

641   atmospheric dust remain the same as orbit parameters change.

642   *Current Understanding of Amazonian Climate*

643   Modeling the Amazonian climate involves running GCMs that are generally capable of

644   capturing the main components of the current Mars climate for different orbit parameters.

645   Because GCMs are complex and require significant computational resources, it is not possible

646   to explicitly simulate changing orbit parameters. Instead, combinations of obliquity,

647   eccentricity, and season of perihelion are chosen to map out trends and branch points in the

648   behavior of the climate. When designing these simulations, the total inventories and available

649   surface reservoirs of CO_2, dust, and water must be considered. The effects of increasing or

650   decreasing the obliquity are generally more substantial than changing the eccentricity or season

651   of perihelion (Laskar et la., 2004).

652   Obliquity variations have important consequences for the CO_2 cycle. As obliquity

653   increases, the annual mean insolation at the poles increases. For obliquities greater than 54°,

654   the poles receive more annual insolation than the equator. This drives more extreme seasonal

655   variations in surface temperature and surface CO_2 ice. Overall, the global average surface

656   pressure decreases with increasing obliquity because more CO_2 cycles into and out of the polar

657   ice caps seasonally (Mischna et al. 2003; Haberle et al. 2003; Newman et al. 2005). At low
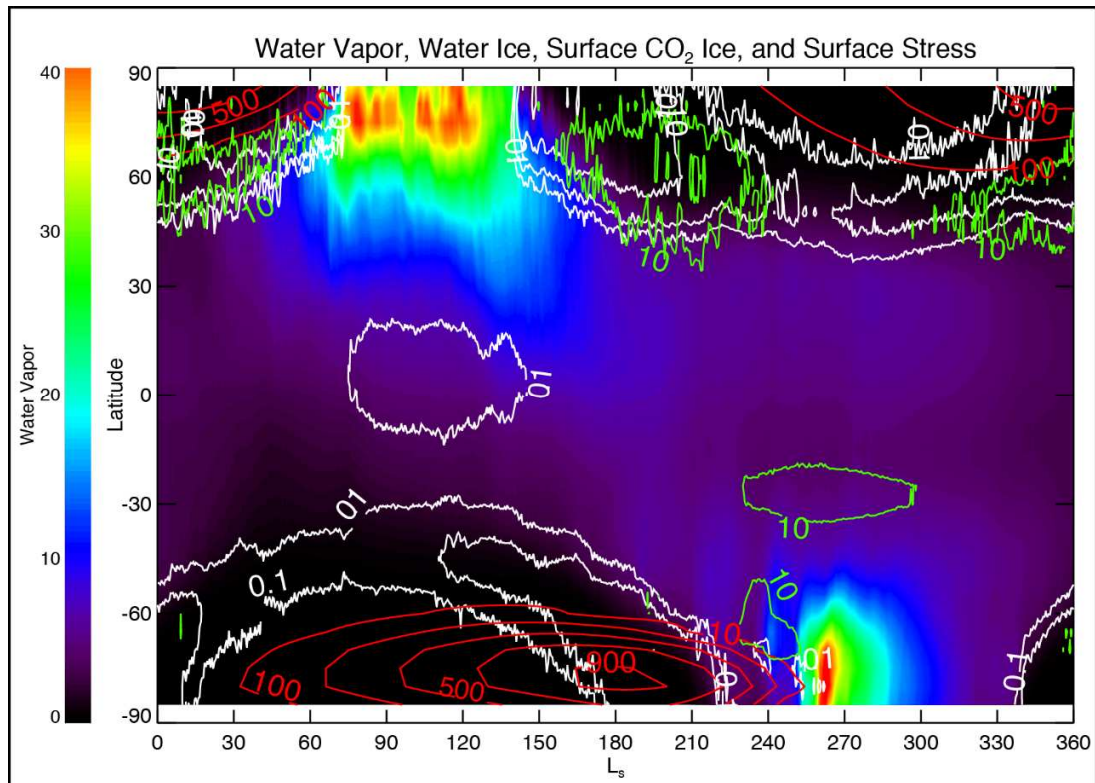
Figure 5: Current-day seasonal cycles by latitude and season of atmospheric water vapor (color fill), atmospheric water ice (white contours), surface carbon dioxide ice (red contours), and surface stress (green contours) as simulated by the NASA/Ames Legacy Mars GCM.

658 obliquities (< ~20°), permanent CO_2 ice caps form and the atmosphere collapses (Haberle et al.

659 2003; Newman et al. 2005; Manning et al., 2006; 2019; Buhler et al., in press). In a collapsed

660 state, the equilibrated atmospheric mass could be quite low (~30 Pa). Recent models have

661 begun considering what would happen if the ~2.6×10^{16} of CO_2 locked in the south pole (Phillips

662 et al., 2011) were available to circulate through the atmosphere.

663   At low obliquities (<30°) when the polar insolation is low, water ice is stable at the pole

664 and the atmosphere is relative dry (Mischna et al, 2003; Forget et al. 2006; Levrard et al. 2007).

665 The hemisphere where the polar water ice resides is likely controlled by the season of

666 perihelion, with the north favored when the perihelion occurs near southern summer solstice

667 and the south favored when perihelion occurs near northern summer solstice (Montmessin et

668 al., 2007). At moderate obliquity (30-40°), water ice becomes stable in the middle latitudes and

669 the atmosphere is considerably wetter (Madeleine et al. 2009). At high obliquity, water ice is

670 destabilized from the poles and becomes stable at low latitudes (Mischna and Richardson 2005

671 Forget et al. 2006; Levrard et al. 2007). The radiatively active ice clouds have significant effects,

672 particularly at moderate to high obliquity. Models predict that optically thick clouds form up

673 high, which allows them to significantly warm the surface, enhance the mean circulation, and

674 produce significant snowfall (Haberle et al. 2012; Madeleine et al 2014; Kahre et al., 2018).

675 From the subsurface, water ice may interact with the atmosphere, and varying orbital

676 parameters controlling insolation will drive transport between the poles and mid- or low-

677 latitudes. This is modulated by slope and thermal lags. Presently, mid-latitude deposits that

678 should not be stable likely exist because of a protective lag (Bramson et al., 2017).

679 As obliquity increases, the Hadley cell is enhanced due to an increased equator-to-pole

680 temperature gradient. The stronger return flow from the overturning circulation increases

681 surface stress and thus wind-stress dust lifting (Haberle et al., 2003). Once dust is lifted, positive

682 radiative/dynamic feedbacks further enhance the Hadley cell and dust lifting (Newman et al.,

683 2005). While this predicted behavior is robust, there are potential caveats that must be

684 considered. The first is the incorrect assumption that an infinite amount of surface dust is

685 available for lifting everywhere on the planet. The second caveat is that early dust cycle

686 simulations at high obliquity did not include water ice clouds. Clouds can scavenge dust and

687 provide additional radiative/dynamic feedbacks that need to be fully understood.

688 *Modeling the Polar Layer Deposits*

689   The PLDs contain a record of the martian climate over time, so realistically modeling this

690   record will require the use of models that are capable of creating an evolving climate state and

691   potential for internal deformation of ice. While there have been some attempts to use results

692   (or general behaviors) from GCMs to model the PLDs, this process has proven very challenging

693   due to the complexities of the processes involved.

694   In the most comprehensive effort, Levrard et al. (2007) predicted polar ice deposition

695   and removal rates over a range of obliquities taken from the computed obliquity history of

696   Laskar (2004) over the past 10 million years. They quantitatively tracked the evolution of polar

697   surface ice reservoirs and found that the north cap could begin accumulating about 4 million

698   years ago (Figure 4). The model predicted ~30 layers that could have been generated by the

699   changing obliquity during the past 4 million years. This number is inconsistent with thousands

700   of visible layers of the NPLD but similar in order to the number of radar reflectors observed.

701   This result implies that visible dusty layers form on a shorter time frame, perhaps related to

702   precession of the argument of perihelion, which should modulate layer formation. However,

703   that study did not use a model with an interactive dust cycle or radiatively active clouds, two

704   major factors required for any successful climate modeling of Mars, especially since the amount

705   of dust deposited in the polar regions could vary significantly with varying orbital configurations

706   (e.g., Newman et al., 2005). Fully coupled dust and water cycle simulations will further our

707   understanding of how the PLDs have formed due to orbit-driven variations in the martian

708   climate (e.g. recently presented work by Emmett et al. (2018)).

709   ## *1.C History of Mars Polar Investigations*

1.C.1 Orbiters

710

711   Spacecraft investigations of the polar regions of Mars began with the Mariner 7 flyby in

712   1969 when the infrared spectrometer observed CO_2 ice, related to seasonal processes (Herr

713   and Pimentel, 1969). Imagery of the polar regions began in 1971 with Mariner 9 and continued

714   with the comprehensive coverage by Viking orbiters (1976-80). In the modern era, imagery at

715   ever increasing spatial resolution has been obtained from the Mars Global Surveyor (MGS),

716   Odyssey, Mars Express, and Mars Reconnaissance Orbiter (MRO) orbiters using the High

717   Resolution Stereo Camera (HRSC), MOC, THEMIS, CTX, and HiRISE instruments. Infrared

718   observations to observe surface properties began with multi-channel instruments (Infrared

719   Thermal Mapper (IRTM) on Viking) and advanced to full spectroscopy and compositional

720   measurements with the MGS Thermal Emission Spectrometer (TES), Mars Odyssey's THEMIS,

721   and continues with Mars Express' Observatoire pour la Minéralogie, l'Eau, les Glaces et

722   l'Activité (OMEGA), and MRO's Compact Reconnaissance Imaging Spectrometer for Mars

723   (CRISM). Infrared spectroscopy began with the Infrared Interferometer Spectrometer (IRIS)

724   instrument on Mariner 9 and continued with MGS' TES, Mars Express' Planetary Fourier

725   Spectrometer (PFS), and MRO's Mars Climate Sounder (MCS) (e.g. Smith, 2008). Gamma ray

726   and neutron spectroscopy on Odyssey has been used to study ice (Feldman et al., 2002), and

727   laser altimetry from the Mars Orbiter Laser Altimeter (MOLA) has been used to estimate the

728   total thickness of the PLD and measure seasonal elevation change with deposition (Smith et al.,

729   2001). Radar measurements to probe the subsurface have been performed from both MARSIS

730   and SHARAD sounders (Picardi et al., 2004; Seu et al., 2007).

731   Polar studies have benefitted from several kinds of orbital observations. Optical and

732 infrared instruments tracked stratigraphy, geomorphology, seasonal geologic processes, inter-

733 annual variability, composition, albedo, and physical state of H_2O and CO_2 ice deposits.

734 Spectrometers track grain size and layer properties on the surface (Calvin et al., 2009; Brown et

735 al., 2016) along with the distribution of hydrated materials, altered glasses and basaltic

736 materials, and the origins of gypsum on the north polar dunes (Langevin, et al., 2005; Horgan et

737 al. 2009; Horgan and Bell, 2012; Massé et al., 2012). Instruments that measure atmospheric

738 properties tell us about thermal and humidity profiles, cloud formation, and snowfall (Hayne et

739 al., 2014). Temperature sensing instruments tell about the thermal inertia of ice-cemented

740 material or the PLD (Putzig et al. 2014). Finally, orbital radars have been instrumental in

741 determining the bulk dielectric properties of the PLD and 3-D stratigraphic relationships

742 inaccessible with cameras.

743 *1.C.2 Landers*

744   The polar regions of Mars have been a high-priority target for landed missions for

745 decades. Since their discovery in Mariner 9 images (Murray et al., 1972), the polar layered

746 deposits were suggested to contain a climate record, which could be accessed in at least a

747 limited number of exposures (Cutts, 1973; Howard et al., 1982). High-resolution images from

748 MOC revealed much more extensive layered deposits than had been previously recognized,

749 especially in the south polar region (Malin et al., 1998).

750   **Mars Polar Lander.** Landing site selection for NASA's Mars '98 mission was guided

751 towards the south polar deposits, where remote sensing data revealed a vast volume of ice just

752 beneath a layer of dust or regolith. This mission became Mars Polar Lander, which had primary

753 science objectives to dig into the subsurface to search for water, to measure the atmospheric

754 composition, and to survey the SPLD to better understand their formation mechanisms. Its

755 landing site was located in a region between 73 – 78°S and 170 – 230°W. In addition to the

756 main lander, the Mars Polar Lander spacecraft also contained two penetrator probes, called

757 Deep Space 2 (DS-2) designed to sample the atmosphere during descent, and the subsurface

758 soil and ice layers following impact. Unfortunately, a malfunction in the Mars Polar Lander's

759 descent stage caused the catastrophic loss of both the primary payload and DS-2 (Albee et al.,

760 2000).

761 **Phoenix.** Resurrected as the Phoenix mission, the 2001 Surveyor Lander was repurposed

762 to a high latitude location. Launched in 2007, Phoenix landed at a position of 68.22° N, 125.7°

763 W on May 25, 2008. Its primary purposes were to study the geologic history and habitability of

764 subsurface water by sampling material at this high-latitude landing site and collect data on how

765 the Martian climate is affected by polar dynamics.

766 Although its location was over 700 km from the NPLD, the Phoenix mission's landing site

767 was on top of a region with well-established ground ice, where remote sensing and model

768 calculations had shown ice likely to be present in the upper few centimeters (Fanale et al.,

769 1986; Mellon and Jakosky, 1993; Feldman et al., 1993; Aharonson and Schorghofer, 2006;

770 Putzig and Mellon, 2007; Mellon et al., 2008). Indeed, the landing thrusters revealed a patch of

771 ice under the lander, and the robotic arm and scoop excavated ice beneath a layer of loose, ice-

772 free soil ~5 cm thick (Mellon et al., 2009). Wet chemistry measurements of soils revealed salts,

773 including perchlorate (Hecht et al., 2009), which are freezing point depressants for water.

774 Significant exchange of water vapor between the surface and atmosphere was detected by the

775 lander's Thermal and Electrical conductivity Probe (TECP; Zent et al., 2010).

1.C.3 Previous Concept Studies

776

777   In the past four decades, numerous missions to the northern polar deposits have been

778   proposed as part of either concept studies or spacecraft proposals. Perhaps the earliest concept

779   was described shortly after the first Viking landing (Staehle, 1976; Staehle et al., 1977). None

780   passed beyond the proposal stage. A subset, from the last 15 years, is summarized here to

781   represent past polar community thinking on observational strategies. One can see that while

782   the technology and exploration platforms have varied, the core observational strategies desired

783   by the polar community have not.

784   *Decadal Survey concept studies*

785   In a mission concept study associated with the SS2012 Planetary Science Decadal

786   Survey, Calvin et al. (2010) identified how to use the following basic architectures for near-

787   future polar missions: Discovery-class orbiters, New Frontiers-class orbiter, Discovery-class

788   lander, New Frontiers-class lander, and New Frontiers-class rover.

789   Discovery and New Frontiers-class orbiters would focus on global climate and seasonal

790   processes, surface energy balance and composition, and atmospheric sounding. Discovery and

791   New Frontiers-class landers have been conceived and proposed to perform cm-scale

792   stratigraphic analysis and surface-atmosphere interactions on ~1 Mars year time scales.

793   Meteorologic packages would be included. Options range from landing at the base of a polar

794   scarp to subsurface access with drills or high-resolution radar remote sensing. New Frontiers-

795   class rovers have also been conceived that would carry a rock corer or drill to collect samples

796   for analysis through traversing across exposed layers. Analysis would have greater coverage

797 than a static lander. Smaller rovers that arrive as part of a larger platform have also been

798 studied. The strawman payload included an imager; navigation cameras; tunable diode laser

799 spectrometer (for distinguishing the various water isotopes); microscopic imager, Raman

800 spectrometer, and chemical sensors.

801   Drilling may be done in multiple ways. Three mission concepts used a thermal energy

802 source to melt water and descend into the melt hole. Analysis of the interior of the polar

803 deposits must be done on the walls of the hole as the drill descends using instrumentation fit

804 within the thermal drill itself, or upon the resulting meltwater pumped through the tether to an

805 instrumented surface platform. Concepts include Cryoscout (Zimmerman et al, 2002; Hecht and

806 Saunders 2003), CHRONOS (Hecht 2006), and Palmer Quest (Carsey et al, 2005a; 2005b), a

807 NASA Vision Study. Instruments for those landed studies included the following to go into the

808 bore hole: nephelometer for recording visible stratigraphy in full color; electrochemical sensors

809 for salt composition; laser hygrometer for H and O abundance; temperature sensors;

810 seismometer. On the surface, a stereoscopic imager; meteorologic package; laser

811 spectrometer; and electrochemical sensors

812   While none of the mission concepts outlined above made it past (or in some cases, to)

813 the proposal stage, common themes of exploration are clear: accessing the local subsurface

814 stratigraphy, placing it in the regional context of the broader polar deposits, assessing the

815 atmosphere above the surface, and relating it to the seasonal evolution of the polar surface.

816 *1.D Terrestrial Climate Studies Using Ice Cores*

817   Terrestrial glaciers and ice sheets provide accessible field sites that can support our

818 understanding of local processes that relate to those on Mars. Terrestrial ice represents a key

819 component of the Earth climate system and interact dynamically with climate through several

820 different processes. During glacial cycles, growth and retreat of glaciers in the northern

821 hemisphere enhances the effects of climate changes through the ice-albedo feedback

822 (Ruddiman, 2006). In the present warming climate, surface melting and mass loss is further

823 enhanced during summer due to the darkening effect of meltwater and dust at the surface of

824 retreating glaciers and ice sheets (Tedesco et al., 2016). Increased discharge from marine

825 terminating glaciers due to warm ocean temperatures may subsequently influence ocean

826 circulation with global effects (Vaughan et al., 2013). Three key themes related to terrestrial

827 glaciers and ice sheets stand out in modern terrestrial climates studies: understanding drivers

828 of the glacial cycles of the Pleistocene (past ~2.6 Myr), deriving the paleo-climatic history from

829 the ice core archives, and estimating the mass loss from glaciers and ice sheets and their

830 contribution to global sea level.

831 *The general flow pattern of ice sheets*

832   On Earth, ice sheets form when climate conditions allow snow to accumulate at the

833 surface over thousands of years, and they initiate and grow from mountainous areas that are

834 colder than lower elevations (Cuffey and Paterson, 2010; Hvidberg et al. 2013). In the large

835 terrestrial ice sheets, ice accumulates in the interior by snowfall, ice flows slowly towards the

836 margin as the ice sheets spread due to gravity, and ice is lost along the margins by surface

837 melting and run off or by discharge into the ocean from marine terminating glaciers. Although

838 ice sheets respond to climate changes, they may gradually reach a steady state where snow

839 accumulation is approximately balanced by discharge and runoff. In the high-elevation interior,

840 the ice sheets are more than 3 km thick. There, layers are compressed and deform as they

841   gradually sink into the ice sheet and flow. Climate proxies from ice cores drilled through these

842   layers need to consider the thinning and stretching of the layers due to flow.

843   *Transformation of snow to ice*

844   Freshly deposited snow in the interior of the Greenland or Antarctic ice sheets has a

845   density of 300-400 km m^{-3}. Density variations in the top tens of meters of the snowpack (firn)

846   reveal an annual stratigraphy due to temperature and impurity content as well as individual

847   events, e.g. wind crusts formed by packing action of wind. Within the top 60-120 m, the firn

848   gradually transforms vis sintering into glacier ice with a density of 830 km m^{-3} (Sowers, 1992;

849   Gow, 1969). Flow and compaction of air bubbles below the firn-ice transition increase the

850   density further to 920 km m^{-3}. Deeper ice does not densify further. The depth of the firn-ice

851   transition depends mainly on the mean annual temperature and rate of snowfall and can vary

852   from 70 to 100+ m. Glacier ice contains air bubbles with samples of the atmosphere from the

853   time of the bubble close off and are used to document variations in past atmospheric

Figure 6: Ice core from 1 km depth of the The East Greenland Ice-core Project (EastGRIP) core in. For most cores in Greenland layers are not visible to the eye, and other methods must be employed to characterize them. Photo by C. Hvidberg

854   composition (Cuffey and Paterson, 2010).

855   *Composition, stratigraphy and timescales*

856 Terrestrial ice sheets generally consist of nearly pure water ice with a small impurity

857 content (Figure 6). Impurities originate from aerosols or particles deposited with the snow

858 (Figure 7, top). Impurity records have an annual variation related to the atmospheric circulation

859 and transport or are related to specific events, e.g. volcanic eruptions or forest fires. The

860 stratigraphy in ice cores is observed by the electrical conductivity measurement (ECM) and

861 dielectrical profiling (DEP), by continuous high-resolution profiles of concentrations of chemical

862 impurities using the continuous flow apparatus (CFA) method, or by concentration of dust

863 particles (e.g. Svensson et al., 2008; Cuffey and Paterson, 2010). ECM is a measure of the acidity

864   of the ice and used to identify volcanic reference horizons due to their high concentration of

865   sulfuric acid, and climate transitions due to the shifts in impurity concentrations and thereby

866   changes in conductivity. CFA provides multiple continuous records of impurities and thereby

867   allows identification of annual layers. In Greenland, the annual accumulation rate is sufficiently

868   high to preserve an annual signal, and it is possible to detect the seasonal cycle in several

869   impurity concentration records, e.g. insoluble dust, Ca^{2+}, NO_3, ECM (Svensson et al. 2008).

870   Insoluble dust particles from continents are carried by winds through the troposphere and

871   deposited over the ice sheets. The particles typically have a size of order 0.1-2 µm and a bulk

872   dust concentration of 50-200 µg per kg of ice in the interior of Antarctica and Greenland,

873   respectively (Lambert et al., 2008; Steffensen et al., 2008). During glacial periods, the

874   concentration of continental dust increases by a factor of 10-100 (Greenland) and a factor of

875   20-50 (Antarctica). In Greenland, the dust concentration in glacial ice is high enough to

876   influence the crystal size, and layers of high dust concentration are associated with small

877   crystals. Crystal size is generally in the order of 0.1-1 cm^2 and increases with depth but drops at

878   the Holocene-Pleistocene transition with a factor of 2. Although the dust is not visible by itself

879   in the glacial ice, dust-rich layers can be identified in the visible stratigraphy of ice cores as

Figure 7: Examples of visible layering in the North Greenland Eemian Ice Drilling (NEEM) ice core. Top: This layer is one of the only major, visible ash layers in Greenland; most are much thinner. Bottom: Layers of rocks and grains in the bottom tens of cm of the 2537.36 m deep NEEM ice core. Large grains are not found above the lowermost section. Photos by C. Hvidberg
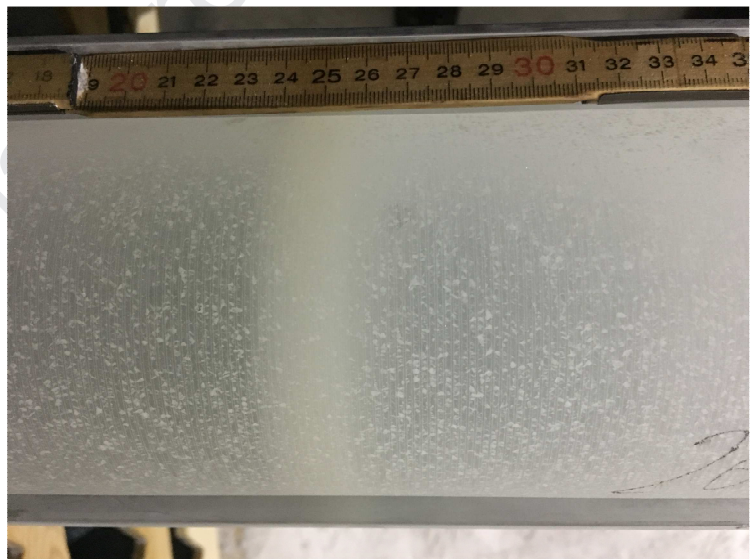
880   cloudy bands. The visible stratigraphy in Greenlandic ice cores has revealed annual layers in the

881   glacial ice down to a resolution of 1 cm (Svensson et al., 2005).

882   In Greenland, ice cores have been dated accurately by layer counting back to 60 kyr ago

883   using a combination of visible stratigraphy, concentration of dust and chemical impurities

884   (Svensson et al., 2008). In the interior of East Antarctica, the annual accumulation is only few

885   centimeters and annual layers cannot be identified. Ice cores in East Antarctica are dated from

886   a combination of reference horizons with dates transferred from Greenlandic ice cores or other

887   paleoclimatic records and ice flow modeling, taking into account thinning of layers due to flow

888   and using consistent relations between climate and snow accumulation rate (Veres et al.,

889   2013).

890   *Radar stratigraphy*

891   As on Mars, radar sounding is used to map the stratigraphy of terrestrial ice sheets. The

892   stratigraphy in the top tens of meters is mapped with higher-frequency snow radar systems,

893   employed from the air or the surface with ground penetrating radar (GPR) systems. The snow

894   structure of the dry snow zone in Greenland has for example been mapped with an airborne

895   Ku-band synthetic aperture radar (SAR) system and linked to in-situ observations from shallow

896   ice cores and pit studies. The observations reveal the annual layer structure in the top 15-20

897   meters related to density variations in the firn, which forms due to seasonal variations in

898   temperature, snowfall and impurity concentrations.

899   The internal radar layers show the past surfaces of the ice sheet as they sink down and

900   are subject to flow, including thinning and stretching, local variations of basal melting, and

901   large-scale evolution of the ice sheet and its flow pattern. Repeated surveys over several years

902 show how layers sink into the ice sheet and new layers form at the surface and allow detailed

903 mapping of spatial and temporal variations of the annual snow accumulation (e.g. Simonsen et

904 al. 2013). Medley et al, (2014) has performed an Antarctic counterpart to the Greenland

905 surveys, and Koenig et al., (2016) have performed a more recent and more extensive survey

906 that improves temporal and spatial resolution.

907 In general, the radar stratigraphy of ice sheets arises from transitions in the bulk

908 electrical conductivity of the media due to density variations, volcanic reference horizons, ice

909 crystal structure, or climatic transitions associated with changes in impurity concentration of

910 the ice. Deep internal radar layers have been linked to ice cores and dated using ice core

911 timescales in Greenland and Antarctica (e.g. MacGregor et al 2015; Winter et al., 2017). In

912 Greenland, they are associated with abrupt climate transitions during the last glacial, known as

913 Dansgaard-Oeschger cycles, or with glacial-interglacial transitions. In both Greenland and

914 Antarctica, echo-free zones occur; however those have now been partially attributed to lack of

915 signal power (Winter et al., 2017), and new radar systems are capable of resolving deep layers

916 there too. In Greenland, ice that deposited during the last glacial maximum, between ~15 and

917 30 kyr, contain no distinct radar-echo layers, possibly due to a generally high level of

918 continental dust ($CaCO_3$ and Ca^{2+} ions), which neutralizes any volcanic acidity peaks during that

919 period. The oldest ice in both Greenland and Antarctica are echo free or have a few blurred

920 layers, and here it has been suggested that flow effects in these deep and old layers could have

921 smeared out the transitions, e.g. by thinning layers or shearing and folding layers of different

922 rheology (NEEM members, 2013).

923 *The climate archive in ice cores*

924   Paleo-climatic records from terrestrial ice cores have revolutionized the understanding

925   of the Earth climate history and, together with ocean sediment cores, provided knowledge of

926   glacial cycles and beyond. The key contributions of ice cores to the paleoclimatic community

927   are their accurate and independent timescales as well as the unique information of past

928   temperatures from oxygen isotopes (e.g. $\delta^{18}O$ and δD) and past atmospheric composition from

929   air trapped within the ice (e.g. CO_2, CH_4) (Cuffey and Paterson, 2010). The ability to detect

930   annual variations in many different parameters, such as oxygen isotopes, insoluble dust, and

931   chemical impurities - and thereby identify and count each year - has contributed to

932   understanding the timing and phases of climate changes in the past. Terrestrial ice cores

933   contain an undisturbed stratigraphic record of ~100 kyr (Greenland) and ~1 Myr (Antarctica)

934   (Cuffey and Paterson, 2010). Older layers are disturbed by flow or removed by basal melt. The

935   climate archive of terrestrial ice cores is continuously expanded with new climate proxies and

936   new techniques that make it possible to detect more parameters and reduce sample size. One

937   example is CFA. Ice is continuously melted along the ice core and analyzed in a semi-automatic

938   wet-chemistry lab to provide records of isotopes, ions, cations, insoluble dust particles,

939   conductivity, black carbon, etc., that contain information about atmospheric and oceanic

940   circulation patterns, sea ice conditions, forest fires, far-field humidity, etc. The interpretation of

941   these proxy records is done in combination with climate modeling and paleo-climatic records

942   from other archives.

943   *Selection of the drill site and recommendations for Mars*

944   Ice cores from the interior Greenland and Antarctica are widely used to infer the climate

945   history of Earth because the timescale is reliable, and the records have been interpreted to

946   provide the hemispheric or global climate history (e.g. EPICA members, 2004; NEEM members,

947   2013). The ice core records contain continuously deposited layers and allow age determination

948   from measurements of constituents known to vary on annual timescales combined with

949   reference horizons known from other stratigraphic records. Comparisons between ice cores

950   spaced over tens of meters show significant local variations in snow accumulation rate due to

951   surface roughness and wind effects, where snow is redistributed at the surface or removed due

952   to wind scouring, but decade-averaged records are similar. Radar stratigraphy from the top

953   meters of the firn to the deep (2-3 km) layers are continuous and smoothly varying and show

954   similarly that the stratigraphy of the large ice sheets represents large-scale climate variations in

955   the past, not local snow accumulation patterns (MacGregor et al. 2015).

956   Prior to an ice core drilling program, data are collected from the area and used for the

957   drill site selection and planning of the campaign (e.g. Dahl-Jensen et al., 2002). Surface

958   campaigns and radar surveys provide information on annual snow accumulation rate, ice

959   thickness, ice flow velocity, surface conditions and local weather, as well as internal layer

960   structure. In general, sites are preferred with the following qualities: smooth bedrock, unfolded

961   internal layers, no signs of basal melting or complicated flow over complex underlying

962   topography (e.g. mountains), only little horizontal movement, with cold surface conditions, and

963   no melting at the surface or at the base. The optimal site has undisturbed layers and no

964   complicating upstream conditions.

965 ## 2. Major Questions to Address and Key Measurements

966 ### 2.A Major Science Questions and Objectives

967   Based on existing knowledge and knowledge gaps that need to be bridged, the KISS

968   workshop members listed numerous questions yet to be answered. Many shared a theme, and

969   taken together four overarching questions about the climate record stored in the PLD :

970

971   *1. What are present and past fluxes of volatiles, dust, and other materials into and out of*

972   *the polar regions?*

973   *2. How do orbital forcing and exchange with other reservoirs affect those fluxes?*

974   *3. What chemical and physical processes form and modify layers?*

975   *4. What is the timespan, completeness, and temporal resolution of the climate history*

976   *recorded in the PLD?*

977   We refer to these questions as, "**Fluxes**," "**Forcings**," "**Layer Processes**," and "**Record**," and in

978   this section we discuss the value of answering each.

979   ### *2.A.1 Fluxes*

980   ### *2.A.1.a Observations*

981   Measuring the modern-day fluxes of volatiles, dust, and other materials from lower

982   latitudes to the polar regions and then onto the polar caps are key steps to interpreting the

983   climate record in the PLDs. Obtaining these measurements would provide the opportunity to

984   link observable modern climatic processes to material arrival at the PLD surface, leading to

985   individual layer formation (Section 2.A.3) and to connect to the polar geologic record (Section

986   2.A.4). We expect that variation in the isotopic and chemical composition and total mass of

987   material exchanging between the atmosphere and polar deposits will yield observable signals in

988   the PLD. Therefore, we focus our attention on measuring these quantities and on quantifying

989   the atmospheric processes that govern these fluxes. To do this, we must measure fluxes at

990   global and regional scales and the exchange between the surface and atmosphere. Four

991   categories of material exchange annually between the atmosphere and the polar deposits. In

992   order of decreasing quantity by volume or mass they are CO_2, H_2O, refractory materials (e.g.

993   dust, salts, volcanic debris, hydrocarbons), and trace volatile species. One big uncertainty is the

994   source reservoirs of these materials, which may have formed in different epochs and contain

995   variable inputs to the current climate, so observations that track the locations of these

996   materials spatially are critical inputs to our modern climate understanding.

997   The largest component of the gross annual flux is CO_2 (Leighton and Murray, 1996)

998   which in condensed form reaches several hundred kg m^{-2} over the PLD. However, orbital

999   observations show that annually, there is no net flux of CO_2 onto the north polar cap and the

1000   mass balance of the SPRC cannot be determined better than ±1 kg m^{-2} per martian year

1001   (Thomas et al., 2016). Additional measurements of surface pressure from landers cannot detect

1002   a secular change in pressure that would imply net mass change at the SPRC (e.g. Haberle et al.,

1003   2010). Nevertheless, measuring the relative proportion of winter CO_2 laid down through direct

1004   deposition vs. snowfall is important because these different modes lead to vastly different

1005   thermal, radiative, and structural properties (e.g. Colaprete et al., 2005). This will affect the

1006   incorporation of co-deposited material into the polar caps. Additionally, measuring seasonal

1007   isotopic variation (e.g. Villanueva et al., 2015) during deposition and sublimation of CO_2 will aid

1008   in the interpretation of the isotopic abundances of trapped gas within the PLD.

1009   The flux of H_2O relative to that of refractory materials under modern climatic conditions

1010 is a key measurement for deciphering what goes into layer formation and for determining the

1011 climatic signal of variable dust fraction stored in the PLD. Measurements from orbit can track

1012 dust movement towards the polar regions, and surface measurements can determine how

1013 much of that falls to the surface either directly or is scavenged to make snow. In addition,

1014 knowledge of the chemical and isotopic composition of this material will yield important

1015 information, such as the reservoir provenance for dust or ice (Vos et al., 2019). Seasonal

1016 isotopic variability in the H_2O flux, including D/H, would come from a combination of mass-

1017 dependent fractionation or changing source reservoirs, and solar activity may influence D/H

1018 ratios on longer time scales (Fisher 2007). This may be used to interpret H_2O isotopic variation

1019 recorded in the PLD, and the current state is critically unconstrained. Importantly, this isotopic

1020 variation may be annual and may provide the smallest resolvable cyclic signal in the PLD.

1021 Finally, the flux of trace volatiles incorporated into the polar cap compared to the ambient

1022 trace volatile composition will support deciphering trapped atmospheric gas bubbles in the PLD.

1023 Several measurements are necessary in order to understand the fluxes of material at all scales:

1024   • Wind speed profile near the surface boundary layer. Near-surface wind speed is

1025 determined by nonlinear processes that are impossible to model *a priori*. When observed

1026 concurrently with the number density of atmospheric refractory material and H_2O, this is a

1027 basic input for calculating regional flux.

1028   • Horizontal and vertical wind speeds globally and over several Mars years. This will be

1029 used to validate GCMs and track movement of dust and other tracers. Tellingly, wind speeds

1030 have never been systematically measured globally that include the full boundary layer.

1031   • 4-dimensional (altitude, latitude, longitude, and time) number density map of

1032   atmospheric dust and H_2O. The ideal minimum resolution for these measurements is a 10-point

1033   vertical grid within the first half-scale height (scale height is ~11 km) and half-scale height

1034   resolution up to 80 km, at a 4x diurnal cadence, resolved across 12 longitudinal bands, all

1035   observed over one full martian year. Isotopic measurements of H_2O (e.g. D/H, $\delta^{18}O$, $\delta^{17}O$) are

1036   also important for tracking its provenance. Combined with wind speed, the number density of

1037   material is a basic input for calculating regional flux.

1038   • *In situ* surface mass flux of H_2O, refractory material, and CO_2. It is most critical to

1039   obtain this measurement at one well-selected location; however, additional measurement

1040   locations would allow the determination of regional variability. Characterizing the chemical and

1041   isotopic makeup of the surface material is also desirable for determining the provenance of the

1042   fluxing material and connecting *in situ* measurements to global measurements.

1043   • Obtaining surface and orbital measurements concurrently is important for accurately

1044   determining fluxes and connecting local deposition to global climatic processes.

1045   *2.A.1.b Modeling*

1046   Atmospheric models will be used in conjunction with observations to quantify the fluxes

1047   of non-volatile and volatile material into and out of the polar caps on Mars. Two steps are

1048   necessary. The first is that models require observations for validation purposes. Second, models

1049   will be invaluable tools for interpreting and expanding the observations beyond measurements.

1050   *Model Validation:*

1051   Before models can be reliably used to extrapolate information gained from one or a few

1052   locations to the entire polar cap region, they must be validated with observations. Winds and

1053 turbulence in the lower atmosphere control the exchange of volatiles and dust between the

1054 surface and atmosphere and transport those materials. However, to date, these processes have

1055 not been comprehensively or reliably measured on Mars. Near surface wind measurements

1056 have been acquired by the Viking Landers, Pathfinder, Phoenix, and Curiosity but these data

1057 sets suffer from calibration issues and other problems. The Interior Exploration using Seismic

1058 Investigations, Geodesy and Heat Transport (InSight), recently landed on Mars, is providing an

1059 improved look at pressure and wind speeds at one low latitude location.

1060 Winds above ~1.5-2.0 m have never been directly measured on Mars apart from a few

1061 entry, descent and landing profiles. Instead, our understanding of the winds throughout the

1062 bulk of the atmosphere have come from deriving thermally balanced winds from observed

1063 thermal structures and atmospheric models (Navarro et al, 2017). Models require wind

1064 observations for validation, particularly near the surface where the thermal wind balance

1065 approximation cannot be used. Well-calibrated measurements of near-surfaces winds or wind

1066 profiles from the surface in conjunction with global wind speed measurements from orbit will

1067 provide this critical model validation. In addition to wind observations, direct observations of

1068 the rates of exchange of dust and volatiles between the surface and the atmosphere in the

1069 polar regions will provide critical constraints for models. Current state-of-the-art global- and

1070 regional-scale models include the physics of dust lifting and removal, and water and CO_2 ice

1071 sublimation, deposition, and snowfall. In the absence of measurements of the fluxes from each

1072 process, however, it is difficult to know if the models are handling these processes correctly.

1073 Once models are fully vetted for present day processes, their value in representing past

1074 behavior grows. At that point, we will be in a much better position to understand how orbital

1075   parameters and other forcings (Section 2.A.2) affect the recorded climate signal (Section 2.A.4).

1076   *Interpreting/Expanding Observations:*

1077   We expect significant spatial and temporal variations in the surface fluxes of dust and

1078   water over PLDs due to regional and local-scale circulations and spatial variations in surface

1079   properties. It would be optimal to have a large network of highly capable meteorological

1080   stations placed strategically around the polar regions. Barring that, models will be critical tools

1081   for extrapolating information from a small number of stations to a comprehensive

1082   understanding of what is occurring over the entire region. Additionally, unless there are

1083   observations from orbit of the global transport of dust and volatiles concurrent with *in situ*

1084   measurements, global-scale climate models will likely be needed to provide this global

1085   perspective.

1086   ### 2.A.2 Forcings

1087   *Observables in the PLD and Climate Signal*

1088   In order to determine the forcings that create the volatile deposits, *in situ*

1089   measurements of the layers of the PLD must be made. The materials to be measured are

1090   discussed in section 2.A.4. By measuring observables in a stratigraphic column, we can track the

1091   variability at each layer, going backwards in time. If those variables are cyclical in nature, then

1092   perhaps we can tie those signals to the periodic nature of seasonal or annual cycles, dust

1093   storms, solar cycles, and longer period cycles driven by orbital changes. Correlating time-series

1094   or possible forcings to stratigraphic measurements will test our hypotheses about the orbital

1095   evolution of Mars.

1096   Part of understanding forcings is to learn how off-polar volatile reservoirs respond to

1097   changes in orbital parameters. In order to do this, the first step is to characterize and inventory

1098   all off-polar reservoirs. Secondly, many are meta-stable in the current climate, so discovering

1099   the processes that stabilize these reservoirs and how that responds to changing insolation is

1100   critical.

2.A.3 Layer-Formation Processes

1102   Modern processes related to layer formation are not well known, and yet the materials

1103   from the present surface will one day become incorporated into the PLD. Reading the variability

1104   in layer composition through time requires an understanding of what goes into making a layer

1105   today. Importantly, layer formation doesn't end upon burial. Communication with the

1106   atmosphere occurs down to an unknown depth; cosmic radiation interacts with materials; and

1107   chemical or physical forces can recrystalize the ice and exclude or incorporate impurities. Thus,

1108   determining all of the processes that affect layers is a critical knowledge gap, and

1109   measurements on the surface will determine what products form on the surface and remain in

1110   the ice or decay.

1111   To measure modern processes, we need access to the surface and the upper 50 cm

1112   away from an outcrop. 50 cm is significant because the processes described above have likely

1113   fully ceased by this depth, so it will be possible to extract the necessary information without

1114   worrying about missing processes. Additionally, based on estimated accumulation rates

1115   (Becerra et al., 2017 and references within), 50 cm is expected to represent the last 1000 years

1116   of Mars history, a period in which the climate should have been nearly identical to present day.

1117   Thus, it will be possible to measure layer formation without complications from variable inputs.

1118   Composition was identified as the top priority because it closely links to the climate

1119   record (Section 2.A.4) and is informative about fluxes of materials to the poles (Section 2.A.1)

1120   by identifying potential sources of materials that make up the layers. The relative abundances

1121   of the highest concentration constituents (water ice, dust, and salts) will be key for

1122   investigations on these topics. Identifying trace quantities of other materials (e.g. organics,

1123   isotopes, clathrate) and identifying composition at multiple spots (if landed) or better vertical

1124   resolution than currently available (from orbit) are also important. These observations will

1125   require an instrument capable of identifying and measuring different constituents to high

1126   precision. Next, an improved understanding of layer formation processes in the recent past (top

1127   50 cm) will then allow us to compare to deeper and older layers exposed at trough outcrops.

1128   Ice microstructure is important for determining the physical properties of the NPLD.

1129   Phase partitioning of salt and impurities from ice grains is likely to be different on Mars because

1130   of the materials involved. Density and grain size distribution of dust can tell us of source

1131   material and perhaps past atmospheric states. These properties affect layers and the strength

1132   of NPLD materials. Measuring the distribution of components within layers will provide

1133   important information about how the layers of the NPLD respond to forces.

1134   The study of current surface and meteorologic processes will illuminate how material

1135   becomes available for layer formation or removed from the system. Meteorologic

1136   measurements at the surface will be compared to global and regional measurements (Section

1137   2.A.1) in order to determine the availability of material through the present epoch. Then, in

1138   combination with GCMs, we can estimate the availability of material and forcings that formed

1139   past layers (Section 2.A.2). Similar to layer formation, measuring meteorological processes

1140 requires *in situ* observation over an entire martian year. Measurements within a single site and

1141 across many sites should be simultaneous to gain the most value. They should include the

1142 ablation and/or accumulation of dust and ice (H_2O and CO_2), saltation and surface transport of

1143 materials, wind speed, insolation, humidity, temperature, pressure, and albedo.

1144 ### *2.A.4 Record*

1145 In order to address the science question "What is the timespan, completeness, and

1146 temporal resolution recorded in the PLD?" we identified three time (and size) scales that need

1147 to be addressed. The largest physical scale is characterizing the bulk stratigraphy of the PLDs.

1148 The geologic relationships between the four packets of radar layers and the basal unit would be

1149 better constrained by radiometric age dates and/or exposure age dates of lithics contained in

1150 the PLD, Cavi, and Rupus units. These constraints would characterize the timespan and the

1151 largest temporal resolution contained within the PLDs.

1152 Trough exposures, on the order of ~100s of meters, is the next scale. Identifying

1153 unconformities is a priority for understanding the completeness of the record contained in the

1154 PLDs because hiatuses in accumulation or periods of ablation could remove or fail to preserve

1155 some of the record, and measurements of stratigraphy better than current assets provide are

1156 necessary to identify all of the periods when materials were not accumulating. At this scale, the

1157 NPLD offers a more likely solution. Observations at the NPLD, whether in optical or radar

1158 wavelengths, are more easily integrated in part because of high internal scattering that hinders

1159 interpretation at the SPLD (Whitten and Campbell, 2018). Elucidating the evolution of the PLDs

1160 requires understanding changes in deposition rates by observing bedding geometry, thickness

1161 and unconformities to understand how deposition has changed through time.

1162   Finally, it is important to study the current surface and upper meter of the PLDs at the

1163   sub-meter scale as described in Section 2.A.3. Understanding the fine-scale structures in the

1164   near-surface of the PLD is key to interpreting the deeper record because the finest layers made

1165   in the current epoch are likely to be created by the same processes that formed layers in the

1166   past.

1167   We identified several key measurements that would address the above areas of needed

1168   knowledge and ranked them according to priority.

1169   • Highest priority is to obtain an absolute age somewhere in the stratigraphy through

1170   cosmogenic/radiogenic nuclei abundance for a well-chosen location within the PLD. There are a

1171   variety of radiosotopic systems and methods available for age determination on the Earth (e.g.

1172 ^{14}C, ^{10}Be, K-Ar, ^{36}Cl, ^{3}He, ^{36}Ar, Ne). These methods may require finding and dating a lithic layer

1173   (e.g., impact or volcanic sediments, Figure 8) or finding a clear climate signal in isotopologues of

1174   atmospheric gasses or water vapor. We discuss age dating in Section 2.A.5.

1175   • Intermediate priority was given to the search for patterns in vertical distribution of

1176   impurity fraction of isotopes (D/H, oxygen, and carbon being most important), and chemistry

1177   (iron, silica, aluminum, sulfur and chlorine) to match orbital history on the 100s of m depth

1178   scale. Annual layers are estimated to be on the microns to mm scale and obtaining that vertical

1179   resolution would assist in determining the smallest time resolution recorded in the PLD layers.

1180   • Intermediate priority was also given to determining the completeness of the PLD by

1181   generating a catalogue of existing unconformities throughout the stack. Such unconformities,

1182   when mapped by radar and compared to climate models, have been useful in constraining ages

1183   (Putzig et al., 2009; Smith et al., 2016). Finer resolution mapping by improved resolution

1184 remote sensing would provide invaluable inputs to determining the PLD record.

1185 • Low priority was given to the measurement of the crater size-frequency distribution

1186 (SFD) with depth to determine relative ages from vertical crater distribution. The vertical crater

1187 SFD would require higher resolution, and therefore higher power, radar than SHARAD to detect

1188 craters below the 7 km detected in initial surveys (Putzig et al., 2018). While absolute age

1189 results would still be crater production-function dependent, quantifying the crater size-

1190 frequency distribution with depth places relative age constraints on the PLDs.

1191 ### 2.A.5 Age Dating the NPLD

1192 In order to tie physical layers seen in radar to obliquity and climate cycles on Mars, age

1193 constraints must be placed on layered

1194 materials. In particular, obtaining at

1195 least one absolute age is critical for

1196 placing all layers above and below in

1197 some context of the greater system.

1198 Formation and exposure ages are

1199 obtained on Earth (and Mars, e.g.

1200 Farley et al. 2014) using radiogenic

1201 and cosmogenic nuclides. Briefly,

Figure 8 Production of ^{34}Ar, ^{3}He, and ^{22}Ne with depth on Mars, modified from Farley et al., 2014

1202 cosmogenic nuclides are produced through any interaction of primary or secondary cosmic

1203 radiation with matter containing a range of target elements. Stable nuclides build up over time

1204 as a surface is exposed to cosmic rays. Radiogenic nuclides are daughter products of radioactive

1205 decay and build up on surfaces to the point of saturation, which refers to the state when the
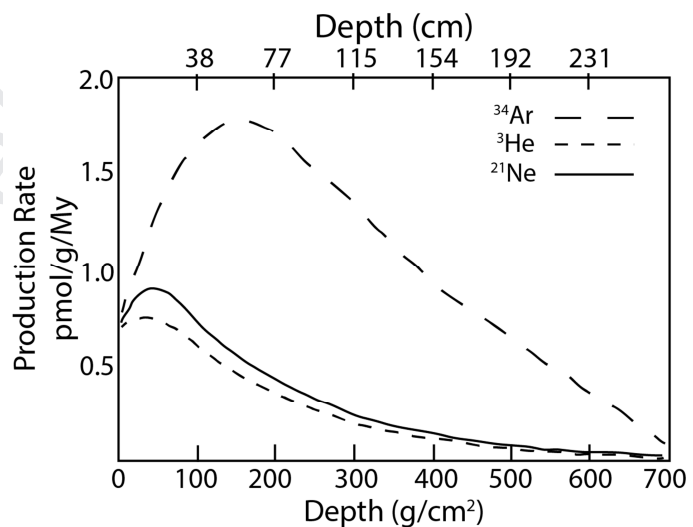
1206   rate of production equals the rate of decay. When a surface is buried, the accumulation of

1207   cosmogenic and radiogenic nuclides slows down or stops entirely, depending on the nuclide

1208   (Figure 8). The cosmogenic stable nuclides remain, while the radiogenic nuclides decay into

1209   stable daughters. The production rate of cosmogenic nuclides on Mars is estimated from

1210   meteorites, and can be used, along with a measurement of the abundance of these nuclides in

1211   a layer, to determine how long the material in the layer sat on the surface. The burial age of the

1212   material can then be determined by the difference between the abundance of cosmogenic

1213   nuclides in currently exposed surface materials vs. buried materials.

1214   Cosmogenic and radiogenic dating techniques are widely used in studies of ice cores and

1215   glacial geomorphology on Earth, with ^{10}Be (half-life ~1.5 My), ^{26}Al (half-life ~700 ky), and ^{14}C

1216   (half-life ~5700 y) as the most frequently used dating systems (e.g., Fabel et al, 2002; Bond et

1217   al., 1993; Rinterknecht et al., 2006). For the most part, age dating is done on lithic material and

1218   volcanic ash entrained in ice, although in some cases trapped gases are analyzed (e.g., Buizert

1219   et al., 2014) with state-of-the-art noble gas mass spectrometers. However, the very large

1220   masses of ice (100s of kg) required for this technique to obtain sufficient material to analyze

1221   with high sensitivity, complicate applying this technique on Mars.

1222   Cosmogenic and radiometric dating on Mars presents significant analytical challenges

1223   due to the amount of material necessary and the requirement (in most techniques) to have a

1224   robust mass estimate of material. A successful application of radiometric (K-Ar) and exposure

1225   age dating on Mars using cosmogenic ^{21}Ne, ^{3}He, and ^{38}Ar has been performed on Gale Crater

1226   mudstone (Farley et al., 2014) using the SAM instrument on Mars Science Laboratory (MSL).

1227   However, this work was done on martian regolith, where rocks with high concentrations of

1228   target elements (e.g., Mg, Ca, Al) ensure the presence of measurable abundances of

1229   cosmogenic nuclides.

1230   Because the NPLD are mostly ice, achieving meaningful ages hinges on finding datable

1231   lithic material in the form of dust, volcanic ash, or impact ejecta that are accessible to robotic

1232   explorers. The estimated ~5×10^6 years age of the NPLD also drives the requirement for

1233   extremely high precision measurements in order to achieve useful ages, with minimum age

1234   resolution on the order of 10^4-10^5 years. For comparison, the exposure age measurements

1235   achieved by SAM were 78 ± 30 million years (Farley et al., 2014), suggesting the need to

1236   improve precision by at least 2 orders of magnitude for meaningful measurements of the NPLD.

1237   A mission to age-date the NPLD would require a highly selective and sensitive mass

1238   spectrometer similar in size, mass, and power to the SAM instrument on MSL. A range of mass

1239   spectrometry techniques to optimize exposure age dating using cosmogenic nuclides are

1240   currently in development to address the need for absolute age dating in planetary science.

1241   These techniques represent improvements in sensitivity, resolution, and selectivity over mass

1242   spectrometers currently used in planetary exploration. One promising technique in

1243   development is resonance ionization mass spectrometry (RIMS), which uses a laser or ion beam

1244   to remove neutral atoms from solids, then uses tuned lasers to excite electrons of a specific

1245   element and ionize it for measurement by mass spectrometer. This technique has been

1246   developed for the Rb-Sr geochronometer (Anderson et al. 2012; 2015) but could be applied to

1247   cosmogenic nuclides as well. In addition, recent developments using isotope dilution remove

1248   the need for obtaining a mass estimate, which should significantly reduce the magnitude of

1249   error (Farley et al., 2013). A precursor mission to confirm the presence and abundance of

1250 datable lithic material in the top 50 cm of the NPLD could inform efforts to refine these and

1251 other age dating techniques (e.g., Cohen et al., 2014) for later applications that access multiple

1252 layers.

1253 ## 2.B Key Properties and Measurements

1254 This section describes measurements to address our science priorities that can be made

1255 with existing and near future technology and the precision requirements associated with them.

1256 ### 2.B.1 Requirements for Measurements of Fluxes in the Polar Regions

1257 Flux measurements will have to be performed at the surface in order to quantify fluxes

1258 that are directly relevant to deposition and ablation processes, and they should be

1259 supplemented by orbital measurements (as discussed above) in order to connect the surface

1260 measurements with the processes that govern the current global climate.

1261 *Measurement requirements*

1262 For fluxes, high frequency sampling of wind speed and direction in combination with

1263 temperature, pressure, and humidity are necessary. Particle flux should also be measured. To

1264 achieve this, wind measurements should have a precision of ten cm/s in three directions at a

1265 temporal resolution of ~20 Hz at least once per hour. Surface pressure measurements should

1266 provide long-term stability of 0.1 mbar with a precision of 0.02 mbar to be fruitful.

1267 Temperature measurements should fulfill a 0.5 K accuracy requirement. Characterization of

1268 heat and momentum fluxes in the lowermost polar atmosphere can develop from these

1269 measurements.

1270 The accuracy requirement for humidity measurements is of order a few parts per million

1271   (ppm). Humidity measurements with a high temporal resolution (~20 Hz) in combination with

1272   wind measurements of the same resolution would allow the determination of water vapor

1273   transport through turbulent eddies. Alternatively, water vapor transport could be derived from

1274   similar frequency measurements of the water vapor gradient at 2-3 heights measured from a

1275   tall tower, the height of which would have to be determined.

1276   Airborne dust and ice particles should be counted in aggregate to distinguish

1277   populations with respect to particle size to 1 micron and type, such as dust, CO_2 ice, and water

1278   ice. Together with hourly wind measurements, particulate measurements would enable the

1279   determination of dust and water ice particle transport through turbulent eddies. Depositional

1280   mass and dust to ices ratio are also required with microgram sensitivity. Furthermore,

1281   measurements of optical surface properties could supplement the characterization of

1282   environmental conditions and the interpretation of deposition and erosion measurements.

1283   Five to six stations would be needed to accurately characterize these fluxes. Flux

1284   variations are expected to vary primarily with latitude and elevation so stations placed on the

1285   polar cap along one longitude at various latitudes, even equatorward of the polar cap margin,

1286   would capture the dependence on latitude and elevation.

1287   *Potential technologies*

1288   Wind speed and direction could be measured by a sonic anemometer or a wind lidar.

1289   The sonic anemometer can be set up to measure in three dimensions and would fulfill

1290   measurement requirements (Banfield and Dissly, 2005). This instrument could also measure

1291   temperature to an accuracy of ~0.2 K. Wind lidars are frequently used in ground-based

1292   applications on Earth; however, no wind lidar has been deployed on Mars. Hot wire or hot film

1293   anemometers, as deployed on Mars Pathfinder, Mars Science Laboratory, and InSight, do not

1294   have the measurement sensitivity to resolve turbulent eddies. Surface pressure can be

1295   measured by magnetic reluctance diaphragm sensors (Hess et al., 1977) or capacitive sensors

1296   (Gómez-Elvira et al., 2012), which have extensive heritage for Mars surface missions.

1297   For humidity measurements a laser hygrometer based on Tunable Diode Laser

1298   technology (TDL) provides high sensitivity at high repetition rates (Webster et al., 2004). Such

1299   an instrument has been deployed on the Mars Science Laboratory.

1300   Measurements of dust and water ice mass flux could be achieved by aerosol optical

1301   detectors or nephelometers. Nephelometers measure particle densities that pass through a

1302   light beam and a light detector (e.g. a laser emitter and a photocell receiver) either in

1303   transmission or scattering geometry. They could also measure particle size distributions and

1304   optical properties. Deposition measurements could be made by a thermogravimeter or

1305   microbalance. These devices work with thermally stabilized piezoelectric transducers, whose

1306   frequency is proportional to the mass deposited on the sensor. They were proposed for the

1307   Martian Environmental Dust Systematic Analyser (MEDUSA) surface instrumentation package

1308   (Ventura et al., 2011). To determine the ratio of accumulation, heating the microbalance to

1309   sublimation temperatures would sublime deposited volatiles leaving just the dust.

1310   Measurement requirements and potential technologies for in-situ measurements are

1311   summarized in Table 2.1.

1312

1313   ***Table 2.1:*** *Measurement requirements and potential technologies for in-situ flux measurements.*

Measurement	Sensitivity requirement	Measurement frequency	# of stations	Potential technology
Wind (near surface)	few cm/s	20 Hz	5-6	Sonic anemometer
Water vapor/ humidity	few ppm	20 Hz	5-6	Tunable Laser Spectrometer
Dust/water ice flux	aggregate of particles, μm radius	< 1 Hz	5-6	Nephelometer
Dust/water ice accumulation	< 1 μg	daily	5-6	Micro-balance (evaporation capabilities)

1314

1315   Simultaneous measurements from orbital assets should supplement *in-situ*

1316 measurements. Globally obtained vertical profiles of dust, water vapor, and water ice clouds

1317 would be necessary to connect the surface measurements with the processes that govern the

1318 current global climate. These kinds of vertical profiles have been provided, for example, by the

1319 MCS (Kleinböhl et al., 2009, 2017, McCleese et al. 2010) on MRO, and future instruments using

1320 lidar or sub mm spectroscopy can provide additional, critical information. Contributions to

1321 deposition and erosion processes could possibly be made using lidar or interferometric

1322 synthetic aperture radar (INSAR). However, it is likely that only the seasonal CO_2 frost could be

1323 measured in this way because other quantities would be beneath the detection limits of either

1324 instrument. It may be possible to support deposition and erosion studies by covering the polar

1325   ice with an artificial surface or a dye. Measuring changes in the optical properties of the surface

1326   over a season from a surface camera or from orbit would provide information on dust and ice

1327   accumulation. The dyed surface will likely change the surface roughness and radiative

1328   properties in comparison to an unmodified surface, so care is warranted in this approach.

1329   **_2.B.2 Requirements for Measurements of Layer Formation and Properties_**

1330   In the following section we consider measurements that would answer questions

1331   related to layer formation, age, composition, and stratification.

1332   _Layer formation_

1333   At the surface, determining the ratio of present-day accumulation of dust to H_2O to CO_2

1334   is exceptionally important. A thermogravimeter with microgram accuracy can accumulate

1335   materials from snowfall and direct grain growth then measure to the microgram before heating

1336   the volatiles to the appropriate temperature for sublimation. These measurements will have to

1337   be made during polar winter, during accumulation of volatiles.

1338   Measurements of surface albedo, texture, grain size (to 100 microns), grain density, and

1339   grain orientation should be made by reflectance spectroscopy in the infrared, a high-resolution

1340   imager, and nephelometry. Surface temperature can be measured with a thermal imager.

1341   Understanding layer formation also requires access to the near subsurface, and drilling

1342   is the most appropriate method for reaching to 50 cm. Direct measurements of samples can

1343   either be done by lowering instruments into the bore hole or by transporting cuttings to lander

1344   deck instruments. Additionally, some techniques may permit thermal and electrical probes or

1345   fiber optic cables to be lowered in. We discuss implementation in later sections.

1346   Drill telemetry can provide some of the required information. A 50 cm drill would offer

1347   rock/ice competency (in Pa) and density measurements within 20% error. Ideally, these

1348   measurements would be taken continuously, but discrete measurements would be sufficient.

1349   Once a borehole is drilled, an optical imager could be lowered into the borehole in order

1350   to identify and count layers, layer thickness, and dip. Vertical resolution is a function of the

1351   device and the logging speed. Since the size of the smallest layer (or for that matter, what

1352   defines a layer) is unknown, we expect to need finer than 1 mm resolution in order to discern

1353   the thinnest, annual layers within the ice. After determining the most interesting layers, a

1354   microscope with ~30 μm resolution would record high-resolution imagery. Resistivity probes

1355   adequately adapted for Martian conditions and lowered within a borehole could be used to

1356   help correlate ground-penetrating radar (GPR) data with visible layers in the subsurface.

1357   To measure grain size as a function of depth, techniques should have precision of 100

1358   microns. The standard approach would be to observe thin sections from ice cores under

1359   polarized light. Within a borehole however, this quantity is difficult to measure. Sublimation

1360   occurs preferentially along grain boundaries (Obbard et al., 2006), so re-imaging the borehole

1361   at high resolutions 10s of days after it is created may allow grain boundaries to be visible.

1362   Alternatively, if the ice remains granular and porous within the uppermost meters then near-IR

1363   spectroscopy can be used to quantify grain sizes.

1364   The distribution of impurities likely varies in the uppermost 50 cm because of active

1365   layer formation processes. To characterize impurity distribution, one option that provides

1366   nondestructive three-dimensional visualization of the internal features is miniaturized

1367   computerized tomography (microCT). This technology uses axial X-ray scans to obtain spatial

1368 resolution down to several microns. The technology uses a series of tomographic images taken

1369 at different sample angles to create a 3D reconstruction that can be analyzed with spatial

1370 resolution down to several microns. Numerous aspects of interest are in a vertical column:

1371 particle size and shape; volume concentration; pore size, shape, and distribution, discrimination

1372 of salts from Fe-rich sediment; and potentially relative atomic weight. It has been used

1373 extensively in the study of depositional processes in sedimentary rock (e.g. Falvard and Paris,

1374 2017) and more recently in ice (Obbard et al., 2009; Iverson et al., 2017). MicroCT analysis has

1375 been able to differentiate ash layers from specific eruptions (Iverson et al., 2017).

1376 *Composition*

1377   On Earth, high precision measurements of impurities within the ice are conducted on

1378 drill cuttings or ice core sections. Analysis includes thin section stereology, ECM, meltwater

1379 analysis, ion and isotope chemistry, and microCT. However, this requires human intervention,

1380 and drilling and withdrawing cores robotically on Mars requires technology that does not exist.

1381 We discuss techniques to address this concern in later sections.

1382   Trapped gases, such as CO_2, N_2, Ar, O_2, CO are in sufficient abundance to measure at a

1383 precision of 0.1% or greater, and minor constituents such as NO, Ne, HDO, Kr, and Xe require

1384 precision of 10-100 ppb. Other important volatile species like S, Cl, and CH_4 also require ppb

1385 precision. Bubble size and density should be measured to 10 μm.

1386   Isotopic measurements should include D/H to a precision of 100/mil over the range of

1387 100-9000 mil, $^{18}O/^{16}O$ at a precision of 3/mil, and $^{13}C/^{12}C$ at a precision of 5/mil. These

1388 measurements could be directly compared to isotopic measurements of the modern upper

1389 atmosphere by MAVEN or ancient hydrated minerals in Gale crater sediments and martian

1390 meteorites to inform models of long-term atmospheric escape. Concentrations of ^{10}Be are

1391 unknown, so determining if it is present in trace quantities will be valuable.

1392   Composition and abundance of organics with a sensitivity of ppm to ppb is required.

1393   Measurements should require determining the mineralogy of refractory minerals such

1394 as dust (an unconstrained assemblage of phases including nanophase ferric oxides and primary

1395 minerals) and primary mafic sediments to a precision of 1 wt%, distribution to 10 μm, and grain

1396 size for 1 μm particles and larger.

1397   Similarly, S/Cl-rich salts (Morris et al., 2004; Yen et al., Hamilton et al., 2005; Yen et al.,

1398 2005) and perchlorate and sulfate salts (Horgan et al., 2009; Calvin et al., 2009; Massé et al.,

1399 2010, 2012) have been detected. Determining the mineralogy and elemental composition of

1400 soluble impurities such as these to a precision of 0.1 wt% is required.

1401 *Structure*

1402   Orbital measurements are better suited for large scale characterization than landed

1403 assets, and 10x higher resolution versions of existing instruments can provide more information

1404 than what we have presently. A stereoscopic optical imager with 10x improved resolution over

1405 HiRISE would identify finer layers and provide their geometries. An orbital sounding radar >100

1406 MHz bandwidth would match present optical imagery. The higher resolution sounding radar

1407 with this bandwidth necessarily has a higher center frequency than existing assets, a trade that

1408 comes with a decrease in penetration depth unless compensated with a significant increase in

1409 transmit power. This trade increases cost and mass.

1410   From the surface, geophysical techniques could be deployed as well. In order to resolve

1411 thin layers, a GPR with very high resolution and bandwidth (order 10 cm and GHz), that reaches

1412 >100 m penetration depth would provide exceptional quality checks on orbital measurements.

1413 Similarly, an advanced active source seismic system could resolve the layers and offer varying

1414 depth penetration depending on the separation of source and receiver.

1415   Surface based optical imagery can aid here. In a borehole, an imager can look for layer

1416 tilt and of course measure layer thickness. Stereoscopic imagery from within the spiral troughs

1417 would have resolutions better than 10 cm and provide the unprecedented structure

1418 measurements. Equipment similar to gigapan cameras would be sufficient.

1419 *Borehole Drilling*

1420   There are numerous technical challenges to overcome when drilling in cryogenic

1421 environments. We list some here:

1422   Sampling resolution: Data acquisition with 0.5 mm spatial resolution would be difficult

1423 because of high data volumes and long duration measurements. Trading resolution for data

1424 rate is one possibility; however, the high value of the data warrants the best resolution

1425 possible.

1426   Instrument integration and resources: Instrument miniaturization technology to fit

1427 within the borehole is required, and accommodation and further trade-offs must be

1428 considered.

1429   Removal of drilled material: The smallest useful diameter of the borehole is likely to be

1430 around 5 cm. Thus, approximately 1,000 cm^3 of material will need to be removed from the

1431 borehole. This material needs to be dumped close to the lander or transported by some means

1432 to the lander deck. Dumped material may alter or be mobilized by winds before measurements

1433 are made. Material moved from within the borehole requires technological advancements.

1434   <u>Borehole integrity</u>: Continued drilling and measurements may be affected by material

1435 falling into the borehole or re-condensation of volatiles that sublimate during the drilling

1436 process and re-condense on the colder walls of the borehole.

1437   <u>Sediment layer</u>: The mixing ratio of non-volatile material in individual layers is variable

1438 and may affect drilling operations. Newly exposed dust may be mobilized.

1439   <u>Diffusive loss of trapped gases</u>: Sample handing may release the gases that were stored

1440 in the ice, losing important information in this investigation.

1441   <u>Other ice evolution</u>: Assessment of how the ice evolves after it becomes exposed (in the

1442 borehole or the cuttings on the surface) is required. This involves volatilization or

1443 recrystallization.

1444   <u>Temperature Profile</u>: Unique to deep borehole measurements, a vertical temperature

1445 profile could be measured, providing an additional insight into recent climate parameters such

1446 as the obliquity thermal wave and even the modern geothermal flux, however the drilling

1447 technique may affect temperature readings.

1448 ## *3 Mission Concepts and Approaches to Measurements*

1449   Based on the science priorities and measurement requirements, we developed a multi-

1450 mission strategy that maximizes science return while maintaining a moderate budget. Some

1451 elements, like global wind speeds, and borehole measurements require a specific class of

1452 mission, while others can be distributed among classes for cost effectiveness.

1453   The multi-mission strategy is to send an orbiter for global atmospheric and subsurface

1454 measurements, a static lander for polar reconnaissance of layers and near surface

1455 environments, a network of small-sats for distributed/network meteorology, and a fast, mobile

1456 platform or deep drill for narrow focus, rapid composition measurements. Each stage can be

1457 independent; however, science returns will be move valuable if the landed meteorology

1458 stations overlap in time with the orbiter. We detail these concepts in the next four sections.

1459 *3.A Orbiter*

1460 An orbiter mission dedicated to the study of the martian polar regions has the potential

1461 to greatly advance our understanding of the present day forcings and fluxes in and out of the

1462 high latitudes and also help characterize fundamental properties of the PLD themselves.

1463 Complete coverage of the planet at all local times would be ideal, but with a single

1464 orbiter trades-offs must be made. The main choices are between repeat coverage at one local

1465 time or greater time of day coverage. Each of these requires a different type of orbit; however,

1466 a hybrid scenario is conceivable, wherein an orbiter performs measurements at one local time

1467 for one Mars year and then changes local time for a second Mars year. Thus, time of day

1468 requirements can be accommodated without sacrificing polar coverage, such as CASSIS. Mars

1469 Odyssey has set the precedent for this option. Furthermore, starting with MRO's orbit would

1470 increase the baseline of current atmospheric observations for MCS and the Mars Color Imager

1471 (MARCI).

1472 The science payload would be selected to fit within two broad themes: 1) Fluxes and

1473 Forcings, and 2) PLD Physical Properties. We note that several instruments have a very strong

1474 flight heritage and could potentially be proposed with slight technological improvements for big

1475 gains. See Table 3.1 for a list of instrument type and key measurement goals.

Fluxes and Forcings

1476

1477   Two instruments capable of meeting the highest priority of measuring global wind

1478 speeds for the first time: a microwave sounder and a LIDAR. Besides measuring wind speeds,

1479 either could provide profiles of temperature, water vapor and other tracers in the atmosphere.

1480   A second instrument, such as an IR sounder inspired by MCS, would measure

1481 temperature, water vapor, dust, CO_2 and H_2O ice cloud profiles as well as surface temperature

1482 and emissivity. This would have the benefit of extending our current atmospheric

1483 measurements. Improvements over MCS to obtain 2-3x higher vertical resolution, better

1484 H_2O/aerosol discrimination, and better coverage closer to the surface are important.

1485   A multi-wavelength visible/IR imager would measure surface frosts and discern water

1486 ice from CO_2. An instrument with heritage from MARCI that included more bands and higher

1487 spatial resolution would fill this role.

1488 *PLD Physical Properties*

1489   To measure fine layer sequences within the top 100s of meters of the PLD, we envision a

1490 radar sounding instrument with higher resolution than SHARAD and MARSIS. A P- or L-band

1491 sounder, with >100 MHz bandwidth could achieve vertical resolution better than one meter. A

1492 synthetic aperture radar polarized (PolSAR) with interferometric capabilities (InSAR) on the

1493 order of 5 cm vertically would determine vertical changes of surface topography at the poles

1494 related to seasonal frost accumulation and mass wasting. This would supplement other

1495 instruments in characterizing energy and mass budgets of the PLD. This instrument, while being

1496 highly valuable for polar observations, would also provide measurements related to the global

1497 water ice and dust inventories.

1498   Very high spatial resolution imagers (multi-wavelength visible, similar to HiRISE, and

1499   hyperspectral visible /near IR spectrometers, similar to CRISM) would have the potential to

1500   resolve finer layer structures within the stratigraphic record and constrain the composition of

1501   surface lags derived from internal dust/lithic layers. We note that to generate fundamentally

1502   new science information, the spatial resolution of these instruments would need to be an order

1503   of magnitude finer than current assets. Cost and sufficient signal to noise ratio are concerns.

1504   A multipurpose scanning LIDAR instrument could provide valuable surface and

1505   atmosphere science. With 1 cm topography and 5 m shot points, it would detect surface

1506   changes and help characterize fluxes towards or out of the PLD. Multiple wavelengths could

1507   allow the discrimination of surface CO_2 and water ice and measure cloud heights within the

1508   polar night.

1509   To fit within a Discovery or New Frontiers class mission, the high spatial resolution

1510   imagers and lidar would be the preferred descope options, in that order, leaving the

1511   meteorological and subsurface measurements.

1512   Besides the obvious advantage of joining orbital meteorological measurements with

1513   landed meteorology (Sections 3.B and 3.C), hybrid missions between orbital and surface

1514   platforms would add value. Surface assets may be able to deploy surface calibration targets,

1515   reflectors, or radio beacons to improve the accuracy and precision for monitoring of changes.

1516   Impactor missions could gather data during descent and provide extremely high spatial

Table 3.1: Straw-man Orbiter Payload. Instruments are for an extremely capable orbiter with abundant power and data rates. The first de-scope options are the Microwave Nadir Sounder, Multi-wavelength visible imager, Near-IR pushbroom spectrometer and the LIDARS.

Instrument (in priority order)	Key Measurement	Performance Characteristics	Notes
Microwave or LIDAR Wind Profiler	Winds Speeds, Isotope tracking	3D wind speeds to 1 m/s	Critical for GCMs, never flown to Mars before
High-Resolution RADAR Sounder	MAP PLD layers and mid-latitude ice at high resolution	50 cm vertical resolution to 100 m	Complementary to SHARAD and MARSIS
PolSAR	Map extent of ground ice	<5 m horizontal resolution, polarimetry	Big power draw and data rates
InSAR	Temporal changes in topography, surface roughness	<1 cm vertical resolution	Big power draw and data rates
IR limb/Nadir Sounder	Vertical profiles of Temperature, Water Vapor, Aerosols	2x MCS + enhanced channels	Global atmospheric processes
Multi wavelength visible/IR imager	Measure surface frosts and discern H_2O from CO_2	Improved channels and resolution over MARCI	Two cameras for stereo observations of clouds
Multi-Wavelength LIDAR	High-resolution topography, CO_2 and H_2O composition, seasonal and interannual variability, cloud profiles	<1 cm vertical resolution, <5 m shot size, >4 wavelengths, atmospheric profiling	Works at night, measure seasonal accumulation, high precision orbit required
Multi-wavelength visible imager	Morphology, Albedo, Composition, Topography	1-10 cm	Resolve layers thinner than HiRISE, Context
Near-IR pushbroom spectrometer	Composition - H_2O and CO_2 Ices, Dust	Better than CRISM	Only works in sunlight

1517 resolution of surface and near surface properties. A surface instrument to disperse reflectors or

1518 a dye on the surface would allow an orbiter to monitor color and albedo changes as a means to

1519 determine the mass balance at specific locations. Color and albedo changes monitored from

1520 orbit could prove a means to determine the mass balance at multiple locations.
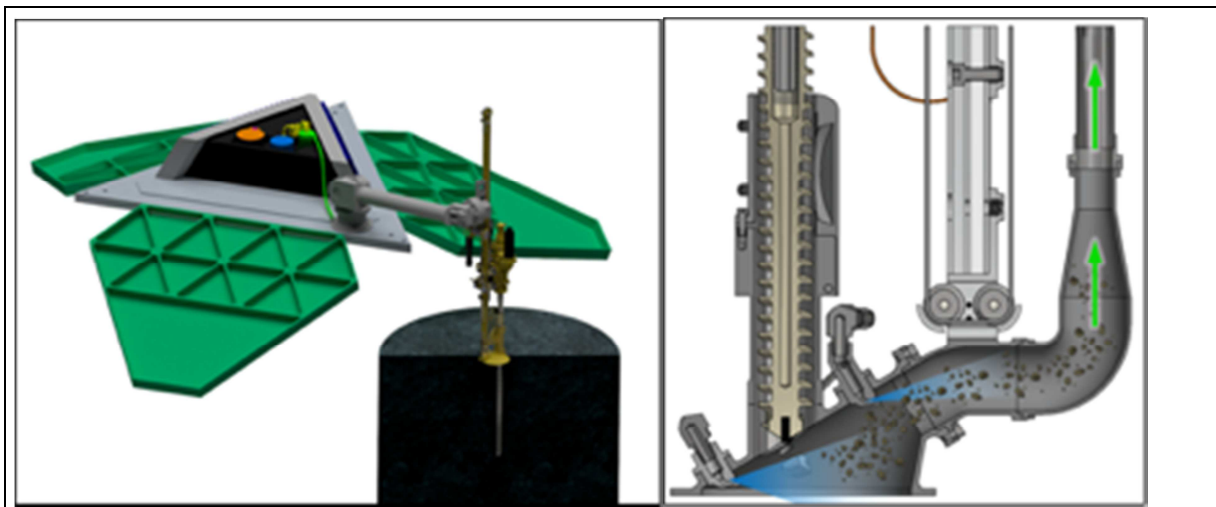
Figure 9: CAD concept of a lander asset using the Mars Exploration Rover (MER) Entry, Descent, and Landing (EDL) architecture. A) A drill arm extends past the landing hardware and mechanically drills ~50 cm into the subsurface using several small steps. B) Pneumatic hardware moves the drill cuttings to the lander deck where they can be analyzed by onboard instruments. Graphic courtesy of Honeybee Robotics

1521 **3.B Static Lander**

1522 Here we discuss a straw-man payload for a single static lander that has drilling

1523 capabilities, ice handling equipment and instruments, and a complete suite of atmospheric

1524 instruments. We anticipate that a static lander is best suited as a reconnaissance mission

1525 designed to characterize the environment at the PLD, including the near subsurface.

1526 This first delivery to the PLD surface should include instrumentation that is capable of

1527 addressing strategic knowledge gaps, including measuring all relevant atmospheric parameters

1528   and processes, observing surface changes and properties, and accessing the top 50 cm with full

1529   physical and chemical analysis. The top 50 cm is chosen to reach layers that are predicted to no

1530   longer interact with the current atmosphere (Bramson et al., 2019). This mission could be of the

1531   NASA New Frontiers class and provide the groundwork for a future mobile mission designed to

1532   use the knowledge gained for rapid acquisition of stratigraphic measurements (see section 3.E).

1533   Potential methods to reach 50 cm depth include thermal and mechanical drilling.

1534   Analysis may take place inside the borehole on the lander deck. Some instruments are too large

1535   to fit in a borehole, so a combination of techniques is considered. Because the 50 cm depth is

1536   very shallow, we concentrate on an approach that includes a mechanical drill, as opposed to a

1537   melt-probe. The main driver for using a mechanical drill, or a combined mechanical and melt

1538   drill, is the power savings. Cryogenic ice is 3-4x more conductive than warm ice, and as such,

1539   the melting approach would require a larger power supply (>80% of heat is lost into

1540   surrounding ice). There is the additional risk of finding layers with significant dust fraction that

1541   the drill could not penetrate, causing it to be stuck. That said, if thermal, or vaporizing drilling

1542   techniques could overcome these obstacles while maintaining high resolution, the benefit of

1543   not handling drill cuttings or risk of getting stuck outweigh a mechanical drill.

1544   *In borehole analysis*

1545   Multiple options exist for in-borehole analysis. The first is to use the drill itself as an

1546   instrument. Drill-integrated instruments would help with the drilling process, reduce

1547   mechanical risks, and provide science data. The instruments and data include, material strength

1548   and density from drilling telemetry, density from ultrasonic velocity, a temperature sensor, and

1549   bulk electrical resistivity (required to detect "slush" formation and salt content) from resistivity

1550   sensor.

1551   The second option is to modify the drill string to include instruments. This approach has

1552   numerous benefits, including in situ analysis of samples, but it also requires miniaturization

Table 3.2: Lander Instrumentation. Drill (D); Borehole Logger (BL); Lander Deck (LD)

Type of measurement	Instrument	Heritage	Location	Comment
Optical	Pan-cam (multi-spec)	Many	D, BL, LD	
Optical	Microscope	Many	D, BL	
Environmental	Ground penetrating radar		LD	
Environmental	Met station	Many	LD	
Environmental	Ice and dust accumulation system		LD	Quartz-crystal microbalance?
Environmental	LIDAR	Phoenix	LD	
Analytical	Tunable laser spectrometer	MSL	LD	
Analytical	Mass spectrometer	Phoenix	LD	Connected via a vacuum pump and tubing to the mouth of the borehole
Analytical	Deep UV, Raman or VNIR (with fiberoptic lead)	Mars 2020	D, BL, LD	Fibre-fed from the borehole
Elemental	LIBS	MSL, Mars2020	D, BL, LD	Fibre-fed from the borehole
Ice structure	micro CT			Examine Core

1553   technologies to be developed. Additionally, a drill string may not be capable of performing all of

1554   the science requirements, meaning that some material may have to be taken to the surface.

1555   A third technique is to lower instruments into the borehole after the drill string is

1556   removed. This option has advantages over using the drill string because it reduces complexity of

1557   a complicated moving part; however, a trade is made because a separate articulating arm

1558   would be required, or the mechanical arm that operated the drill would have to detach from

1559   the drill and operate the borehole logger.

1560   Instruments that could be built into the drill string or lowered separately include an

1561   optical camera system and/or a LED-driven VNIR spectrometer system, a microscope, a

1562   spectrometer (such as Ma_MISS on ExoMars, De Sanctis et al., 2017), a fine-scale electrical

1563   resistivity probe, a temperature sensor, and a laser. The optical camera system should provide a

1564   wide field of view, such as a fish eye or acquire images by rotation. The microscope should have

1565   a short working distance and be able to reach micron resolutions. An optical camera,

1566   spectrometer, and the microscope will require some illumination. In addition, we foresee the

1567   inclusion of a laser in the borehole as a source for performing Laser Induced Breakdown

1568   Spectroscopy (LIBS) and deepUV/Raman (Bazalgette Courrèges-Lacoste et al., 2002)). The

1569   spectrometer would reside on the deck of the lander and be fed via fiber optic cable, while the

1570   laser would be integrated in the borehole logger. These instruments are ideal for measuring

1571   D/H or $^{18}O/^{16}O$, critical measurements for this mission. The alternative of keeping the laser on

1572   deck and using fiber optic cable to transmit the light increases risk of damage to the cable.

1573   Heritage of this type of instrument comes from the Mars 2020 Scanning Habitable

1574   Environments with Raman & Luminescence for Organics & Chemicals (SHERLOC) and SuperCam

1575   spectrometers.

1576   Ice composition and ice grain size as well as the mineralogy of impurities could all be

1577   assessed rapidly via short-wave infrared reflectance spectroscopy (SWIR; 1.0-4.0 microns),

1578   which has been shown via orbital remote sensing to be highly sensitive to key phases in the PLD

1579   (references above) and has been successfully miniaturized for small applications.

1580   Bulk chemistry of borehole walls or other solid samples could be assessed via X-ray

1581   fluorescence (XRF), as implemented in the Planetary Instrument for X-ray Lithochemistry (PIXL)

1582   instrument on Mars 2020, via alpha particle X-ray spectroscopy (APXS), as implemented on

1583   multiple Mars rovers, or via laser-induced breakdown spectroscopy (LIBS), as implemented in

1584   the MSL ChemCam and Mars 2020 SuperCam instruments. LIBS has been implemented with

1585   long fiber optics cables and may be more applicable to small diameter boreholes.

1586   Additional instruments could also be packaged inside a borehole logger or drill string,

1587   but the extent of what can be included largely depends on several parameters. Increasing the

1588   diameter of the borehole would permit larger instruments to perform analysis, but this comes

1589   at an energy cost. Resistance to shock, vibrations and temperature are also concerns.

1590   *Sample analysis on the lander deck*

1591   The final option is to remove samples from the borehole for analysis on the lander deck.

1592   This may be done as a single core, drill cuttings, melting the cutting and transporting as a liquid,

1593   or volatilizing the sample. Each has advantages and disadvantages, and Technological

1594   advancements for robotic core handling would be required. Drill cuttings (also known as chips)

1595   of ~ 1 cm have to be transported to instruments many times, requiring a separate and durable

1596   sample handling system. Cuttings could be approximately 1 cm thick, and a pneumatic sample

1597   handling system integrated into the drilling apparatus could transport several cm^3 at a time to

1598   instruments on the lander deck (Figure 9).

1599   Instruments that we propose would remain on the lander deck to perform analysis

1600   include the high technology readiness level (TRL) pyrolysis gas chromatography-mass

1601   spectrometer with a laser desorption mass spectrometer (cf. the Mars Organic Molecule

1602   Analyser (MOMA) onboard the upcoming ExoMars Rover, Arevalo et al., 2015). These could be

1603   applied to detect and characterize organics, or potentially utilized for exposure age dating of

1604   sediments via cosmogenic nuclides. Tunable laser spectroscopy (TLS), as implemented on

1605   Curiosity, could provide information on the bulk and isotopic composition of major gases. Prior

1606   to destruction of the sample, a microCT should be employed to study the internal structure of

1607   the ice. Technology development for a flight ready microCT is necessary to complete these

1608   measurements.

1609   *Landing Site Selection*

1610   Landing site choice will be influenced by 1) safety to the mission and 2) completing our

1611   science requirements. If all sites are determined to be equally safe, then the optimal landing

1612   site will be one that maximizes science returns. Locations with greater surface-atmosphere

1613   activity (e.g. high mass balance and wind speeds) are preferred.

1614   Another important consideration is subsurface layering, and we should avoid a location

1615   that has unique or local processes that do not represent the wider PLD. Compared to Earth, the

1616   PLDs are not as dynamic as the terrestrial ice sheets because layers are not significantly

1617   influenced by flow (Karlsson et al., 2011), and no melting is expected to occur at the surface or

1618   the base today. Radar surveys show continuous, sub-horizontal layers (Phillips et al., 2011) and

1619   small thickness variations (Nerozzi and Holt 2017) across the lower ½ of the NPLD for more than

1620   1000 km, so identifying an ice divide far from strong basal topography is not a priority.

3.C Small-Sat Network

1621

1622   Numerous options are available for small-sat, short-lived missions that can perform

1623   rapid measurements while being scattered over the NPLD. In particular, the Mars$_{Drop}$ platform is

1624   of interest (Staehle, et al., 2015). These units are approximately the size of a 6U cubesat and

1625   shaped like an ice-cream cone. The dome carries a parawing but no other EDL components, and

1626   descent is not guided. This is not critical for the types of investigations identified here, and

1627   distributing up to five landers along a longitude that reaches a band >10° latitude is entirely

1628   sufficient. Landing on a target more specific than the 1000 km diameter polar cap is not

1629   required. Once on the surface, several solar panels would deploy, revealing the payload (Figure
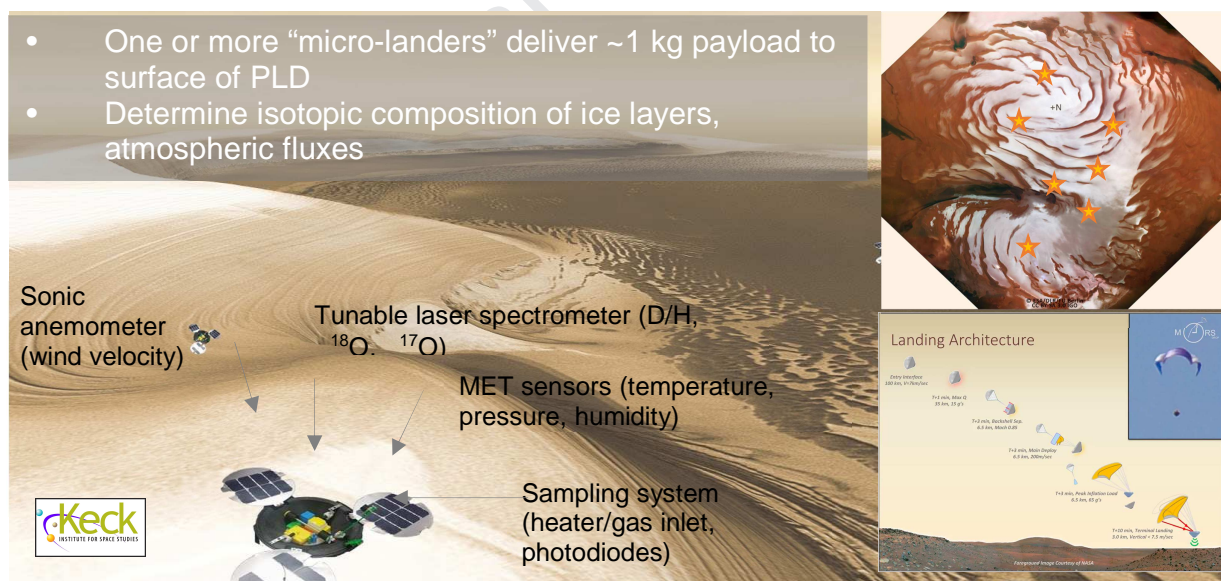
1630   10).

Figure 10: Deployment of a network of small-sat MarsDrop spacecraft carrying either atmospheric or surface measurement instrumentation. Background from THEMIS draped over MOLA topography. Inset image from HRSC.

1631

1632

1633   Because of their small size, Mars$_{Drop}$ spacecraft must contain targeted investigations.

1634   Multiple missions of this scale could be sent simultaneously to measure atmospheric

1635   properties, atmospheric constituents, or surface and subsurface properties. For the

1636   atmosphere, a sonic anemometer coupled with temperature, pressure, and humidity

1637   instruments would be a desirable component of a meteorological network scattered across the

1638   polar landscape. Sending a TLS to measure the atmospheric components could also be of high

1639   value. Finally, a package that is able to measure ice properties including electro-conductivity or

1640   ground penetrating radar that could fit within the Mars$_{Drop}$ package would significantly

1641   contribute to the mission science.

1642   ***3.D Program Architecture with Two Landed Missions***

1643   Completion of the program to extract the climate record requires vertical sampling of

1644   ~500 m of stratigraphy, enough to obtain 1 Myr of climate history. This critical aspect is difficult

1645   to do economically while also performing all other science experiments desired. Therefore, we

1646   developed a two landed mission program that could complete all science objectives for the cost

1647   of two New Frontiers missions. This is a cost saving measure that has the additional benefits of

1648   being funded over multiple decades at the same time as reducing risk.

1649   The first landed mission was a reconnaissance lander sent to measure all relevant

1650   atmospheric, surface, and subsurface properties and processes. The second landed mission

1651   could then concentrate on measuring only a narrow set of properties in a vertical section that

1652   directly tell of the climatic history. Repeating measurements related to ice and atmospheric

1653   properties is desirable but unnecessary, so the second landed mission could have a very small

1654   instrument set that acquired data very quickly. Because of the reduced number of

1655 investigations, this mission could potentially be completed in a single Mars spring and summer

1656 campaign rather than require capabilities to over winter. This mission, like the first, could fit

1657 into the New Frontiers program.

1658 The two landed mission architecture has significant advantages over sending one

1659 extremely capable rover or deep drill capable of making every measurement that we identified

1660 as a priority. A single rover would certainly fall in the Flagship class and likely be the most

1661 capable robot ever sent to Mars with multiple technology programs for cold technology and

1662 miniaturization, increasing the total program cost by several times, reducing science return per

1663 dollar decreases. Further, in order to be cost conscious, science instruments would probably be

1664 de-scoped, leaving critical science goals unmet. Finally, the risk of a failure puts the entire

1665 program at jeopardy and ties NASA's hands for increased testing to guarantee success. This

1666 strategy bloats budgets with no compensatory gain. The complexity and cost of large, single

1667 missions and the risk of unmet science goals make them un-selectable.

1668 Because the first landed mission would fall within the 2023-2032 decade, this second

1669 landed mission should come in the following decade, providing more time to develop platforms

1670 (Section 3.E) and spread the cost over many years.

1671 *3.E Obtaining a Long Climate Profile with Extended Vertical Sampling*

1672 After the reconnaissance lander completes its task, we can complete the task of

1673 unlocking the climate record by accessing 500 m of vertical section in multiple ways that involve

1674 mobile or static landers. Three concepts are viable for follow-on landed missions. The first

1675 is a stationary platform with deep drilling capabilities, and the other two involve mobile

1676 platforms.

1677   *Viable Second Landed Mission Concepts*

1678   For a deep drill, instruments, would have to fit on the drill string to transmit information

1679   back to the surface via cables. Alternatives, such as extracting the drill and lowering

1680   instruments 500 m or handling 500 m of core without human intervention are technologically

1681   unfavorable.

1682   Mechanical deep drilling technology for planetary missions is only at TRL 4 or 5

1683   (AugoGopher2, WATSON), so sampling ~500 m of vertical stratigraphy would require an

1684   ambitious technology advancement program. Because of the reduced scientific payload (over a

1685   single landed mission), thermal drilling to complete the mission objectives becomes more

1686   viable, and thermal drilling has been proven at TRLs >5, reducing overall technological

1687   investments.

1688   The first mobile platform option would involve sampling layers along a gently sloping

1689   trough wall. A rover that covers ten km of transect would access more than five hundred

1690   meters of outcrop. Local slopes, on 1 to 2 m thick layers could reach upwards of 15°, well within

1691   the capabilities of all modern rovers sent to Mars. Sliding is unlikely but could be mitigated with

1692   appropriate selection of traction. With a reduced payload and one high priority science

1693   objective, this rover would traverse more quickly than previous rovers, potentially in one Earth

1694   year.

1695   The second option is a rappelling platform capable of descending a steep scarp near the

1696   margin of the PLD. The Axle-Rover is one possibility because it could land at a safe distance

1697   from the scarp and drive to it. Similar to the rover option, the limited instrument suite would

1698   mean very rapid measurements and quick mission completion.

1699   Both mobile platforms would require abrading up to 10 cm of surface lag before making

1700   measurements. These technologies exist today, so little technological advancement is required.

1701   The exact instruments on board these platforms cannot be decided until the first landed

1702   mission completes; however, we believe that some or all of the following suite may be

1703   necessary: a navigation camera that doubles for layer analysis; a chemistry suite encompassing

1704   wet geochemistry and a mass spectrometer; ground penetrating radar. Arm mounted

1705   instruments may include an optical imager, thermal and electrical conductivity, TLS,

1706   nephelometer, and micro-spectroscopy. *Any mission that accesses numerous layers should have*

1707   *instrumentation capable of finding an absolute age based on the first landed mission's*

1708   *reconnaissance.*

1709   ### *3.F Surviving a polar night.*

1710   Many of the desired measurements require surviving or operating in the polar night. At

1711   very high latitudes, a mission would have to survive extreme temperatures (~150 K) and endure

1712   approximately one earth year without solar energy. This is not achievable with current battery

1713   technology, so landed missions would be required to bring energy with them or create energy

1714   *in situ*. Options exist for both techniques, and each comes with risks.

1715   One option would be to bring a radioisotope thermoelectric generator (RTG). The

1716   constant supply of power would enable measurements in the polar night, but the heat

1717   generated would likely alter the local environment and disturb the atmospheric and surface

1718   measurements. Mitigation would require some distance or insulation between the RTG and

1719   measurements.

1720   Another option would be to bring chemical energy with the spacecraft. Materials may

1721 include fuel and oxygen for burning. This option requires extra mass and has risk associated

1722 with transporting volatiles. An advantage is that power could be on demand, so it would only

1723 be consumed when needed to charge batteries, or during heavy drill operation.

1724 Creating energy *in situ* is currently an important topic of discussion. In lieu of bringing

1725 fuel, landers could use solar energy to create fuel such as hydrogen and oxygen through

1726 photolysis. On launch the tanks could begin empty, saving mass, and then be filled during the

1727 abundant energy period of summer. This requires splitting water molecules and storage and a

1728 technology development program.

1729 Alternatively, recent research has found that CO_2 can react with lithium metal to

1730 produce large quantities of heat and electricity in the form of a battery (Xu et al., 2013; Qie et

1731 al., 2017). This choice would use the abundantly available CO_2 atmosphere to provide energy at

1732 significant cost savings over transporting energy to Mars. The technology has not yet been

1733 developed for planetary missions, so investments are required now to advance to high TRL by

1734 the next decade.

1735 ***3.G Planetary Protection.***

1736 Finally, a mission to locations with H_2O raises questions about forward contamination of

1737 biota to Mars. Under planetary protection definitions, the PLD are not considered special

1738 regions because they are not "a region within which terrestrial organisms are likely to

1739 propagate, or a region which is interpreted to have a high potential for the existence of extant

1740 Martian life forms." This is because of the long history without sufficient energy and

1741 temperatures to melt water. However, there is the possibility that an RTG could induce a

1742 special region by warming the ice to the melting point, and this possibility warrants

1743 consideration for mission planning.

1744   That said, any forward contamination that takes hold in the induced special region is

1745 expected to be temporary. The PLD are many thousands of km away and geologically isolated

1746 from a location that could feature high enough water activity (e.g. subsurface near the

1747 equator), so terrestrial organisms are unlikely to survive transport through the irradiated

1748 atmosphere to find a habitat, possibly making this concern moot.

1749 *4. Conclusions*

1750   In this paper we outlined some of the overarching questions for Mars climate science

1751 going forward and have developed a roadmap for answering the questions with specific focus

1752 on the highest priority science. This plan uses experience gained from past and ongoing

1753 missions, as well as former proposal concepts, terrestrial field, and lab work.

1754   The four most encompassing science question for unlocking the climate record are:

1755   *1. What are present and past fluxes of volatiles, dust, and other materials into and out of*

1756   *the polar regions?*

1757   *2. How do orbital forcing and exchange with other reservoirs affect those fluxes?*

1758   *3. What chemical and physical processes form and modify layers?*

1759   *4. What is the timespan, completeness, and temporal resolution of the climate history*

1760   *recorded in the PLD?*

1761   Each question requires numerous measurements to address, and the climate record can

1762 only be fully extracted by answering all questions. That said, individual steps towards answering

1763 these questions would improve our knowledge of the state of Mars, and missions that address

1764 these core questions can be spread out over several decades. Thus, a program of multiple

1765 missions is the best route to understanding the climate record from the PLD.

1766 Regarding the required missions, we carefully considered science return versus total

1767 cost and presented a multi-staged program that would address all of the highest priority

1768 science in a logical progression that eventually returns the climate record of Mars going back ~1

1769 Myr.

1770 The multi-mission program discussed here utilizes assets in orbit and on the surface. Of

1771 primary importance is new understanding of the present-day climate through enhanced and

1772 continued investigations of volatile and dust fluxes into and out of the polar regions and at the

1773 surface-atmosphere boundary. This is accomplished by making orbital measurements of dust,

1774 water vapor, and CO_2 transport globally through a suite of meteorological instruments. From

1775 orbit, subsurface measurements of volume, extent, purity, and porosity of volatile reservoirs is

1776 also critical to understanding the current climatic state. Simultaneously, if possible, a network

1777 of small, SIMPLEX level spacecraft distributed along a latitude band across >10° of latitude

1778 would provide the ground truth atmospheric observations necessary in order to calibrate the

1779 orbital measurements and observe surface-atmosphere interactions, including accumulation

1780 and ablation of volatiles at the poles.

1781 Larger assets on the ground, in the form of a static reconnaissance lander followed by a

1782 mobile platform or deep drill, would then complete the task of extracting the climate record.

1783 First, a New Frontiers-class static lander would assess all qualities of the materials at the PLD

1784 surface and near (50 cm) subsurface in order to determine the most appropriate techniques for

1785 extracting the climate record, most likely by radio isotope measurements. Subsurface access

1786   would also enable us to determine how atmospheric properties and processes create and

1787   modify layers, including sintering and densification to the preserved layers.

1788   We envision the final mission to be a highly focused mission that is designed to make

1789   very specific measurements through 500 m of vertical stratigraphy, accessing ~ 1 Myr of

1790   martian climate history. Three options include a rover to descend the shallow spiral troughs, a

1791   rappelling platform to descend the steep marginal scarps, or a deep drill. All would carry a

1792   narrow suite of instruments designed to only extract the information needed for obtaining the

1793   past climate, keeping this final mission within the New Frontiers Program.

1794   The two-lander architecture reduces costs, complexity, and risk over sending a single

1795   extremely capable mission while being better adapted to accomplish the science goals.

1796   Further, the two landed-mission concept could be spread over multiple decades, leaving budget

1797   room for other missions. Multiple smaller missions have numerous advantages over single

1798   missions that are too large to fail.

1799   As we discuss here, there are numerous reasons to investigate the polar regions of

1800   Mars. The modern climate state and the climate record are scientifically compelling targets, but

1801   the data required to advance our scientific understanding of ice and climate processes and

1802   history would also support the potential for human exploration by providing critical inputs to

1803   modern climate and available resources. In addition, the astrobiological potential of the polar

1804   ice also makes these compelling targets for future missions.

1805   The polar layered deposits of Mars are the only other known place in the universe to

1806   host a detailed climate record on a terrestrial planet. Accessing that climate record is one of the

1807   most compelling objectives of NASA and a Holy Grail planetary science. By reading that climate

1808   record we can learn about the climate history of planets like our own throughout the universe.

1809   Our hypotheses are fully matured, and the time to begin this project is now.

1810   ***5. Acknowledgements***

1815

1816

6. References

1817

1818   Anderson, F. Scott, et al. "A laser desorption resonance ionization mass spectrometer for Rb-Sr

1819   geochronology: Sr isotope results." Aerospace Conference, 2012 IEEE. IEEE, 2012.

1820   Anderson, F. Scott, et al. "Rb-Sr resonance ionization geochronology of the Duluth Gabbro: A

1821   proof of concept for in situ dating on the Moon." Rapid Communications in Mass

1822   Spectrometry 29.16 (2015): 1457-1464.

1823   Appéré, T., B. Schmitt, Y. Langevin, S. Doute, A. Pommerol, F. Forget, A. Spiga, B. Gondet, and J.

1824   P. Bibring (2011), Winter and spring evolution of northern seasonal deposits on Mars

1825   from OMEGA on Mars Express, *Journal of Geophysical Research-Planets*, *116*,

1826   doi:10.1029/2010je003762.

1827   Arthern, R. J., D. P. Winebrenner, and E. D. Waddington (2000), Densification of Water Ice

1828   Deposits on the Residual North Polar Cap of Mars, Icarus, 144, 367-381.

1829   Bazalgette Courrèges-Lacoste, G., Ahlers, B., Pérez, F.R., 2007. Combined Raman

1830   spectrometer/laser-induced breakdown spectrometer for the next ESA mission to Mars.

1831   Spectrochimica Acta Part A: Molecular and Biomolecular Spectroscopy, Seventh

1832   International Conference on Raman Spectroscopy Applied to the Earth and Planetary

1833   Sciences 68, 1023–1028. https://doi.org/10.1016/j.saa.2007.03.026

1834   Banfield, D. and R. Dissly (2005), A Martian sonic anemometer, *IEEE Aerospace Conference,*

1835   doi:10.1109/AERO.2005.1559354.

1836   Banks, M.E., Byrne, S., Galla, K., McEwen, A.S., Bray, V.J., Dundas, C.M., Fishbaugh, K.E.,

1837   Herkenhoff, K.E., Murray, B.C., 2010. Crater population and resurfacing of the Martian

1838   north polar layered deposits. Journal of Geophysical Research 115, E08006.

1839 Bapst, J., Byrne, S., Brown, A.J., 2018. On the icy edge at Louth and Korolev craters. Icarus, Mars

1840 Polar Science VI 308, 15–26. https://doi.org/10.1016/j.icarus.2017.10.004

1841 Bar-Cohen Y., and K. Zacny [editors], Drilling in Extreme Environments Penetration and

1842 Sampling on Earth and Other Planets, John Wiley & Sons, 2009

1843 Barr, A.C. and Milkovich, S.M., 2008. Ice grain size and the rheology of the martian polar

1844 deposits. Icarus, 194(2), pp.513-518.

1845 Basu, S., Richardson, M.I. and Wilson, R.J., 2004. Simulation of the Martian dust cycle with the

1846 GFDL Mars GCM. Journal of Geophysical Research: Planets, 109(E11).

1847 Becerra, P., S. Byrne, and A. J. Brown (2015), Transient bright "halos"; on the South Polar

1848 Residual Cap of Mars: Implications for mass-balance, *Icarus*, *251*, 211-225,

1849 doi:10.1016/j.icarus.2014.04.050.

1850 Becerra, P., Byrne, S., Sori, M.M., Sutton, S., Herkenhoff, K.E., 2016. Stratigraphy of the north

1851 polar layered deposits of Mars from high-resolution topography. J. Geophys. Res.

1852 Planets 1–27. doi:10.1002/(ISSN)2169-9100

1853 Becerra, P., Smith, I.B., Nunes, D.C., Sori, M.M., Thomas, N., Brouet, Y., Guallini, L., 2017a.

1854 Correlation of Radar and Visible Data of Mars' North Polar Layered Deposits, European

1855 Planetary Science Congress.

1856 Becerra, P., Sori, M.M., Byrne, S., 2017b. Signals of astronomical climate forcing in the exposure

1857 topography of the North Polar Layered Deposits of Mars. *Geophys. Res. Lett.* 44, 62–70

1858 2016GL071197. doi:10.1002/2016GL071197

1859 Becerra, P., Sori, M.M., Thomas, N., Pommerol, A., Simioni, E., Sutton, S.S., Tulyakov, S.,

1860 Cremonese, G., 2019. Timescales of the Climate Record in the South Polar Ice Cap of

1861   Mars. Geophysical Research Letters 46, 7268–7277.

1862   https://doi.org/10.1029/2019GL083588

1863 Berman, D.C. and Hartmann, W.K., 2002. Recent fluvial, volcanic, and tectonic activity on the

1864   Cerberus plains of Mars. Icarus, 159(1), pp.1-17.

1865 Bibring, J.-P., Langevin, Y., Gendrin, A., Gondet, B., Poulet, F., Berthé, M., Soufflot, A., Arvidson,

1866   R., Mangold, N., Mustard, J., others, 2005. Mars surface diversity as revealed by the

1867   OMEGA/Mars Express observations. Science 307, 1576–1581.

1868 Bierson, C. J., R. J. Phillips, I. B. Smith, S. E. Wood, N. E. Putzig, D. Nunes, and S. Byrne (2016),

1869   Stratigraphy and evolution of the buried CO_2 deposit in the Martian south polar cap,

1870   *Geophysical Research Letters*, *43*(9), 4172-4179, doi:10.1002/2016gl068457.

1871 Bond, Gerard, et al. "Correlations between climate records from North Atlantic sediments and

1872   Greenland ice." Nature365.6442 (1993): 143-147.

1873 Böttger, H.M., Lewis, S.R., Read, P.L. and Forget, F., 2005. The effects of the martian regolith on

1874   GCM water cycle simulations. Icarus, 177(1), pp.174-189.

1875 Bramson, A.M., Byrne, S., Bapst, J., 2017. Preservation of Midlatitude Ice Sheets on Mars.

1876   Journal of Geophysical Research: Planets 122, 2250–2266.

1877   https://doi.org/10.1002/2017JE005357

1878 Bramson, A.M., Byrne, S., Bapst, J., Smith, I.B., McClintock, T., 2019. A Migration Model for the

1879   Polar Spiral Troughs of Mars. Journal of Geophysical Research: Planets.

1880 Brothers, T.C., Holt, J.W., Spiga, A., 2015. Planum Boreum basal unit topography, Mars:

1881   Irregularities and insights from SHARAD. Journal of Geophysical Research: Planets 120,

1882   1357–1375.

1883   Brown, A. J., W. M. Calvin, and S. L. Murchie (2012), Compact Reconnaissance Imaging

1884   Spectrometer for Mars (CRISM) north polar springtime recession mapping: First 3 Mars

1885   years of observations, *Journal of Geophysical Research-Planets*, *117*,

1886   doi:10.1029/2012je004113.

1887   Brown, A. J., Piqueux, S. & Titus, T. N, 2014. Interannual observations and quantification of

1888   summertime H2O ice deposition on the Martian CO2 ice south polar cap. *Earth Planet.*

1889   *Sci. Lett.* **406,** 102–109.

1890   Brown, A. J., W. M. Calvin, P. Becerra, and S. Byrne (2016), Martian north polar cap summer

1891   water cycle, *Icarus*, *277*, 401-415, doi:10.1016/j.icarus.2016.05.007.

1892   Buhler, P.B., Ingersoll, A.P., Ehlmann, B.L., Fassett, C.I., Head, J.W. (2017). How the Martian

1893   Residual South Polar Cap Develops Quasi-Circular and Heart-Shaped Pits, Troughs, and

1894   Moats. Icarus 286, 69-93. doi:10.1016/j.icarus.2017.01.012

1895   Buhler, P. B., Ingersoll, A.P., Piqueux, S., Ehlmann, B.E., Hayne, P.O. (in press). Coevolution of

1896   Mars's atmosphere and massive south polar CO2 ice deposit. Nature

1897   Astronomy. doi:10.1038/s41550-019-0976-8

1898   Buizert, Christo, et al. "Radiometric 81Kr dating identifies 120,000-year-old ice at Taylor Glacier,

1899   Antarctica." Proceedings of the National Academy of Sciences 111.19 (2014): 6876-6881.

1900   Byrne, S., (2004). Internal structure of the Martian south polar layered deposits. J. Geophys.

1901   Res. 109, 43–20. doi:10.1029/2004JE002267

1902   Byrne, S., (2009). The Polar Deposits of Mars. Annu. Rev. Earth Planet. Sci. 37, 535–560.

1903   doi:10.1146/annurev.earth.031208.100101

1904   Byrne, S., Ingersoll, A.P., 2003. A Sublimation Model for Martian South Polar Ice Features.

1905   Science 299, 1051–1053. https://doi.org/10.1126/science.1080148

1906   Calvin, W. M., L. H. Roach, F. P. Seelos, K. D. Seelos, R. O. Green, S. L. Murchie, and J. F. Mustard

1907   (2009), Compact Reconnaissance Imaging Spectrometer for Mars observations of

1908   northern Martian latitudes in summer, *Journal of Geophysical Research-Planets*, *114*,

1909   doi:10.1029/2009je003348.

1910   Calvin, W. et al, 2010. Planetary Science Decadal Survey: Mars Polar Climate Concepts

1911   https://sites.nationalacademies.org/cs/groups/ssbsite/documents/webpage/ssb_05931

1912   2.pdf

1913   Calvin, W. M. P. B. James, B. A. Cantor, and E. M. Dixon (2015), Interannual and seasonal

1914   changes in the north polar ice deposits of Mars: Observations from MY 29-31 using

1915   MARCI, *Icarus*, **251**, 181-190, DOI: 10.1016/j.icarus.2014.08.026

1916   Carsey, F. D., et al, (2005a). NASA Vision Mission: Palmer Quest: Search for Life at the Bed of

1917   the Mars Polar Cap. California Institute of Technology, Jet Propulsion Laboratory.

1918   Carsey, F. D. et al, (2005b). Palmer Quest: A Feasible Nuclear Fission "Vision Mission" To The

1919   Mars Polar Caps. LPSC #1844

1920   Chamberlain, M.A., Boynton, W.V., 2007. Response of Martian ground ice to orbit-induced

1921   climate change. Journal of Geophysical Research: Planets 112.

1922   https://doi.org/10.1029/2006JE002801

1923   Christian, S., Holt, J.W., Byrne, S., Fishbaugh, K.E., 2013. Integrating radar stratigraphy with high

1924   resolution visible stratigraphy of the north polar layered deposits, Mars. ICARUS 226,

1925   1241–1251. doi:10.1016/j.icarus.2013.07.003

1926 Cohen et al. (2014) The Potassium-Argon Laser Experiment (KArLE): In situ geochronology for

1927   Mars and beyond. 8th Int. Conf. on Mars, Pasadena, #1791.

1928 Colaprete, A., Barnes, J.R., Haberle, R.M., Hollingsworth, J.L., Kieffer, H.H., Titus, T.N., 2005.

1929   Albedo of the south pole on Mars determined by topographic forcing of atmosphere

1930   dynamics. Nature 435, 184–188.

1931 Colaprete, A., Barnes, J.R., Haberle, R.M. and Montmessin, F., 2008. CO2 clouds, CAPE and

1932   convection on Mars: Observations and general circulation modeling. Planetary and

1933   Space Science, 56(2), pp.150-180.

1934 Craddock, R.A. and Greeley, R., 2009. Minimum estimates of the amount and timing of gases

1935   released into the martian atmosphere from volcanic eruptions. Icarus, 204(2), pp.512-

1936   526.

1937 Cuffey, K. and W.S.B. Paterson (2010) The Physics of Glaciers, 4th Edition, Academic Press,

1938   Elsevier. 704 pages. Hardcover ISBN: 9780123694614

1939 Cutts, J.A., 1973. Nature and origin of layered deposits of the Martian polar regions. J. Geophys.

1940   Res. Planets 78, 4231–4249. doi:10.1029/JB078i020p04231

1941 Dahl-Jensen, D., Gundestrup, N.S., Miller, H., Watanabe, O., Johnsen, S.J., Steffensen, J.P.,

1942   Clausen, H.B., Svensson, A., Larsen, L.B., (2002). The NorthGRIP deep drilling

1943   programme. Annals of Glaciology 35, 1–4.

1944   https://doi.org/10.3189/172756402781817275

1945 De Sanctis, M.C., Altieri, F., Ammannito, E., Biondi, D., De Angelis, S., Meini, M., Mondello, G.,

1946   Novi, S., Paolinetti, R., Soldani, M., Mugnuolo, R., Pirrotta, S., Vago, J.L., the Ma_MISS

1947   team, (2017). Ma_MISS on ExoMars: Mineralogical Characterization of the Martian

1948   Subsurface. Astrobiology 17, 612–620. https://doi.org/10.1089/ast.2016.1541

1949   Dequaire, J.M., Kahre, M.A., Haberle, R.M. and Hollingsworth, J.L., (2014), July. Radiative Effects

1950   of CO_2 Ice Clouds in the Martian Polar Nights. In Eighth International Conference on

1951   Mars (Vol. 1791, p. 1429).

1952   Diniega, S., Smith, I.B., (in press) High-priority science questions identified at the Mars

1953   Workshop on Amazonian and Present-Day Climate, Planetary and Space Science,

1954   https://doi.org/10.1016/j.pss.2019.104813

1955   Durand, G., and 10 colleagues (2006), Effect of impurities on grain growth in cold ice sheets,

1956   Journal of Geophysical Research (Earth Surface), 111, F01015.

1957   Emmett, J. A., J. R. Murphy (2018), Formation of the Martian Polar Layered Deposits:

1958   Quantifying Polar Water Ice and Dust Surface Deposition During Current and Past

1959   Orbital Epochs with the NASA Ames Mars GCM. Mars Workshop on Amazonian Climate,

1960   Abst. 4006.

1961   EPICA community members. 2004. Eight glacial cycles from an Antarctic ice core. Nature, Vol.

1962   429, p. 623-628, 2004. Doi: https://doi.org/10.1038/nature02599.

1963   Fabel, Derek, et al. (2002) "Landscape preservation under Fennoscandian ice sheets determined

1964   from in situ produced 10 Be and 26 Al." *Earth and Planetary Science Letters* 201.2: 397-

1965   406.

1966   Farley, K. A., et al. "A double-spike method for K–Ar measurement: A technique for high

1967   precision in situ dating on Mars and other planetary surfaces." Geochimica et

1968   Cosmochimica Acta 110 (2013): 1-12.

1969   Farley, K. A., et al. (2014), In Situ Radiometric and Exposure Age Dating of the Martian Surface,

1970   Science, 343(6169), 1247166, doi: 10.1126/science.1247166.

1971   Feldman, W.C., Boynton, W.V., Tokar, R.L., Prettyman, T.H., Gasnault, O., Squyres, S.W., Elphic,

1972   R.C., Lawrence, D.J., Lawson, S.L., Maurice, S., McKinney, G.W., Moore, K.R., Reedy, R.C.,

1973   2002. Global Distribution of Neutrons from Mars: Results from Mars Odyssey. Science

1974   297, 75–78. https://doi.org/10.1126/science.1073541

1975   Fishbaugh, K.E., Head, J.W., 2005. Origin and characteristics of the Mars north polar basal unit

1976   and implications for polar geologic history. Icarus 174, 444–474.

1977   Fishbaugh, K.E., Hvidberg, C.S., 2006. Martian north polar layered deposits stratigraphy:

1978   Implications for accumulation rates and flow. J. Geophys. Res. 111, 26819–21.

1979   doi:10.1029/2005JE002571

1980   Fishbaugh, K.E., Byrne, S., Herkenhoff, K.E., Kirk, R.L., Fortezzo, C., Russell, P.S., McEwen, A.,

1981   2010a. Evaluating the meaning of "layer" in the martian north polar layered deposits

1982   and the impact on the climate connection. ICARUS 205, 269–282.

1983   doi:10.1016/j.icarus.2009.04.011

1984   Fishbaugh, K.E., Hvidberg, C.S., Byrne, S., Russell, P.S., Herkenhoff, K.E., Winstrup, M., Kirk, R.,

1985   2010b. First high-resolution stratigraphic column of the Martian north polar layered

1986   deposits. Geophys. Res. Lett. 37, n/a–n/a. doi:10.1029/2009GL041642

1987   Fisher, D.A., 1993. If Martian Ice Caps Flow: Ablation Mechanisms and Appearance. Icarus 105,

1988   501–511.

1989   Fisher, D.A., 2000. Internal Layers in an "Accublation" Ice Cap: A Test for Flow. Icarus 144, 289–

1990   294.

1991   Fisher, D.A., 2007. Mars' water isotope (D/H) history in the strata of the North Polar Cap:

1992   Inferences about the water cycle. Icarus 187, 430–441.

1993   https://doi.org/10.1016/j.icarus.2006.10.032

1994   Fisher, D.A., Hecht, M.H., Kounaves, S.P., Catling, D.C., 2010. A perchlorate brine lubricated

1995   deformable bed facilitating flow of the north polar cap of Mars: Possible mechanism for

1996   water table recharging. Journal of Geophysical Research: Planets 115.

1997   Forget, F., Pollack, J.B., 1996. Thermal infrared observations of the condensing Martian polar

1998   caps: CO2 ice temperatures and radiative budget. Journal of Geophysical Research:

1999   Planets 101, 16865–16879.

2000   Forget, F., Hourdin, F., Fournier, R., Hourdin, C., Talagrand, O., Collins, M., Lewis, S.R., Read, P.L.

2001   and Huot, J.P., 1999. Improved general circulation models of the Martian atmosphere

2002   from the surface to above 80 km. Journal of Geophysical Research: Planets, 104(E10),

2003   pp.24155-24175.

2004   Forget, F., Haberle, R.M., Montmessin, F., Levrard, B. and Head, J.W., 2006. Formation of

2005   glaciers on Mars by atmospheric precipitation at high obliquity. science, 311(5759),

2006   pp.368-371.

2007   Foss II, F. J., Putzig, N. E., Campbell, B. A., Phillips, R. J., 2017. 3-D Imaging of Mars' Polar Ice

2008   Caps Using Orbital Radar Data. *The Leading Edge* 36(1), 43-57,

2009   doi:10.1190/tle36010043.1.

2010   Gómez-Elvira, J., et al. (2012), REMS: The environmental sensor suite for the Mars Science

2011   Laboratory rover, *Space Sci. Rev., 170,* 583–640.

2012   Gómez-Elvira, J., Armiens, C., Castañer, L., Domínguez, M., Genzer, M., Gómez, F., Haberle, R.,

2013   Harri, A.-M., Jiménez, V., Kahanpää, H., Kowalski, L., Lepinette, A., Martín, J., Martínez-

2014   Frías, J., McEwan, I., Mora, L., Moreno, J., Navarro, S., de Pablo, M.A., Peinado, V., Peña,

2015   A., Polkko, J., Ramos, M., Renno, N.O., Ricart, J., Richardson, M., Rodríguez-Manfredi, J.,

2016   Romeral, J., Sebastián, E., Serrano, J., de la Torre Juárez, M., Torres, J., Torrero, F., Urquí,

2017   R., Vázquez, L., Velasco, T., Verdasca, J., Zorzano, M.-P., Martín-Torres, J., 2012. REMS:

2018   The Environmental Sensor Suite for the Mars Science Laboratory Rover. Space Sci Rev

2019   170, 583–640. https://doi.org/10.1007/s11214-012-9921-1

2020   Gow, A. J. (1969), On the rates of growth of grains and crystals in South Polar firn, Journal of

2021   Glaciology, 8, 241-252.

2022   Grima, C., Kofman, W., Mouginot, J., Phillips, R.J., Hérique, A., Biccari, D., Seu, R., Cutigni, M.,

2023   2009. North polar deposits of Mars: Extreme purity of the water ice. Geophys. Res. Lett.

2024   36, n/a–n/a. doi:10.1029/2008GL036326

2025   Grimm, R.E., Harrison, K.P., Stillman, D.E., Kirchoff, M.R., 2017. On the secular retention of

2026   ground water and ice on Mars. Journal of Geophysical Research: Planets 122, 94–109.

2027   https://doi.org/10.1002/2016JE005132

2028   Guo, X., Lawson, W.G., Richardson, M.I. and Toigo, A., 2009. Fitting the Viking lander surface

2029   pressure cycle with a Mars General Circulation Model. Journal of Geophysical Research:

2030   Planets, 114(E7).

2031   Haberle, R., Kahre M. A. (2010). Detecting secular climate change on Mars. Mars 5, 68–75.

2032   https://doi.org/10.1555/mars.2010.0003

2033   Haberle, R.M., Murphy, J.R. and Schaeffer, J., (2003). Orbital change experiments with a Mars

2034   general circulation model. Icarus, 161(1), pp.66-89.

2035   Haberle, R.M., Forget, F., Colaprete, A., Schaeffer, J., Boynton, W.V., Kelly, N.J. and

2036   Chamberlain, M.A., 2008. The effect of ground ice on the Martian seasonal CO_2

2037   cycle. Planetary and Space Science, 56(2), pp.251-255.

2038   Haberle, R.M., Kahre, M.A., Schaeffer, J.R., Montmessin, F. and Phillips, R.J., 2012. A cloud

2039   greenhouse effect on Mars: Significant climate change in the recent past.

2040   Haberle, R.M., Juárez, M. de la T., Kahre, M.A., Kass, D.M., Barnes, J.R., Hollingsworth, J.L.,

2041   Harri, A.-M., Kahanpää, H., 2018. Detection of Northern Hemisphere transient eddies at

2042   Gale Crater Mars. Icarus 307, 150–160. https://doi.org/10.1016/j.icarus.2018.02.013

2043   Hamilton, V. E., H. Y. Mcsween, and B. Hapke (2005), Mineralogy of Martian atmospheric dust

2044   inferred from thermal infrared spectra of aerosols,, 110, 12006,

2045   doi:10.1029/2005JE002501.

2046   Hayne, P.O., Paige, D.A. , Heavens, N.G. Mars Climate Sounder Science Team, 2014. The role of

2047   snowfall in forming the seasonal ice caps of Mars: Models and constraints from the

2048   Mars Climate Sounder. Icarus 231, 122–130.

2049   Head, J.W., Mustard, J.F., Kreslavsky, M.A., Milliken, R.E., Marchant, D.R., 2003. Recent ice ages

2050   on Mars. Nature 426, 797–802.

2051   Hecht, M. H., 2006. CHRONOS: A journey through martian history. Fourth International Mars

2052   Polar Science Conference, #8096

2053   Hecht, M. H. and R. S. Saunders, 2003. Cryoscout: A Descent Through The Mars Polar Cap. Third

2054   International Mars Polar Science Conference, #8078

2055 Hecht, M.H., Kounaves, S.P., Quinn, R.C., West, S.J., Young, S.M.M., Ming, D.W., Catling, D.C.,

2056   Clark, B.C., Boynton, W.V., Hoffman, J., DeFlores, L.P., Gospodinova, K., Kapit, J., Smith,

2057   P.H., 2009. Detection of Perchlorate and the Soluble Chemistry of Martian Soil at the

2058   Phoenix Lander Site. Science 325, 64–67. https://doi.org/10.1126/science.1172466

2059 Herkenhoff, K., Plaut, J.G., 2000. Surface Ages and Resurfacing Rates of the Polar Layered

2060   Deposits on Mars. Icarus 144, 243–253. https://doi.org/10.1006/icar.1999.6287

2061 Herkenhoff, K.E., Byrne, S., Russell, P.S., Fishbaugh, K.E., McEwen, A.S., 2007. Meter-Scale

2062   Morphology of the North Polar Region of Mars. Science 317, 1711–1715.

2063   doi:10.1126/science.1143544

2064 Herny, C., Massé, M., Bourgeois, O., Carpy, S., Le Mouélic, S., Appéré, T., Smith, I.B., Spiga, A.,

2065   Rodriguez, S., 2014. Sedimentation waves on the Martian North Polar Cap: analogy with

2066   megadunes in Antarctica. Earth and Planetary Science Letters 403, 56–66.

2067   https://doi.org/10.1016/j.epsl.2014.06.033

2068 Herr, K.C. and G.C. Pimentel, Infrared absorptions near 3 microns recorded over the polar cap

2069   of Mars, Science, 166, 496-499, 1969.

2070 Hess, S. L., R. M. Henry, C. B. Leovy, J. A. Ryan, and J. E. Tillman (1977), Meteorological results

2071   from the surface of Mars: Viking 1 and 2, J. Geophys. Res., 82, 4559–4574.

2072 Holt, J.W., Fishbaugh, K.E., Byrne, S., Christian, S., Tanaka, K., Russell, P.S., Herkenhoff, K.E.,

2073   Safaeinili, A., Putzig, N.E., Phillips, R.J., 2010. The construction of Chasma Boreale on

2074   Mars. Nature 465, 446–449. doi:10.1038/nature09050

2075 Horgan, B., and J. F. Bell (2012), Widespread weathered glass on the surface of Mars, Geology,

2076   40(5), 391-394, doi:10.1130/g32755.1.

2077 Horgan, B. H., J. F. Bell, E. Z. Noe Dobrea, E. A. Cloutis, D. T. Bailey, M. A. Craig, L. H. Roach, and

2078 J. F. Mustard (2009), Distribution of hydrated minerals in the north polar region of Mars,

2079 Journal of Geophysical Research: Planets, 114(E1), 27, doi:10.1029/2008JE003187.

2080 Horgan, B. H. N., E. A. Cloutis, P. Mann, and J. F. Bell (2014), Near-infrared spectra of ferrous

2081 mineral mixtures and methods for their identification in planetary surface spectra,

2082 Icarus, 234, 132–154, doi:10.1016/j.icarus.2014.02.031.

2083 Howard, A.D., Cutts, J.A., Blasius, K.R., 1982. Stratigraphic relationships within Martian polar

2084 cap deposits. Icarus 50, 161–215.

2085 Howard, A.D., 2000. The Role of Eolian Processes in Forming Surface Features of the Martian

2086 Polar Layered Deposits. Icarus 144, 267–288.

2087 Hvidberg, C.S., Fishbaugh, K.E., Winstrup, M., Svensson, A., Byrne, S., Herkenhoff, K.E., 2012.

2088 Reading the climate record of the martian polar layered deposits. ICARUS 221, 405–419.

2089 doi:10.1016/j.icarus.2012.08.009

2090 Hvidberg, C.S., Svensson, A., Buchardt, S.L., (2013). Ice dynamcis of the Greenland Ice Sheet, in:

2091 Encyclopedia of Quaternary Science, 2nd Edition (Eds. Scott Elias and Cary Mock).

2092 ICESAG (2019), Report from the Ice and Climate Evolution Science Analysis group (ICE-SAG),

2093 Mars Exploration Program Analysis Group Topical Analysis Reports

2094 Iverson, N.A., Lieb-Lappen, R., Dunbar, N.W., Obbard, R., Kim, E., Golden, E., 2017. The first

2095 physical evidence of subglacial volcanism under the West Antarctic Ice Sheet. Scientific

2096 Reports 7, 11457. https://doi.org/10.1038/s41598-017-11515-3

2097 Jakosky, B., Phillips, R. Mars' volatile and climate history. Nature 412, 237–244 (2001)

2098 doi:10.1038/35084184

2099   James, P.B., North, G.R., 1982. The seasonal CO2 cycle on Mars: An application of an energy

2100   balance climate model. Journal of Geophysical Research: Solid Earth 87, 10271–10283.

2101   https://doi.org/10.1029/JB087iB12p10271

2102   James, P.B., H.H. Kieffer and D.A. Paige, Seasonal cycle of carbon dioxide on Mars, in Mars, Ed.

2103   H.H. Kieffer et al., pp. 934-968, Univ. of AZ Press, 1992.

2104   Kadish, S.J., Head, J.W., Barlow, N.G. and Marchant, D.R., 2008. Martian pedestal craters:

2105   Marginal sublimation pits implicate a climate‐related formation

2106   mechanism. Geophysical Research Letters, 35(16).

2107   Kahre, M.A., Murphy, J.R. and Haberle, R.M., 2006. Modeling the Martian dust cycle and

2108   surface dust reservoirs with the NASA Ames general circulation model. Journal of

2109   Geophysical Research: Planets, 111(E6).

2110   Kahre, M.A., Haberle, R.M., Hollingsworth, J.L. and Wilson, R.J., 2018. Could a Significant Water

2111   Ice Cloud Greenhouse Have Persisted Throughout Much of the Amazonian?. LPI

2112   Contributions, 2086.

2113   Karlsson, N. B., J. W. Holt, and R. C. A. Hindmarsh (2011), Testing for flow in the north polar

2114   layered deposits of Mars using radar stratigraphy and a simple 3D ice-flow model,

2115   Geophys. Res. Lett., 38, L24204

2116   Karlsson, N.B., Schmidt, L.S., Hvidberg, C.S., 2015. Volume of Martian mid-latitude glaciers from

2117   radar observations and ice-flow modelling. Geophys. Res. Lett. 2015GL063219.

2118   https://doi.org/10.1002/2015GL063219

2119   Kieffer, H. H. (1990), H_2O grain size and the amount of dust in Mars' residual north polar CAP, J.

2120   Geophys. Res., 95, 1481-1493.

2121   Kleinböhl, A., J. T. Schofield, D. M. Kass, W. A. Abdou, C. R. Backus, B. Sen, J. H. Shirley,W. G.

2122   Lawson, M. I. Richardson, F. W. Taylor, N. A. Teanby, and D. J. McCleese (2009), Mars

2123   Climate Sounder limb profile retrieval of atmospheric temperature, pressure, dust and

2124   water ice opacity, *J. Geophys. Res., 114,* E10006, doi:10.1029/2009JE003358.

2125   Kleinböhl, A., A. J. Friedson, J. T. Schofield (2017) , Two-dimensional radiative transfer for the

2126   retrieval of limb emission measurements in the martian atmosphere, *J. Quant.*

2127   *Spectrosc. Rad. Transfer, 187,* 511–522.

2128   Koenig, L.S., Ivanoff, A., Alexander, P.M., MacGregor, J.A., Fettweis, X., Panzer, B., Paden, J.D.,

2129   Forster, R.R., Das, I., McConnell, J.R., Tedesco, M., Leuschen, C., Gogineni, P., 2016.

2130   Annual Greenland accumulation rates (2009–2012) from airborne snow radar. The

2131   Cryosphere 10, 1739–1752. https://doi.org/10.5194/tc-10-1739-2016

2132   Koutnik, M., Byrne, S., Murray, B., 2002. South Polar Layered Deposits of Mars: The cratering

2133   record. J. Geophys. Res. Planets 107, 5100–1. doi:10.1029/2001JE001805

2134   Lalich, D.E., Holt, J.W., 2017. New Martian climate constraints from radar reflectivity within the

2135   north polar layered deposits. Geophys. Res. Lett. 44, 657–664.

2136   doi:10.1002/2016GL071323

2137   Lambert, F., Delmonte, B., Petit, J.R., Bigler, M., Kaufmann, P.R., Hutterli, M.A., Stocker, T.F.,

2138   Ruth, U., Steffensen, J.P., Maggi, V., (2008). Dust-climate couplings over the past

2139   800,000 years from the EPICA Dome C ice core. Nature 452, 616–619.

2140   https://doi.org/10.1038/nature06763

2141 Landis, M.E., Byrne, S., Daubar, I.J., Herkenhoff, K.E., Dundas, C.M., 2016. A revised surface age

2142   for the North Polar Layered Deposits of Mars. Geophys. Res. Lett. 43, 3060–3068.

2143   doi:10.1002/2016GL068434

2144 Langevin, Y., F. Poulet, J. P. Bibring, and B. Gondet (2005), Summer evolution of the north polar

2145   cap of Mars as observed by OMEGA/Mars express, *Science*, *307*(5715), 1581-1584.

2146 Langevin, Y., Bibring, J.-P., Montmessin, F., Forget, F., Vincendon, M., Douté, S., Poulet, F.,

2147   Gondet, B., 2007. Observations of the south seasonal cap of Mars during recession in

2148   2004–2006 by the OMEGA visible/near-infrared imaging spectrometer on board Mars

2149   Express. Journal of Geophysical Research: Planets 112.

2150   https://doi.org/10.1029/2006JE002841

2151 Laskar, J., Correia, A.C.M., Gastineau, M., Joutel, F., Levrard, B., Robutel, P., 2004. Long term

2152   evolution and chaotic diffusion of the insolation quantities of Mars. ICARUS 170, 343–

2153   364. doi:10.1016/j.icarus.2004.04.005

2154 Laskar, J., Levrard, B., Mustard, J.F., 2002. Orbital forcing of the martian polar layered deposits.

2155   Nature 419, 375–377. doi:10.1038/nature01066

2156 Leighton, R.R. and B.C. Murray, Behavior of carbon dioxide and other volatiles on Mars, *Science,*

2157   *153,* 136-144, 1966.

2158 Levrard, B., Forget, F., Montmessin, F., Laskar, J., 2007. Recent formation and evolution of

2159   northern Martian polar layered deposits as inferred from a Global Climate Model. J.

2160   Geophys. Res. 112, 5044–18. doi:10.1029/2006JE002772

2161 Levy, J.S., Fassett, C.I., Head, J.W., Schwartz, C., Watters, J.L., 2014. Sequestered glacial ice

2162   contribution to the global Martian water budget: Geometric constraints on the volume

2163   of remnant, midlatitude debris-covered glaciers. J. Geophys. Res. Planets 119,

2164   2014JE004685. https://doi.org/10.1002/2014JE004685

2165 Limaye, A.B.S., Aharonson, O., Perron, J.T., 2012. Detailed stratigraphy and bed thickness of the

2166   Mars north and south polar layered deposits. J. Geophys. Res. 117, n/a–n/a.

2167   doi:10.1029/2011JE003961

2168 Listowski, C., Määttänen, A., Riipinen, I., Montmessin, F. and Lefèvre, F., 2013. Near-pure vapor

2169   condensation in the Martian atmosphere: CO_2 ice crystal growth. Journal of Geophysical

2170   Research: Planets, 118(10), pp.2153-2171.

2171 MacGregor, J. A., M. A. Fahnestock, G. A. Catania, J. D. Paden, S. P. Gogineni, S. K. Young, S. C.

2172   Rybarski, A. N. Mabrey, B. M. Wagman, and M. Morlighem (2015), Radiostratigraphy

2173   and age structure of the Greenland Ice Sheet, J. Geophys. Res. Earth Surf., 120,

2174   doi:10.1002/2014JF003215.Massé, M., O. Bourgeois, S. Le Mouélic, C. Verpoorter, L. Le

2175   Deit, and J.-P. Bibring (2010), Martian polar and circum-polar sulfate-bearing deposits:

2176   Sublimation tills derived from the North Polar Cap, Icarus, 209(2), 434–451,

2177   doi:10.1016/j.icarus.2010.04.017.

2178 Madeleine, J.B., Forget, F., Head, J.W., Levrard, B., Montmessin, F. and Millour, E., 2009.

2179   Amazonian northern mid-latitude glaciation on Mars: A proposed climate

2180   scenario. Icarus, 203(2), pp.390-405.

2181 Madeleine, J.B., Head, J.W., Forget, F., Navarro, T., Millour, E., Spiga, A., Colaïtis, A., Määttänen,

2182   A., Montmessin, F. and Dickson, J.L., 2014. Recent ice ages on Mars: the role of

2183   radiatively active clouds and cloud microphysics. Geophysical Research Letters, 41(14),

2184   pp.4873-4879.

2185   Malin, M.C., Carr, M.H., Danielson, G.E., Davies, M.E., Hartmann, W.K., Ingersoll, A.P., James,

2186   P.B., Masursky, H., McEwen, A.S., Soderblom, L.A., Thomas, P., Veverka, J., Caplinger,

2187   M.A., Ravine, M.A., Soulanille, T.A., Warren, J.L., 1998. Early Views of the Martian

2188   Surface from the Mars Orbiter Camera of Mars Global Surveyor. Science 279, 1681–

2189   1685. https://doi.org/10.1126/science.279.5357.1681

2190   Malin, M.C., Edgett, K.S., 2001. Mars Global Surveyor Mars Orbiter Camera: Interplanetary

2191   cruise through primary mission. Journal of Geophysical Research: Planets 106, 23429–

2192   23570. https://doi.org/10.1029/2000JE001455

2193   Manning, C.V., McKay, C.P., Zahnle, K.J., (2006). Thick and thin models of the evolution of

2194   carbon dioxide on Mars. Icarus 180, 38–59.

2195   Manning, C.V., Bierson, C., Putzig, N.E., McKay, C.P., (2019). The formation and stability of

2196   buried polar CO2 deposits on Mars. Icarus 317, 509–517.

2197   https://doi.org/10.1016/j.icarus.2018.07.021

2198   Massé, M., Bourgeois, O., Le Mouélic, S., Verpoorter, C., Spiga, A., Le Deit, L., 2012. Wide

2199   distribution and glacial origin of polar gypsum on Mars. Earth and Planetary Science

2200   Letters 317–318, 44–55. https://doi.org/10.1016/j.epsl.2011.11.035

2201   McCleese, D.J., Heavens, N.G., Schofield, J.T., Abdou, W.A., Bandfield, J.L., Calcutt, S.B., Irwin,

2202   P.G.J., Kass, D.M., Kleinböhl, A., Lewis, S.R., Paige, D.A., Read, P.L., Richardson, M.I.,

2203   Shirley, J.H., Taylor, F.W., Teanby, N., Zurek, R.W., 2010. Structure and dynamics of the

2204   Martian lower and middle atmosphere as observed by the Mars Climate Sounder:

2205   Seasonal variations in zonal mean temperature, dust, and water ice aerosols. J.

2206   Geophys. Res. 115, E12016. https://doi.org/10.1029/2010JE003677

2207   McEwen, A.S., Eliason, E.M., Bergstrom, J.W., Bridges, N.T., Hansen, C.J., Delamere, W.A., Grant,

2208   J.A., Gulick, V.C., Herkenhoff, K.E., Keszthelyi, L., Kirk, R.L., Mellon, M.T., Squyres, S.W.,

2209   Thomas, N., Weitz, C.M., 2007. Mars Reconnaissance Orbiter's High Resolution Imaging

2210   Science Experiment (HiRISE). J. Geophys. Res. 112, 8048–40. doi:10.1029/2005JE002605

2211   Medley, B., Joughin, I., Smith, B.E., Das, S.B., Steig, E.J., Conway, H., Gogineni, S., Lewis, C.,

2212   Criscitiello, A.S., McConnell, J.R., van den Broeke, M.R., Lenaerts, J.T.M., Bromwich, D.H.,

2213   Nicolas, J.P., Leuschen, C., 2014. Constraining the recent mass balance of Pine Island and

2214   Thwaites glaciers, West Antarctica, with airborne observations of snow accumulation.

2215   The Cryosphere 8, 1375–1392. https://doi.org/10.5194/tc-8-1375-2014

2216   Mellon, M.T., Boynton, W.V., Feldman, W.C., Arvidson, R.E., Titus, T.N., Bandfield, J.L., Putzig,

2217   N.E., Sizemore, H.G., (2018). A prelanding assessment of the ice table depth and ground

2218   ice characteristics in Martian permafrost at the Phoenix landing site. Journal of

2219   Geophysical Research: Planets. https://doi.org/10.1029/2007JE003067@10.1002/(ISSN)2169-

2220   9100.PHOENIX1

2221   Mischna, M.A., Richardson, M.I., 2005. A reanalysis of water abundances in the Martian

2222   atmosphere at high obliquity. Geophysical Research Letters 32.

2223   https://doi.org/10.1029/2004GL021865

2224   Milkovich, S.M., Head, J.W., 2005. North polar cap of Mars: Polar layered deposit

2225   characterization and identification of a fundamental climate signal. J. Geophys. Res 110,

2226   140–21. doi:10.1029/2004JE002349

2227 Milkovich, S.M., Plaut, J.J., 2008. Martian South Polar Layered Deposit stratigraphy and

2228   implications for accumulation history. J. Geophys. Res. 113, 6983–17.

2229   doi:10.1029/2007JE002987

2230 Milkovich, S.M., Plaut, J.J., Safaeinili, A., Picardi, G., Seu, R., Phillips, R.J., 2009. Stratigraphy of

2231   Promethei Lingula, south polar layered deposits, Mars, in radar and imaging data sets. J.

2232   Geophys. Res. 114, 420–21. doi:10.1029/2008JE003162

2233 Mischna, M.A., Richardson, M.I., Wilson, R.J. and McCleese, D.J., 2003. On the orbital forcing of

2234   Martian water and CO_2 cycles: A general circulation model study with simplified volatile

2235   schemes. Journal of Geophysical Research: Planets, 108(E6).

2236 Montabone, L., Forget, F., Millour, E., Wilson, R.J., Lewis, S.R., Cantor, B., Kass, D., Kleinböhl, A.,

2237   Lemmon, M.T., Smith, M.D., others, 2015. Eight-year climatology of dust optical depth

2238   on Mars. Icarus 251, 65–95.

2239 Montmessin, F., Rannou, P. and Cabane, M., (2002) New insights into Martian dust distribution

2240   and water-ice cloud microphysics. Journal of Geophysical Research: Planets, 107(E6).

2241 Montmessin, F., Forget, F., Rannou, P., Cabane, M. and Haberle, R.M., (2004) Origin and role of

2242   water ice clouds in the Martian water cycle as inferred from a general circulation

2243   model. Journal of Geophysical Research: Planets, 109(E10).

2244 Montmessin, F., T. Fouchet, and F. Forget (2005), Modeling the annual cycle of HDO in the

2245   Martian atmosphere, J. Geophys. Res., 110, E03006, doi:10.1029/2004JE002357.

2246 Montmessin, F., Haberle, R.M., Forget, F., Langevin, Y., Clancy, R.T. and Bibring, J.P., 2007. On

2247   the origin of perennial water ice at the south pole of Mars: A precession-controlled

2248   mechanism?. Journal of Geophysical Research: Planets, 112(E8).

2249   Morris, R. V. et al. (2004), Mineralogy at Gusev Crater from the Mössbauer Spectrometer on the

2250   Spirit Rover, Science, 305(5), 833–837, doi:10.1126/science.1100020.

2251   Murchie, S., Arvidson, R., Bedini, P., Beisser, K., Bibring, J.-P., Bishop, J., Boldt, J., Cavender, P.,

2252   Choo, T., Clancy, R.T., Darlington, E.H., Des Marais, D., Espiritu, R., Fort, D., Green, R.,

2253   Guinness, E., Hayes, J., Hash, C., Heffernan, K., Hemmler, J., Heyler, G., Humm, D.,

2254   Hutcheson, J., Izenberg, N., Lee, R., Lees, J., Lohr, D., Malaret, E., Martin, T., McGovern,

2255   J.A., McGuire, P., Morris, R., Mustard, J., Pelkey, S., Rhodes, E., Robinson, M., Roush, T.,

2256   Schaefer, E., Seagrave, G., Seelos, F., Silverglate, P., Slavney, S., Smith, M., Shyong, W.-J.,

2257   Strohbehn, K., Taylor, H., Thompson, P., Tossman, B., Wirzburger, M., Wolff, M., 2007.

2258   Compact Reconnaissance Imaging Spectrometer for Mars (CRISM) on Mars

2259   Reconnaissance Orbiter (MRO). J. Geophys. Res. 112, E05S03.

2260   https://doi.org/10.1029/2006JE002682

2261   Murray, B.C., Soderblom, L.A., Cutts, J.A., Sharp, R.P., Milton, D.J., Leighton, R.B., 1972.

2262   Geological framework of the south polar region of Mars. Icarus 17, 328–345.

2263   National Research Council (2011). Vision and Voyages for PLanetary Science in the Decade

2264   2013-2022. Washington, DC: The National Academies Press.

2265   Navarro, T., Madeleine, J.B., Forget, F., Spiga, A., Millour, E., Montmessin, F. and Määttänen, A.,

2266   2014. Global climate modeling of the Martian water cycle with improved microphysics

2267   and radiatively active water ice clouds. Journal of Geophysical Research: Planets, 119(7),

2268   pp.1479-1495.

2269   Navarro, T., Forget, F., Millour, E., Greybush, S.J., Kalnay, E., Miyoshi, T., 2017. The Challenge of

2270   Atmospheric Data Assimilation on Mars. Earth and Space Science 4, 690–722.

2271   https://doi.org/10.1002/2017EA000274

2272   NEEM Community members. 2013. Eemian interglacial reconstructed from a Greenland folded

2273   ice core. Nature, 493, 489-494, doi:10.1038/nature11789.

2274   Nerozzi, S., W Holt, J., 2017. Earliest accumulation history of the north polar layered deposits,

2275   Mars from SHARAD. ICARUS. doi:10.1016/j.icarus.2017.05.027

2276   Nerozzi, S., Holt, J.W., 2019. Buried Ice and Sand Caps at the North Pole of Mars: Revealing a

2277   Record of Climate Change in the Cavi Unit With SHARAD. Geophysical Research Letters

2278   46, 7278–7286. https://doi.org/10.1029/2019GL082114

2279   Newman, C.E., Lewis, S.R., Read, P.L. and Forget, F., 2002. Modeling the Martian dust cycle 2.

2280   Multiannual radiatively active dust transport simulations. Journal of Geophysical

2281   Research: Planets, 107(E12), pp.7-1.

2282   Newman, C.E., Lewis, S.R. and Read, P.L., 2005. The atmospheric circulation and dust activity in

2283   different orbital epochs on Mars. Icarus, 174(1), pp.135-160.

2284   Nunes, D.C., Phillips, R.J., 2006. Radar subsurface mapping of the polar layered deposits on

2285   Mars. J. Geophys. Res. 111, 5042–16. doi:10.1029/2005JE002609

2286   Nunes, D.C., Smrekar, S.E., Fisher, B., Plaut, J.J., Holt, J.W., Head, J.W., Kadish, S.J., Phillips, R.J.,

2287   2011. Shallow Radar (SHARAD), pedestal craters, and the lost Martian layers: Initial

2288   assessments. Journal of Geophysical Research: Planets 116.

2289   https://doi.org/10.1029/2010JE003690

2290   Obbard, R., I. Baker, and K. Sieg (2006), Using electron backscatter diffraction patterns to

2291   examine recrystallization in polar ice sheets, Journal of Glaciology, 52, 546-557.

2292   Orosei, R., Lauro, S.E., Pettinelli, E., Cicchetti, A., Coradini, M., Cosciotti, B., Paolo, F.D., Flamini,

2293   E., Mattei, E., Pajola, M., Soldovieri, F., Cartacci, M., Cassenti, F., Frigeri, A., Giuppi, S.,

2294   Martufi, R., Masdea, A., Mitri, G., Nenna, C., Noschese, R., Restano, M., Seu, R., 2018.

2295   Radar evidence of subglacial liquid water on Mars. Science 361, 490–493.

2296   https://doi.org/10.1126/science.aar7268

2297   Pathare, A.V., Paige, D.A., 2005. The effects of martian orbital variations upon the sublimation

2298   and relaxation of north polar troughs and scarps. Icarus 174, 419–443.

2299   Perron, J.T., Huybers, P., 2009. Is there an orbital signal in the polar layered deposits on Mars?

2300   Geology 37, 155–158. doi:10.1130/G25143A.1

2301   Piqueux, S., Kleinbohl, A., Hayne, P. O., Kass, D. M., Schofield, J. T., McCleese, D. J., 2015.

2302   Variability of the Martian seasonal CO_2 cap extent over eight Mars Years. Icarus. 251**,**

2303   164-180.

2304   Phillips, R.J., Davis, B.J., Tanaka, K.L., Byrne, S., Mellon, M.T., Putzig, N.E., Haberle, R.M., Kahre,

2305   M.A., Campbell, B.A., Carter, L.M., Smith, I.B., Holt, J.W., Smrekar, S.E., Nunes, D.C.,

2306   Plaut, J.J., Egan, A.F., Titus, T.N., Seu, R., 2011. Massive CO_2 Ice Deposits Sequestered in

2307   the South Polar Layered Deposits of Mars. Science 332, 838–.

2308   doi:10.1126/science.1203091

2309   Phillips, R.J., Zuber, M.T., Smrekar, S.E., Mellon, M.T., Head, J.W., Tanaka, K.L., Putzig, N.E.,

2310   Milkovich, S.M., Campbell, B.A., Plaut, J.J., Safaeinili, A., Seu, R., Biccari, D., Carter, L.M.,

2311   Picardi, G., Orosei, R., Mohit, P.S., Heggy, E., Zurek, R.W., Egan, A.F., Giacomoni, E.,

2312   Russo, F., Cutigni, M., Pettinelli, E., Holt, J.W., Leuschen, C.J., Marinangeli, L., 2008. Mars

2313   North Polar Deposits: Stratigraphy, Age, and Geodynamical Response. Science 320,

2314   1182–1185. doi:10.1126/science.1157546

2315   Picardi, G., Biccari, D., Seu, R., Marinangeli, L., Johnson, W.T.K., Jordan, R.L., Plaut, J., Safaenili,

2316   A., Gurnett, D.A., Ori, G.G., Orosei, R., Calabrese, D., Zampolini, E., 2004. Performance

2317   and surface scattering models for the Mars Advanced Radar for Subsurface and

2318   Ionosphere Sounding (MARSIS). Planetary and Space Science 52, 149–156.

2319   doi:10.1016/j.pss.2003.08.020

2320   Plaut, J.J., Picardi, G., Safaeinili, A., Ivanov, A.B., Milkovich, S.M., Cicchetti, A., Kofman, W.,

2321   Mouginot, J., Farrell, W.M., Phillips, R.J., Clifford, S.M., Frigeri, A., Orosei, R., Federico,

2322   C., Williams, I.P., Gurnett, D.A., Nielsen, E., Hagfors, T., Heggy, E., Stofan, E.R.,

2323   Plettemeier, D., Watters, T.R., Leuschen, C.J., Edenhofer, P., 2007. Subsurface Radar

2324   Sounding of the South Polar Layered Deposits of Mars. Science 316, 92–95.

2325   doi:10.1126/science.1139672

2326   Putzig, N.E., Mellon, M.T., 2007. Apparent thermal inertia and the surface heterogeneity of

2327   Mars. Icarus 191, 68–94. https://doi.org/10.1016/j.icarus.2007.05.013

2328   Putzig, N.E., Phillips, R.J., Campbell, B.A., Holt, J.W., Plaut, J.J., Carter, L.M., Egan, A.F.,

2329   Bernardini, F., Safaeinili, A., Seu, R., 2009. Subsurface structure of Planum Boreum from

2330   Mars Reconnaissance Orbiter Shallow Radar soundings. ICARUS 204, 443–457.

2331   doi:10.1016/j.icarus.2009.07.034

2332   Putzig, N.E., Mellon, M.T., Herkenhoff, K.E., Phillips, R.J., Davis, B.J., Ewer, K.J., Bowers, L.M.,

2333   2014. Thermal behavior and ice-table depth within the north polar erg of Mars. Icarus,

2334   Third Planetary Dunes Systems 230, 64–76.

2335   https://doi.org/10.1016/j.icarus.2013.07.010

2336   Putzig, N.E., Smith, I.B., Perry, M.R., Foss, F.J., Campbell, B.A., Phillips, R.J., Seu, R., 2018. Three-

2337   dimensional radar imaging of structures and craters in the Martian polar caps. Icarus,

2338   Mars Polar Science VI 308, 138–147. https://doi.org/10.1016/j.icarus.2017.09.023

2339   Qie, L., Lin, Y., Connell, J.W., Xu, J., Dai, L., 2017. Highly Rechargeable Lithium-CO2 Batteries

2340   with a Boron-and Nitrogen-Codoped Holey-Graphene Cathode. Angewandte Chemie

2341   International Edition 56, 6970–6974.

2342   Rinterknecht, V. R., et al. "The last deglaciation of the southeastern sector of the Scandinavian

2343   Ice Sheet." Science311.5766 (2006): 1449-1452.

2344   Ruddiman, W.F., (2006). Orbital changes and climate. Quaternary Science Reviews 25, 3092–

2345   3112.Russell, P., Thomas, N., Byrne, S., Herkenhoff, K., Fishbaugh, K., Bridges, N., Okubo,

2346   C., Milazzo, M., Daubar, I., Hansen, C., McEwen, A., 2008. Seasonally active frost-dust

2347   avalanches on a north polar scarp of Mars captured by HiRISE. Geophysical Research

2348   Letters 35. https://doi.org/10.1029/2008GL035790

2349   Schenk, P.M., Moore, J.M., 2000. Stereo topography of the south polar region of Mars: Volatile

2350   inventory and Mars Polar Lander landing site. J. Geophys. Res. 105, 24529–24546.

2351   doi:10.1029/1999JE001054

2352   Schmidt, F., et al., 2009. Albedo control of seasonal south polar cap recession on Mars. Icarus

2353   200, 374–394.

2354   Seu, R., Phillips, R.J., Biccari, D., Orosei, R., Masdea, A., Picardi, G., Safaeinili, A., Campbell, B.A.,

2355   Plaut, J.J., Marinangeli, L., Smrekar, S.E., Nunes, D.C., 2007. SHARAD sounding radar on

2356   the Mars Reconnaissance Orbiter. J. Geophys. Res. 112, 8073–18.

2357   doi:10.1029/2006JE002745

2358   Simonsen, S. B., L. Stenseng, G. Adalgeirsdottir, R. S. Fausto, and C. S. Hvidberg (2013) Assessing

2359   a multi-layered dynamic firn-compaction model for Greenland with ASIRAS radar

2360   measurements. Journal of Glaciology, 59(215), 545-558, doi: 10.3189/2013JoG12J158.

2361   Sinha, P., Horgan, B., Seelos, F., 2019. Dateable Volcanic and Impact Sediments within the North

2362   Polar Layered Deposits on Mars, in: Lunar and Planetary Science Conference. Abst 2132.

2363   Smith, D.E., Zuber, M.T., Frey, H.V., Garvin, J.B., Head, J.W., Muhleman, D.O., Pettengill, G.H.,

2364   Phillips, R.J., Solomon, S.C., Zwally, H.J., 2001. Mars Orbiter Laser Altimeter: Experiment

2365   summary after the first year of global mapping of Mars (Paper 2000JE001364). JOURNAL

2366   OF GEOPHYSICAL RESEARCH-ALL SERIES- 106, 23–689.

2367   Smith, M. D. (2008), Spacecraft observations of the Martian atmosphere, *Annual Review of*

2368   *Earth and Planetary Sciences*, *36*, 191-219,

2369   doi:10.1146/annurev.earth.36.031207.124335.

2370   Smith, I. B., and J. W. Holt (2010), Onset and migration of spiral troughs on Mars revealed by

2371   orbital radar,, 465(7297), 450–453, doi:10.1038/nature09049.

2372   Smith, I.B., Holt, J.W., (2015). Spiral trough diversity on the north pole of Mars, as seen by

2373   Shallow Radar (SHARAD). J. Geophys. Res. Planets 120, 362–387.

2374   doi:10.1002/2014JE004720

2375   Smith, I.B., Holt, J.W., Spiga, A., Howard, A.D., Parker, G., (2013). The spiral troughs of Mars as

2376   cyclic steps. Journal of Geophysical Research: Planets.

2377   https://doi.org/10.1002/jgre.20142

2378   Smith, I.B., Putzig, N.E., Holt, J.W., Phillips, R.J., (2016). An ice age recorded in the polar deposits

2379   of Mars. Science 352, 1075–1078. doi:10.1126/science.aad6968

2380   Smith, I.B., Diniega, S., Beaty, D.W., Thorsteinsson, T., Becerra, P., Bramson, A.M., Clifford, S.M.,

2381   Hvidberg, C.S., Portyankina, G., Piqueux, S., Spiga, A., Titus, T.N., (2018). 6th

2382   international conference on Mars polar science and exploration: Conference summary

2383   and five top questions. *Icarus*. doi:10.1016/j.icarus.2017.06.027

2384   Staehle, Robert L., "Mars Polar Ice Sample Return Mission" (Part 1), *Spaceflight*, November

2385   1976.

2386   Staehle, Robert L, Sheryl A. Fine, Andrew Roberts, Carl R. Schulenberg & David L. Skinner, "Mars

2387   Polar Ice Sample Return Mission" (Parts 2 & 3), *Spaceflight*, November & December

2388   1977.

2389   Steffensen, J.P., K.K. Andersen, M. Bigler, H.B. Clausen, D. Dahl-Jensen, H. Fischer, K. Goto-

2390   Azuma, M. Hansson, S.J. Johnsen, J. Jouzel, V. Masson-Delmotte, T. Popp, S.O.

2391   Rasmussen, R. Röthlisberger, U. Ruth, B. Stauffer, M.-L. Siggaard-Andersen, A.E.

2392   Sveinbjörnsdóttir, A. Svensson, J.W.C. White. (2008). High resolution Greenland ice core

2393   data show abrupt climate change happens in few years. Science, 321, 5889, 680-684.

2394   DOI: 10.1126/science.1157707.

2395   Sori, M. M., S. Byrne, C. W. Hamilton, and M. E. Landis (2016), Viscous flow rates of icy

2396   topography on the north polar layered deposits of Mars, Geophys. Res. Lett., 43, 541-

2397   549.

2398 Sowers, T., M. Bender, D. Raynaud, and I. S. Korotkevich (1992), Delta N-15 of N2 in air trapped

2399   in polar ice - A tracer of gas transport in the firn and a possible constraint on ice age-gas

2400   age differences, J. Geophys. Res., 97, 15.

2401 Svensson, A., S. W. Nielsen, S. Kipfstuhl, S. J. Johnsen, J. P. Steffensen, M. Bigler, U. Ruth and R.

2402   Röthlisberger. (2005). Visual Stratigraphy of the North Greenland Ice Core Project

2403   (NorthGRIP) ice core during the last glacial period. Journal of Geophysical Research, Vol.

2404   110, D02108, doi:10.1029/2004JD005134.

2405 Svensson, A., Andersen, K.K., Bigler, M., Clausen, H.B., Dahl-Jensen, D., Davies, S.M., Johnsen,

2406   S.J., Muscheler, R., Parrenin, F., Rasmussen, S.O., Röthlisberger, R., Seierstad, I.,

2407   Steffensen, J.P., Vinther, B.M., (2008). A 60 000 year Greenland stratigraphic ice core

2408   chronology. Climate of the Past 4, 47–57.

2409 Robert L. Staehle, Sara Spangelo, Matthew Eby, Marc S. Lane, Kim M. Aaron, Rohit Bhartia,

2410   Justin S. Boland, Lance E. Christiansen, Siamak Forouhar, Manuel de la Torre Juarez,

2411   David A. Paige, Nikolas Trawny, Chris R. Webster, Rebecca M. E. Williams "Multiplying

2412   Mars Lander Opportunities with MARSDROP Microlanders," conference paper for:

2413   AIAA/USU Small Satellite Conference SSC15-XI-3, Logan, Utah, 2015 August 13. DOI

2414   10.13140/RG.2.1.3599.1127

2415 Tanaka, K.L., 2005. Geology and insolation-driven climatic history of Amazonian north polar

2416   materials on Mars. Nature 437, 991–994. https://doi.org/10.1038/nature04065

2417 Tanaka, K.L., Fortezzo, C.M., 2012. Geologic map of the north polar region of Mars: U.S.

2418   Geological Survey Scientific Investigations Map 3177 [WWW Document].

2419 Tanaka, K., Rodriguez, J., Skinner jr, J., Bourke, M., Fortezzo, C., Herkenhoff, K., Kolb, E., Okubo,

2420   C., (2008). North polar region of Mars: Advances in stratigraphy, structure, and erosional

2421   modification. ICARUS 196, 318–358. doi:10.1016/j.icarus.2008.01.021

2422 Tanaka, K.L., Kolb, E.J., Fortezzo, C., (2007). Recent Advances In The Stratigraphy Of The Polar

2423   Regions Of Mars. 1–4.

2424 Tedesco, M., Doherty, S., Fettweis, X., Alexander, P., Jeyaratnam, J., Stroeve, J., (2016). The

2425   darkening of the Greenland ice sheet: trends, drivers, and projections (1981–2100) 10,

2426   477–496. https://doi.org/10.7916/D8ZG84R3

2427 Thomas, P. C., W. Calvin, B. Cantor, R. Haberle, P. B. James, and S. W. Lee (2016), Mass balance

2428   of Mars' residual south polar cap from CTX images and other data, *Icarus*, *268*, 118-130,

2429   doi:10.1016/j.icarus.2015.12.038.

2430 Thomas, P. C., P. B. James, W. M. Calvin, R. Haberle, and M. C. Malin (2009), Residual south

2431   polar cap of Mars: Stratigraphy, history, and implications of recent changes, *Icarus*,

2432   *203*(2), 352-375, doi:10.1016/j.icarus.2009.05.014.

2433 Tillman, J.E., Johnson, N.C., Guttorp, P., Percival, D.B., (1993). The martian annual atmospheric

2434   pressure cycle: Years without great dust storms. Journal of Geophysical Research:

2435   Planets (1991–2012) 98, 10963–10971.

2436 Titus, T.N., Kieffer, H.H., Christensen, P.R., 2003. Exposed Water Ice Discovered near the South

2437   Pole of Mars. Science 299, 1048–1051. https://doi.org/10.1126/science.1080497

2438 Toon, O.B., Pollack, J.B., Ward, W., Burns, J.A. and Bilski, K., 1980. The astronomical theory of

2439   climatic change on Mars. Icarus, 44(3), pp.552-607.

2440   Vaughan, D.G., J.C. Comiso, I. Allison, J. Carrasco, G. Kaser, R. Kwok, P. Mote, T. Murray, F. Paul,

2441   J. Ren, E. Rignot, O. Solomina, K. Steffen and T. Zhang, 2013: Observations: Cryosphere.

2442   In: Climate Change 2013: The Physical Science Basis. Contribution of Working Group I to

2443   the Fifth Assessment Report of the Intergovernmental Panel on Climate Change

2444   [Stocker, T.F., D. Qin, G.-K. Plattner, M. Tignor, S.K. Allen, J. Boschung, A. Nauels, Y. Xia,

2445   V. Bex and P.M. Midgley (eds.)]. Cambridge University Press, Cambridge, United

2446   Kingdom and New York, NY, USA.

2447   Ventura, S., 2011. The MEDUSA and MicroMED Experiments for the ExoMars Space Programme

2448   to Perform In Situ Analysis of Martian Dust [WWW Document].

2449   https://doi.org/10.6092/UNINA/FEDOA/8541

2450   Veres, D., Bazin, L., Landais, A., Toyé Mahamadou Kele, H., Lemieux-Dudon, B., Parrenin, F.,

2451   Martinerie, P., Blayo, E., Blunier, T., Capron, E., (2013). The Antarctic ice core chronology

2452   (AICC2012): an optimized multi-parameter and multi-site dating approach for the last

2453   120 thousand years. Climate of the Past 9, 1733–1748.

2454   Villanueva, G. L., M. J. Mumma, R. E. Novak, H. U. Käufl, P. Hartogh, T. Encrenaz, A. Tokunaga,

2455   A. Khayat, and M. D. Smith. "Strong water isotopic anomalies in the martian

2456   atmosphere: Probing current and ancient reservoirs." Science 348, no. 6231 (2015): 218-

2457   221.

2458   Vos, E., Aharonson, O., Schorghofer, N., 2019. Dynamic and isotopic evolution of ice reservoirs

2459   on Mars. Icarus 324, 1–7. https://doi.org/10.1016/j.icarus.2019.01.018

2460   Webster, C. R., G. J. Flesch, K. Mansour, R. Haberle, and J. Bauman (2004), Mars Laser

2461   Hygrometer, *Appl. Opt., 43,* 4436-4445.

2462   Whiteway, J. A., L. Komguem, C. Dickinson, C. Cook, M. Illnicki, J. Seabrook, V. Popovici, T. J.

2463   Duck, R. Davy, P. A. Taylor, J. Pathak, D. Fisher, A. I. Carswell, M. Daly, V. Hipkin, A. P.

2464   Zent, M. H. Hecht, S. E. Wood, L. K. Tamppari, N. Renno, J. E. Moores, M. T. Lemmon, F.

2465   Daerden, P. H. Smith. Mars water-ice clouds and precipitation. Science 325, 68–70

2466   (2009).

2467   Whitten, J.L., Campbell, B.A., (2018). Lateral Continuity of Layering in the Mars South Polar

2468   Layered Deposits From SHARAD Sounding Data. Journal of Geophysical Research:

2469   Planets 123, 1541–1554. https://doi.org/10.1029/2018JE005578

2470   Winter, A., Steinhage, D., Arnold, E.J., Blankenship, D.D., Cavitte, M.G.P., Corr, H.F.J., Paden,

2471   J.D., Urbini, S., Young, D.A., Eisen, O., (2017). Comparison of measurements from

2472   different radio-echo sounding systems and synchronization with the ice core at Dome C,

2473   Antarctica. The Cryosphere 11, 653–668. https://doi.org/10.5194/tc-11-653-2017

2474   Xu, S., Das, S.K., Archer, L.A., (2013). The Li–CO 2 battery: A novel method for CO 2 capture and

2475   utilization. RSC Advances 3, 6656–6660.

2476   Yen, A. S. et al. (2005), An integrated view of the chemistry and mineralogy of martian soils,

2477   Nature, 436(7047), 49–54, doi:10.1038/nature03637.

2478   Zacny, K., and Y. Bar-Cohen, "Drilling and excavation for construction and in situ resource

2479   utilization", Chapter 14 in Mars: Prospective Energy and Material Resources, Badescu

2480   (ed), Springer, 2010

2481   Zimmerman, W, et al, 2002. The Mars '07 North Polar Cap Deep Penetration Cryo-Scout

2482   Mission. Proceedings, IEEE Aerospace Conference, 10.1109/AERO.2002.1036850

2483   Zuber, M. T., R. J. Phillips, J. C. Andrews-Hanna, S. W. Asmar, A. S. Konopliv, F. G. Lemoine, J. J.

2484   Plaut, D. E. Smith, and S. E. Smrekar (2007), Density of Mars' south polar layered

2485   deposits, *Science*, *317*(5845), 1718-1719, doi:10.1126/science.1146995.

We have no conflicts of interest.